General Aviation Interior Noise: Part I – Source/Path Identification Technology

James F. Unruh, and Paul D. Till
Southwest Research Institute, San Antonio, Texas

May 2002

The NASA STI Program Office ... in Profile

Since its founding, NASA has been dedicated to the advancement of aeronautics and space science. The NASA Scientific and Technical Information (STI) Program Office plays a key part in helping NASA maintain this important role.

The NASA STI Program Office is operated by Langley Research Center, the lead center for NASA's scientific and technical information. The NASA STI Program Office provides access to the NASA STI Database, the largest collection of aeronautical and space science STI in the world. The Program Office is also NASA's institutional mechanism for disseminating the results of its research and development activities. These results are published by NASA in the NASA STI Report Series, which includes the following report types:

- TECHNICAL PUBLICATION. Reports of completed research or a major significant phase of research that present the results of NASA programs and include extensive data or theoretical analysis. Includes compilations of significant scientific and technical data and information deemed to be of continuing reference value. NASA counterpart of peer-reviewed formal professional papers, but having less stringent limitations on manuscript length and extent of graphic presentations.

- TECHNICAL MEMORANDUM. Scientific and technical findings that are preliminary or of specialized interest, e.g., quick release reports, working papers, and bibliographies that contain minimal annotation. Does not contain extensive analysis.

- CONTRACTOR REPORT. Scientific and technical findings by NASA-sponsored contractors and grantees.

- CONFERENCE PUBLICATION. Collected papers from scientific and technical conferences, symposia, seminars, or other meetings sponsored or co-sponsored by NASA.

- SPECIAL PUBLICATION. Scientific, technical, or historical information from NASA programs, projects, and missions, often concerned with subjects having substantial public interest.

- TECHNICAL TRANSLATION. English-language translations of foreign scientific and technical material pertinent to NASA's mission.

Specialized services that complement the STI Program Office's diverse offerings include creating custom thesauri, building customized databases, organizing and publishing research results ... even providing videos.

For more information about the NASA STI Program Office, see the following:

- Access the NASA STI Program Home Page at ***http://www.sti.nasa.gov***

- E-mail your question via the Internet to help@sti.nasa.gov

- Fax your question to the NASA STI Help Desk at (301) 621-0134

- Phone the NASA STI Help Desk at (301) 621-0390

- Write to:
  NASA STI Help Desk
  NASA Center for AeroSpace Information
  7121 Standard Drive
  Hanover, MD 21076-1320

NASA/CR-2002-211665

General Aviation Interior Noise: Part I – Source/Path Identification Technology

James F. Unruh, and Paul D. Till
Southwest Research Institute, San Antonio, Texas

May 2002

ACKNOWLEDGMENTS

Available from:

NASA Center for AeroSpace Information (CASI)	National Technical Information Service (NTIS)
7121 Standard Drive	5285 Port Royal Road
Hanover, MD 21076-1320	Springfield, VA 22161-2171
(301) 621-0390	(703) 605-6000

EXECUTIVE SUMMARY

Excessive interior noise and vibration in propeller driven general aviation aircraft can result in poor pilot communications with ground control personnel and passengers, and, during extended duration flights, can lead to pilot and passenger fatigue. The typical cabin noise spectrum is dominated by discrete tones generated from propeller, engine exhaust, or engine case radiation airborne impingement onto the fuselage and/or from direct structure-borne engine vibration. To develop efficient noise control measures, the source of each of the offending tones and their respective paths of propagation need to be understood. Signal analysis techniques applicable to tone excitation have been looked at over the past decade; however, a solidified approach to noise source/path identification is not presently available for the General Aviation Community.

There were two primary objectives of the research effort reported herein. The first objective was to identify and evaluate noise source/path identification technology applicable to single engine propeller driven aircraft that can be used to identify interior noise sources originating from structure-borne engine/propeller vibration, airborne propeller transmission, airborne engine exhaust noise, and engine case radiation. The approach taken to identify the contributions of each of these possible sources was first to conduct a Principal Component Analysis (PCA) of an in-flight noise and vibration database acquired on a Cessna Model 182E aircraft. The purpose of the PCA was to obtain an in-flight correlated data set as viewed by a fixed set of cabin microphones. A Conditioned Response Analysis (CRA), combining ground test noise source simulation frequency response function data with the in-flight PCA vectors, was then carried out to identify the relative contributions of each of the simulated sources to the cabin noise levels as measured by the fixed set of cabin microphones. The second objective was to develop and evaluate advanced technology for noise source ranking of interior panel groups such as the aircraft windshield, instrument panel, firewall, and door/window panels within the cabin of a single engine propeller driven aircraft. The technology employed was that of Acoustic Holography (AH). AH was applied to the test aircraft by acquiring a series of in-flight microphone array measurements within the aircraft cabin and correlating the measurements via PCA. A boundary element model of the aircraft cabin interior was then constructed, with pressure recovery nodes at the array measurement locations. The source contributions of the various panel groups leading to the array measurements were then synthesized by solving the inverse problem using the boundary element model.

Analysis of the in-flight and ground test databases for the Cessna Model 182 showed the aircraft interior noise to be generated from several airborne sources, including the propeller, exhaust, and engine case radiation. Structure-borne engine/propeller vibration was not identified to be a significant contributor to interior noise. The major paths of noise propagation were identified to be the aircraft windshield and firewall. Further work in the area of experimental verification and extended acoustic holography modeling is needed to verify the source/paths identified in the PCA and CRA evaluations.

TABLE OF CONTENTS

LIST OF FIGURES

LIST OF FIGURES (continued)

LIST OF FIGURES (continued)

LIST OF FIGURES (continued)

LIST OF TABLES

1. INTRODUCTION

1.1 Background

Excessive interior noise and vibration in aircraft can result in poor pilot communications with ground control personnel and passengers, and, during extended duration flights, can lead to pilot and passenger fatigue. A typical interior noise spectrum taken from a single engine propeller driven General Aviation aircraft is shown in Figure 1.1. The spectrum is dominated by discrete tones generated from propeller, engine exhaust, or engine case radiation airborne impingement onto the fuselage and/or from direct structure-borne engine vibration. Identification of the sources of individual tones can, to some extent, be facilitated by knowing the number of engine cylinders and number of propeller blades, except for the cases where engine firing and propeller tones align. The paths of propagation are not easily identified for either case. To develop efficient noise source/path control measures, the source of each of the offending tones and their respective paths of propagation need to be understood. Signal analysis techniques applicable to tone excitation have been looked at over the past decade [1-5]; however, a solidified approach to noise source/path identification is not presently available for the General Aviation Community.

Aside from direct air vent leaks, all interior noise is structure-borne via the surrounding vibrating panels within the cabin. If source/path control is not possible, then control at the interior radiating panel must be undertaken, requiring identification of the offending panels. Due to the varying degree to which panel vibrations couple with the cabin acoustic volume, direct measurement of panel vibration, which is straightforward, will not directly identify those panels that are major noise radiators. Limited success has been found in the use of sound intensity in the low frequency regions applicable to the General Aviation aircraft cabin [5-6]. A more promising technique, that of near-field acoustic holography [7-8], is gaining much attention and appears to be applicable to the General Aviation cabin geometries when coupled with modern day Helmholtz' Integral Equation solvers.

1.2 Program Objectives and Approach

There were two primary objectives of this research effort reported herein. The first objective was to identify and evaluate noise source/path identification technology applicable to single engine propeller driven aircraft that can be used to determine interior noise sources originating from structure-borne engine/propeller vibration, airborne propeller transmission, airborne engine exhaust noise, and engine case radiation. The approach taken to identify the contributions of each of these possible sources was first to conduct a Principal Component Analysis (PCA) of an in-flight noise and vibration database acquired on a Cessna Model 182E aircraft. The purpose of the PCA was to obtain an in-flight correlated data set as viewed by a fixed set of cabin microphones. A Conditioned Response Analysis (CRA), combining ground test noise source simulation frequency response function data with the in-flight PCA vectors, was then carried out to identify the relative contributions of each of the simulated sources to the cabin noise levels as measured by the fixed set of cabin microphones. These activities are described in Section 2 of the report.

The second objective of the work reported herein was to develop and evaluate advanced technology for noise source ranking of interior panel groups such as the aircraft windshield, instrument panel, firewall, and door/window panels within the cabin of a single engine propeller driven aircraft. The technology employed was that of Acoustic Holography (AH). AH was applied to the test aircraft by acquiring a series of in-flight microphone array measurements within the aircraft cabin and correlating the measurements via PCA. A boundary element model of the aircraft cabin interior was then constructed, with pressure recovery nodes at the array measurement locations. The source contributions of the various panel groups leading to the array measurements were then synthesized by solving the inverse problem using the boundary element model. Details of the analysis procedures and the results obtained are described in Section 3 of the report. Concluding remarks are given in Section 4. Recommendations for experimental verification of the noise source/paths and panel groups contributing to cabin noise in the Cessna 182E are given in Section 5.
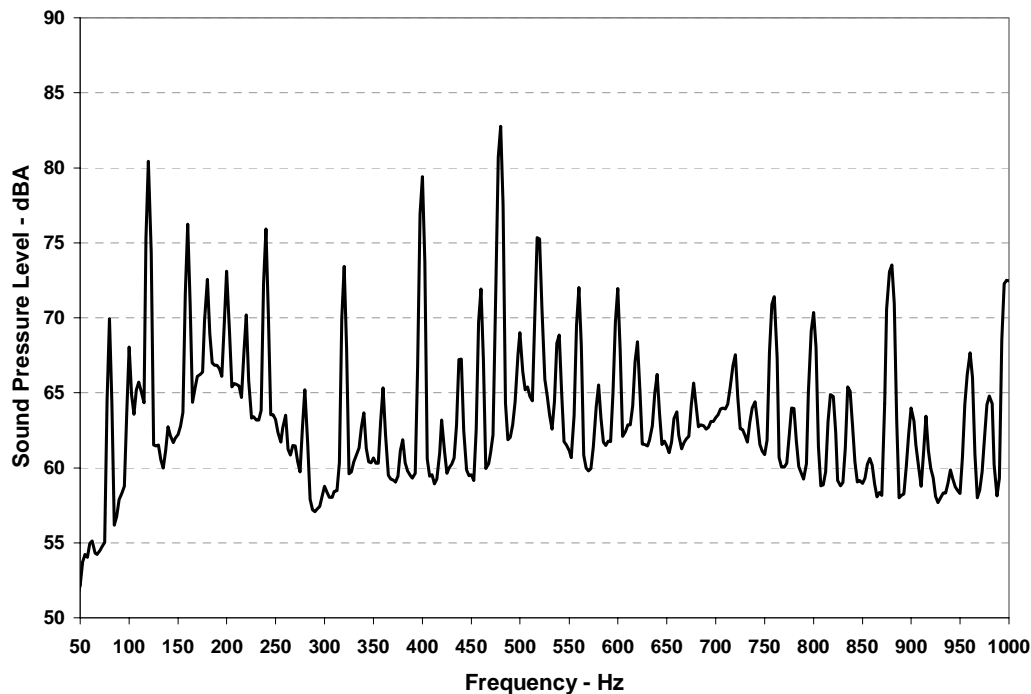
Figure 1.1 Typical General Aviation Interior Noise Spectrum.

2. NOISE SOURCE/PATH IDENTIFICATION

2.1   Principal Component Analysis

A Principal Component Analysis (PCA) of an aircraft in-flight noise and vibration database is necessary to identify the relative contributions of each of the measured responses to a fixed set of cabin reference microphones and to identify the number of partial sources contributing to the cabin noise field. The database of aircraft response parameter measurements may be acquired in a number of subsets; however, with each subset a fixed set of cabin reference microphones must be included. Sample averaged cross spectra between each of the system response parameters and the cabin fixed references are then developed. From this series of cross-spectral matrices, a set of partial correlated sources are generated to identify the relative contributions of each of the response parameters to the cabin fixed reference microphones.

When evaluating the source characteristics of an arbitrary source, a unique signal that is correlated with the acoustic source may not be observable without interference from other sources. Such is the case for a propeller driven aircraft where the engine structure-borne vibration and propeller airborne radiation, engine case radiation, and exhaust sources cannot be separated during in-flight operation. In general, for a vehicle sound field that consists of a series of partial sources, no such signal exists within the physical system. However, at some frequencies, the responses may be attributed to a particular source/path by virtue of its rotational order while other rotational orders can be a combination of several sources. The general case is assumed for most practical engineering applications. The following also addresses the case where, at most, a limited set of parameter instrumentation is available for the measurements and this instrumentation must be moved about the vehicle to span the required measurements.

The approach taken for this most general case will be to use a cross-spectral representation of the sound and vibration field and extract a coherent source description therefrom [8]. Let us assume that the vehicle noise source consists of a finite (small) number of partial sources, say L of them. The sources could be engine/propeller vibration, propeller airborne noise, engine case radiation, etc. Each partial source transmits a partial field that is perfectly coherent within the vehicle structure. The cross-spectral matrix for the lth partial source is:

$$\left[c_l \right] = \left\{ p_l^* \right\} \lfloor p_l \rfloor = \left\{ p_l^* \right\} \left\{ p_l \right\}^T, \quad l = 1, 2, \ldots L. \tag{2.1}$$

Here we use p to represent any combination of vibration or acoustic response parameters. The cross spectrum matrix for the total system would be the linear sum of each of the partial fields which can be written, for three partial sources, as:

$$[C] = \begin{bmatrix} p_1^* & p_2^* & p_3^* \end{bmatrix} \begin{bmatrix} p_1 \\ p_2 \\ p_3 \end{bmatrix} = \begin{bmatrix} P^* \end{bmatrix} \begin{bmatrix} P^T \end{bmatrix}. \tag{2.2}$$

If we could turn on each of the partial fields one at a time, we could construct the total vehicle response field; however, this is not possible for the general case. If one or more of the partial

sources cannot be seen by the vehicle response field measurements, the cross spectrum matrix for L partial fields will have a rank less than L. Let us assume that the rank of the cross spectrum matrix, C, is J, where $J < L$. This being the case, there exists a matrix of responses A of size J x N, where N is the number of response measurements in the vehicle response field that can replace the response matrix P, such that:

$$[C] = [A^*][A^T].$$
(2.3)

In order to determine a set of composite sources; i.e., columns of the A matrix, we employ a principal component technique. Let us place several stationary reference transducers within the vehicle cabin. These reference signals could be surface accelerometers, microphones, etc., which are to remain fixed during all measurements. It is assumed that these stationary references can in total see each of the L partial sources. Let the matrix R be defined as

$$[R] = [r_1 \quad r_2 \quad r_L] \,,$$
(2.4)

where the columns are the reference traces for the L partial sources and the rows are views of the L partial fields seen by a particular stationary reference. Now let us add the vehicle response parameters to these stationary references to form an extended partial system matrix as:

$$[Q] = \begin{bmatrix} r_1 & r_2 & r_L \\ p_1 & p_2 & p_L \end{bmatrix} = \begin{bmatrix} R \\ P \end{bmatrix}.$$
(2.5)

The extended cross spectra matrix may then be written as:

$$[C^E] = [Q^*][Q^T] = \begin{bmatrix} C_R & C_{RP} \\ C_{RP}^{*T} & C \end{bmatrix} = \begin{bmatrix} R^*R^T & R^*P^T \\ P^*R^T & P^*P^T \end{bmatrix} = [C_1 \quad C_2].$$
(2.6)

If one could measure directly the individual contributions of the L partial sources as indicated in Equation 2.5, the system measurement would be complete; however, this is not the case. We do not have the ability to selectively turn off and on the partial sources so that such measurements can be made. Instead, for a set of R stationary reference signals and a number of N system measurements (this can be several sets of say M response parameters) we can obtain the reference cross spectrum matrix C_R and the cross spectra from the references to the system measurement points C_{RP}. From these measurements, the full system cross spectrum matrix, C, can be determined as follows:

1. We assume that the rank of the C^E matrix must be that of the C_R matrix. By the very definition of a partial source, the rank of the C_R matrix cannot be any greater than the number of partial sources, L. (A good check on the number of partial sources is to select the number of stationary references, R, increasingly larger until the rank of the reference cross spectrum matrix, C_R, becomes rank deficient. At this point, the number of partial sources is just one less than the number of stationary references.)

2. The rank of the C_1 matrix must then also be that of C^E; consequently, the columns of C_2 are linear combinations of C_1 and we may write $C_2 = C_1 E$, where the matrix E is of size R by N.

3. Substitute this relationship into Equation 2.6 and we have a set of linear equations to be solved for E and C, namely:

$$E = C_R^{-1} C_{RP} \text{ and}$$

$$C = C_{RP}^{*T} C_R^{-1} C_{RP} . \qquad (2.7)$$

The inverse of the reference cross spectrum matrix may, as discussed above, be rank deficient at some spectral frequencies where a particular partial source is not present. In this case, a single value decomposition (SVD) of the cross spectrum matrix will be computed and the principal singular values will be used to represent the inverse with C_R^{-1} replaced by C_R^{+} to denote the pseudo inverse, which is exact if C_R has the rank of R. The pseudo inverse takes the form

$$C_R^{+} = S^* D^{+} S^T \qquad S^* S^T = S^T S^* = I_R \qquad (2.8)$$

where D is a diagonal matrix of the eigenvalues (singular values) squared, and S is a $R \times R$ orthonormal matrix of eignvectors. When C_R is rank deficient, say of rank $J < R$, then the eigenvalue matrix will contain only J non-zero eigenvalues. For this case, we use only the non-zero eigenvalues and form the inverse D^{+}. The corresponding J eigenvectors, S, are of size R.

With the above representation of the reference cross spectrum matrix we may, after considerable mathematical operation, obtain the principal component representation of the system cross spectrum matrix as given in Equation 2.3 as:

$$[C] = \left[A^*\right]\left[A^T\right] = [C_{RP}^T S_J D_J^{-1/2}]^* [C_{RP}^T S_J D_J^{-1/2}]^T , \qquad (2.9)$$

from which follows:

$$[A] = [C_{RP}^T S_J D_J^{-1/2}] . \qquad (2.10)$$

The columns of A are the principal system responses extracted from the reference cross spectrum matrix, or:

$$\{a_j\} = d_j^{-1/2} \left[C_{RP}^T\right]\{s_j\} \quad j = 1, 2, 3, \dots J. \qquad (2.11)$$

The system source vectors may then be examined for relative source contributions.

2.2 In-Flight Database

In-flight noise and vibration data were acquired on a Cessna Model 182E single engine propeller driven aircraft to provide a database of cabin interior noise, external pressure field excitation, and airframe vibration. The frequency range of interest was out to 1,000 Hz. The

tests were conducted during the week of November 30, 1998 at the Cessna Aircraft Company, Single-Engine Division, located in Wichita, Kansas.

2.2.1 Cessna Model 182E Aircraft

A photograph of the test aircraft is given in Figure 2.1 and the basic overall dimensions of the aircraft are given in Table 2.1. The approximate empty weight of the 182E aircraft was 1,580 lb. (716 kg). The aircraft is equipped with a six-cylinder, bed-mounted engine driving a constant speed two-bladed propeller. The test aircraft bears the Serial Number 182-54068.

2.2.2 Instrumentation Layout

There were three groups of instrumentation installed in the aircraft; namely, a set of primary and secondary sensors in the aircraft cabin (AC), a set of secondary sensors under the engine cowling (EC), and a third set that covered the aircraft exterior (AE) in the area of the cabin. In the following discussions, reference is made to the instrumentation layouts given in Figure 2.2.

Aircraft Cabin

The primary sensors in the aircraft cabin were four microphones. Two microphones were centered above the pilot's and copilot's control column, level with the top of the glare-shield and in-line with the forward doorpost. Two additional microphones were mounted at the ear level of would be rear seat passengers. In addition to these microphones, several surface mounted accelerometers were placed within the cabin as denoted in Table 2.2.

Engine Cowling

A number of transducers were placed within the engine cowling to record engine and airframe motion and direct airborne engine case radiation. Three high temperature accelerometers were placed on top of the engine to record engine vibrations in the axial, lateral, and vertical directions. Pairs of accelerometers were placed on either side of a forward engine mount to record vibration mount transmissibility in the shear and axial directions. Accelerometers were also attached to the firewall, one adjacent to a microphone to sense firewall noise transmission, potentially from engine case radiation. The list of sensors installed in the engine cowling area is given in Table 2.3.

Aircraft Exterior

The aircraft exterior was fitted with a series of microphones to record the propeller source noise impinging on the windshield and fuselage structure. Engine exhaust excitation and local fuselage response were also recorded. The aircraft exterior instrumentation are listed in Table 2.4

The accelerometers used were of a lightweight design (2 grams) and were bonded to the local structure. High temperature accelerometers were used on the engine. The interior and exterior microphones were ¼-inch ICP. Flush mounting of the external microphones was not

---

possible. The microphones on the exterior of the aircraft were soft mounted and shielded from the direct air stream via a porous teardrop shaped cover, as shown in Figure 2.3. While this mounting arrangement was not ideal, tone penetration above the flow noise occurred out to 500 Hz, as will be seen in the data to be presented. The original test plan included a tachometer to be recorded on data channel 32 to provide a timing trigger for spectral analysis of the data. This would have been most helpful in sample averaging out the broadband random noise in the external microphones. Unfortunately, the tachometer was removed from the test aircraft the evening prior to the flight test and was not available for the duration of testing.

2.2.3 Flight Conditions

The 31 channels of noise and vibration data on the 182E aircraft were recorded for the following flight conditions:

- **Normal Climb (500 fpm) - NCL** – Initiated climb at 2,000 ft altitude at 500 fpm and ended climb at 6,000 ft altitude. Vehicle indicated speed ranged from 91 kias to 105 kias. Engine speed constant at 2,400 rpm with manifold pressure at 23 inches.

- **Best Rate of Climb** - **BCR** – Initiated climb at 2,000 ft altitude and ended climb at 6,000 ft altitude. Vehicle indicated speed ranged from 76 kias to 88 kias. Engine speed constant at 2,400 rpm with manifold pressure at 23 inches.

- **65% Power Cruise** - **C65** – Cruise at 5,000 ft altitude with vehicle speed at 115 kias. Engine speed constant at 2,400 rpm with manifold pressure at 23 inches.

- **75% Power Cruise - C75** – Cruise at 5,000 ft altitude with vehicle speed at 120 kias. Engine speed constant at 2,400 rpm with manifold pressure at 21 inches.

- **Cruise Descent (500 fpm) - DES** – Descent initiated at 6,000 ft altitude at 500 fpm and ended descent at 2,500 ft. Vehicle indicated speed was 130 kias. Engine speed constant at 2,400 rpm with manifold pressure at 19 inches.

2.2.4 Typical Noise and Vibration Response

A summary of the overall noise and vibration levels recorded for the various flight conditions is given in Table 2.5. Typically 400 sample averages of all auto and cross spectra were acquired during steady state operation of the vehicle. Overall engine vibration isolation effectiveness can be seen when comparing the vibration responses of EC4 to EC8 and EC5 to EC9. At first it appears that the engine mounts are less than 50 percent effective in reducing transmitted engine vibrations; however, one must look at the frequency spectrum before making any judgments on isolator effectiveness. The vibration levels of the firewall, at EC12 and EC13, appear to warrant some interest along with the local sound pressure level in this area, given by EC14.

The noise and vibration spectra for the 75 percent power cruise condition are presented in Figures 2.4 through 2.18 as typical in-flight spectra. As expected for the propeller driven

aircraft, the spectra are rich with engine and propeller harmonics. Likewise, the vibration spectra show similar harmonic response. The data were recorded at an engine speed of 2,400 rpm. The engine fundamental is at 40 Hz, the propeller fundamental at 80 Hz (two-bladed propeller), and the engine firing fundamental is at 120 Hz (six-cylinder engine).

Cabin Spectra

The cabin sound pressure level spectra are dominated by the engine, propeller, and firing (exhaust) fundamentals and higher order harmonics. There are also harmonic responses occurring at half of the engine fundamental, which are associated with valve closure. The A-weighted noise spectra in the forward cabin, reference Figure 2.4, are surprisingly high in the mid frequency range, 400 to 500 Hz, while the aft cabin spectra, reference Figure 2.5, are low frequency, 50 to 250 Hz, dominated. The right side of the instrument panel exhibits a high level of vibration as compared to the left side, as shown in Figure 2.6. As should be expected, the windshield vibration spectra are dominated by propeller tones. The fuselage window vibration spectra exhibit a high level of response at the propeller harmonics as well, reference Figures 2.8 and 2.9.

Engine Spectra

The engine and engine mount truss vibration spectra are rich in tonal response with the fundamental at 20 Hz, half the engine speed, as seen in Figures 2.10 through 2.15. However, the major tonal responses align with the engine speed fundamental of 40 Hz as do the cabin noise spectra. Comparison of the vibration transmission across the engine mount, Figure 2.13, indicates that engine vibration isolation does not begin until around 200 Hz and 250 Hz, respectively, in the axial and transverse directions. The isolation is shorted by engine mount resonances. The axial vibration component in the engine mount truss members exhibits a broad band resonance around 500 Hz, with the firewall vibration spectra reflecting similar behavior, see Figure 2.15. The sound pressure level spectrum in the mid center of the firewall area also indicates a high level of noise in the low and mid frequency regions of the spectrum.

Fuselage Spectra

The sound pressure level spectra external to the fuselage are dominated by flow (boundary layer noise) beyond 500 Hz, see Figure 2.17. While the propeller and exhaust tones can be identified in the spectra below 500 Hz, the signal to broad band noise is not very good for several of the tones. The accelerometer AE5, mounted on the fuselage structure adjacent to the microphone, exhibits similar broad band noise characteristics. The high level of broad band vibration above 350 Hz leads one to believe that a high level of air turbulence exists in this area.

For interior noise control, the spectral response at the engine harmonics appears to be of primary concern. The various engine harmonics, out to 1,000 Hz, are identified in Table 2.6 along with the amplitude responses for the 75 percent power cruise flight condition. Table 2.6 shows that the individual harmonics that contribute to interior noise are at 1P, 1F, 2P, 2F-3P, 5P, 4F-6P, and 13E, all lying above 75 dBA. This is typical for all flight conditions with some variation. It is these engine harmonics that are of interest for further noise source/path analyses employing Principal Component Analysis (PCA).

2.3   Principal Component Analysis Results

Principal component analyses of each of the five vehicle flight conditions were carried out to determine if such analysis procedures will indicate source/path relationships for the aircraft and if the relationships are consistent for the various flight conditions. The initial analysis consisted of a singular value analysis of the four interior microphones to determine if sufficient fixed references are available to capture the source field. The results of the analyses at each of the engine harmonics are given in Tables 2.7 through 2.11, respectively, for the five flight conditions. At many of the dominant tones, such as, 1P, 1F, 2P, 2F-3P, 5P, 4F-6P, and 13E, a single partial source was indicated with some exceptions.

The primary source contributions to each of a select number of tones are given in Tables 2.12 through 2.16, for each of the flight conditions. The eigenvector components corresponding to the microphone responses were converted to sound pressure levels. The major contributing components for each response vector are highlighted. While the first propeller tone was not one of the dominant tones, it was included in the evaluation to see if PCA would pick out the intuitive source/path relationship. As can be seen by the indicated contributors to the 80 Hz fundamental propeller tone, PCA indicates the intuitive path, being the windshield and cabin side walls along with the firewall. Likewise, the downstream exhaust is shown to dominate at the 120 Hz fundamental firing frequency with the transverse acceleration of the engine mount on the airframe side being quite high, indicating a torsion-like motion of the engine.

2.4   Conditioned Response Analysis

A brief outline of the concept of Conditioned Response Analysis (CRA) is given below to provide a rationale for the supporting ground tests described in Section 2.4. The concept of CRA used herein is to enhance the knowledge gained from the PCA of the aircraft flight test data with a series of ground test simulations of postulated airborne or structure-borne noise sources.

Several years ago in-flight structure-borne noise transmission detection techniques were developed by researchers at Southwest Research Institute[TM] employing a combination of ground based frequency response function testing and in-flight response parameter measurements [1]. The detection technique was applied to the PTA aircraft to determine the level of propeller induced structure-borne interior noise transmission [2]. In the PTA study, the propeller wake excitation was simulated via dual shaker out of phase excitation applied to the wing main spar producing a dynamic moment about the propeller axis of rotation. For this particular investigation, a single structure-borne source excitation was evaluated.

In most general investigations, the noise source is not so well understood nor can it be as easily characterized as it was for the PTA aircraft evaluation. This being the case, several possible airborne and/or structure-borne noise sources should be applied during ground testing to establish a series of potential path/receiver relationships, which can, in the end, be used in some linear combination to simulate the actual in-flight noise source(s). For example, engine induced structure-borne noise in a piston driven general aviation aircraft due to engine imbalance and/or propeller vibration is transmitted past the engine isolation system through the engine support structure directly into the fuselage cabin. Likewise, the propeller direct airborne noise is transmitted to the cabin via the windshield and/or other responding structures. Simulation of

such noise sources during ground testing may require several possible types, locations and directions of excitation to completely characterize the source field.

2.4.1 Instrumentation

<u>Cabin Microphones</u>

The instrumentation for the CRA should consist of a set of interior microphones placed within the cabin at would be pilot, co-pilot, and passenger head heights and at other locations where interior noise is of interest. The locations should be identical to those used during acquisition of the in-flight data noise and vibration database. The following nomenclature is used to describe the responses at the cabin microphones:

$$\{\,\mathbf{p^f}\,\} = \{\,\mathbf{p_s^f}\,\} + \{\,\mathbf{p_a^f}\,\}\,, \tag{2.12}$$

where,

$\{\,\mathbf{p^f}\,\}$ - in-flight microphone response vector (M x 1),

$\{\,\mathbf{p_s^f}\,\}$ - in-flight <u>structure-borne</u> noise component vector,

and

$\{\,\mathbf{p_a^f}\,\}$ - in-flight <u>airborne noise</u> component vector.

Likewise, during ground testing,

$\{\,\mathbf{p^g}\,\}$ - <u>ground test</u> noise vector (M x 1),

consisting of components from both simulated airborne and structure-borne noise sources.

The aircraft may be equipped with microphones to record the external airborne noise source directly as well as accelerometers to record vibrations due to structure-borne noise transmission. The primary response instrumentation recorded during flight and during ground tests provides the link between the ground source simulation vectors and the in-flight measured cabin noise levels.

<u>Airframe Structural Response</u>

Airframe structural response instrumentation is to be placed along potential SBN paths leading to the aircraft cabin. These primary structural response parameters should be chosen such that in-flight airborne noise sources would produce insignificant structural response at these locations. The structural response vectors are:

$\{\,\mathbf{as^f}\,\}$ - <u>in-flight</u> structural response vector (Ns x 1),

and

$\{\,\mathbf{as^g}\,\}$ - <u>ground test</u> structural response vector (Ns x 1).

There may be cabin interior structural response parameters of interest, such as instrument panel or bulkhead responses. These parameters could assume the same role as the interior microphones and may be viewed as an extension to the microphone response vector without loss in generality or assume the role as primary structural responses.

Airframe Acoustic Response

Microphones may be placed directly on the airframe to record direct airborne noise radiation from the propeller. The acoustic response vectors are:

$$\{ \mathbf{aa^f} \} \text{ - \underline{in-flight} airborne response vector } (Na \text{ x } 1),$$

and

$$\{ \mathbf{aa^g} \} \text{ - \underline{ground test} airborne response vector } (Na \text{ x } 1).$$

Combined Responses

For the purposes of representation, the airframe structural and acoustic responses may be combined into one airframe response set:

$$\{ \mathbf{a^f} \} = \{ \mathbf{as^f : aa^f} \}^{\mathbf{T}} \text{ - \underline{in-flight} airframe response vector } (N \text{ x } 1), \tag{2.13}$$

and

$$\{ \mathbf{a^g} \} = \{ \mathbf{as^g : aa^g} \}^{\mathbf{T}} \text{ - \underline{ground test} airframe response vector } (N \text{ x } 1), \tag{2.14}$$

where N is now the sum of Ns and Na.

The reason for breaking out the airframe structural and acoustic responses will be made clear in the improved procedures discussed in Section 2.5.4 to follow.

2.4.2 Data Acquisition

During ground test, assume that $j = 1,2,3, ...J$ sets of microphone interior responses and airframe responses are acquired during J combined structure-borne and airborne noise source simulations. In these simulations, the sources of excitation are to be unique. During structure-borne excitation, every caution must be taken to shield the airframe from any airborne noise, especially that radiated from the shakers used to provide airframe excitation. Frequency response functions between the cabin primary microphone and airframe primary responses with respect to one of the airframe primary response parameters shall be recorded during the ground test simulations. For a given source simulation, the reference response would be chosen to provide excellent correlation with the simulated source. During flight, data are to be acquired at identical microphone locations, say $m = 1,2,3, ...M$, and at identical airframe response parameter locations, say $n = 1,2,3, ...N$, as those used during ground testing. The in-flight data would be phase correlated to the cabin microphone responses.

2.4.3 Data Analysis

The procedure to use for relating the ground test response data to the in-flight response data begins with determining the linear sum of ground test airframe response parameter vectors which best fit the in-flight airframe response parameters measured during flight. Thus, we seek the vector $\{\alpha\}$ such that:

$$\{\ \tilde{\mathbf{a}}^{\mathbf{f}}\ \} = [\ \mathbf{A}^{\mathbf{G}}\ ]\ \{\ \alpha\ \} \tag{2.15}$$

where,

> $\{\ \tilde{\mathbf{a}}^{\mathbf{f}}\ \}$ - is to be a close approximation to $\{\ \mathbf{a}^{\mathbf{f}}\ \}$, the <u>in-flight</u> airframe response vector,
>
> $[\ \mathbf{A}^{\mathbf{G}}\ ]$ - is a matrix of selected $\{\ \mathbf{a}^{\mathbf{g}}\ \}$ response vectors (N x J),

and

> $\{\ \alpha\ \}$ - the desired source simulation weight vector (J x 1).

This being the case, we may then estimate the in-flight structure-borne and airborne noise components from:

$$\{\ \tilde{\mathbf{p}}\ \} = [\ \mathbf{P}^{\mathbf{G}}\ ]\ \{\ \alpha\ \} \tag{2.16}$$

where,

> $\{\ \tilde{\mathbf{p}}\ \}$ - is an estimate of the in-flight response vector,
>
> $[\ \mathbf{P}^{\mathbf{G}}\ ]$ - is a matrix of the $\{\ \mathbf{p}^{\mathbf{g}}\ \}$ response vectors (N x J), consistent
>
> with $\{\ \alpha\ \}$ and
>
> $\{\ \alpha\ \}$ - is the source simulation weight vector determined from the best fit to the in-flight structural response parameters.

The solution approach initially taken was to include all the ground simulation information in a single evaluation and to use a Moore-Penrose pseudoinverse [9] of the over determined system of equations to obtain a solution.

$$\{\ \alpha_{k}\ \} = \ \mathbf{pinv}[\ \mathbf{A}^{\mathbf{G}}\ ]\ \{\ \tilde{\mathbf{a}}^{\mathbf{f}}\ \}. \tag{2.17}$$

The extent to which the above formulation of CRA facilitates noise source/path identification for the Cessna Model 182E aircraft was evaluated using the ground test source simulation data sets described in the following section. As will be seen, analysis of this data resulted in a modification to the general CRA procedures, as is described in Section 2.5.4.

2.5   Ground Test Noise Source Simulation

Ground test noise source simulation data were acquired on the Cessna Model 182E aircraft during the week of April 5, 1999 at Stinson Airport, San Antonio, Texas. A photograph

---

of the aircraft suspended on wing jacks ready for ground test is shown in Figure 2.19. The wing jack suspension was used to better simulate in-flight loading of the structure.

2.5.1 Source Simulations

The following noise source simulations were carried out while the aircraft was in the ground test configuration:

Propeller Airborne Noise Source Radiation

The array of 8- to 10-inch speakers shown in Figure 2.20 was used to provide simulation of the propeller acoustic radiation. The speakers were time delayed to provide simulation of the rotational speed of the propeller at 2,400 rpm. The drive signal was a terminal peak saw tooth with a fundamental at 80 Hz resulting in a broad spectrum of harmonics, as is shown in Figure 2.21. To maintain phase correlation across all installed instrumentation, the windshield microphone response signal, AE1, was used as a reference signal to generate the frequency response functions (FRF) required for the CRA. The cabin sound pressure levels recorded during the propeller simulation were well above the background noise levels, as is shown in Figure 2.22.

Engine Exhaust Noise Radiation

While the first and third harmonics of the engine firing frequency at 120 Hz were dominant in the exterior noise field, reference AE4 of Figure 2.17, the exhaust simulation included all engine harmonics. A speaker, placed near the engine exhaust, was driven at the engine fundamental of 40 Hz to simulate the engine exhaust noise, see Figure 2.23. The drive signal was a terminal peak saw tooth that produced downstream levels at AE4 well above 80 dB throughout the spectrum, as is shown in Figure 2.24. AE4 was chosen as the reference signal to generate the FRF's required for the CRA. The cabin noise levels generated by the exhaust speaker were well above the noise floor, as can be seen in Figure 2.25.

Engine Noise Radiation

A speaker was also placed in the area between the engine and firewall to produce direct airborne impingement on the firewall to simulate engine noise radiation, see Figure 2.26. The engine cowling was replaced and the speaker was driven with a terminal peak saw tooth at the engine fundamental of 40 Hz. The microphone mounted near the firewall, EC14, was chosen as the reference signal. The microphone exhibited good signal to noise ratios, as shown in Figure 2.27. Likewise, the cabin microphone responses were adequately above the noise floor to generate the FRF's required for the CRA, as shown in Figure 2.28.

Direct Structure-Borne Noise

An electrodynamic shaker was attached to the aircraft engine to impose torsional excitation simulating engine or propeller imbalance vibrations, generally considered as direct structure-borne noise transmission. The shaker sting was attached to the engine block at one of the oil pan bolts off from the engine centerline, as shown in Figure 2.29. The imposed force level spectrum produced with a terminal peak saw tooth waveform at 40 Hz is shown in Figure 2.30.

The resulting cabin noise levels, given in Figure 2.31, confirmed the adequacy of the drive signal. The load cell output was chosen as the reference signal for the data set. While the engine cowling was not replaced for this simulation, the shaker was covered with a high transmission loss blanket to minimize airborne radiation from the shaker. An overall view of the direct structure-borne noise shaker test setup is shown in Figure 2.32.

2.5.2 Instrumentation Layout

The instrumentation employed during the ground simulation tests were located at identical locations and maintained identical polarity as those used during the flight test. Reference is made to Figure 2.2 for a schematic of the instrumentation layout and to Table 2.5 for a general description of the location of each transducer.

2.5.3 Frequency Response Functions

During the ground test simulations, the FRF's required for the CRA were recorded directly using the reference signals described in Section 2.5.1. Approximately 400 sample averages were acquired in the frequency range out to 1,000 Hz. The bandwidth of the analysis was 2.5 Hz, the same as the in-flight database. The four cabin microphone FRF's were placed into one of the columns of the $[\mathbf{P^G}]$ matrix, defined in Equation 2.16. The four independent source simulations resulted in $[\mathbf{P^G}]$ being a 4x4 matrix. Likewise, the FRF's of the various aircraft response parameters were placed into a corresponding column of the $[\mathbf{P^G}]$ matrix, as defined in Equation 2.15. The 27 aircraft response parameters for the four source simulations resulted in $[\mathbf{A^G}]$ being a 27x4 matrix. The magnitudes of the FRF's were non-dimensional for the microphone responses due to airborne excitation and the units of the accelerometer FRF's were g's/(P/P$_{ref}$). For shaker induced structure-borne noise transmission simulation, the units were g's/lbf.

The FRF's for several response locations for the various noise source simulations are given in Figures 2.33 through 2.36. It is of interest to note the increased amplitude of the firewall mounted microphone (EC14) above the reference at selected tones for both the propeller and exhaust simulations, see Figures 2.33a and 2.34a. This may indicate a possible resonant buildup within the engine cowling. Similar levels of firewall acceleration (EC13) are also present during these airborne source simulations. The firewall acceleration response is most pronounced for the engine airborne simulation, see Figure 2.35b, as should be expected with the source being very close to the firewall. FRF's generated during the direct structure-borne noise source simulation for the firewall and instrument panel are given in Figures 2.36a and 2.36b, respectively. As expected, the response levels per pound of shaker force are considerably higher than those generated by any one of the airborne source simulations.

2.5.4 Improved CRA Procedures

Brute Force Analysis

In the following discussions, the "auxiliary responses" are defined as all the aircraft response parameters except for the four cabin microphones. A brute force conditioned response

---

analysis approach would be to weigh all auxiliary responses equally and use a least squares solution to Equation 2.15 to solve the highly over-determined system of equations for an estimate of source simulation weight vector, $\{\alpha\}$. The results of the brute force predictions versus measured in-flight cabin responses during Cruise at 75% Power are given in Table 2.17 for all measured spectral tones above 80 dBA. The contributions from the propeller airborne vector are listed under "AB-Prop," the exhaust airborne under "AB-Exhst," the engine airborne under "AB-Eng," and the engine direct structure-borne under "SB-Eng."

Several observations are made from the data in Table 2.17:

1. In general, the predictions are generally much higher than the measured in-flight levels, the only exception being the response at 400 Hz, which does not appear to be generated from any one of the simulated airborne or structure-borne noise sources.

2. Airborne noise radiation appears to dominate the cabin interior response. The predicted structure-borne noise levels do not appear to be significant.

3. The measured sound pressure level variation within the cabin for the 80 Hz propeller fundamental exhibits a possible modal behavior with the forward cabin responses being lower than the aft cabin. The predictions do not exhibit this trend.

4. Source phasing appears to be very important, as can be seen by attempting to sum the individual source contributions to obtain the combined levels.

It is to be noted that at an engine speed of 2,400 rpm, the propeller tones are multiples of 80 Hz, the engine firing tones are multiples of 120 Hz, and the engine case radiation and associated structure-borne vibrations are multiples of 40 Hz. This is the reason for the zero contributions from the airborne propeller and airborne exhaust at several of the spectral tones.

Primary and Secondary Auxiliary Response Parameters

Many of the auxiliary response parameters recorded during flight will respond to several of the airborne and structure-borne noise sources. However, for a given source simulation, there is a set of auxiliary response parameters that are most sensitive to that simulated source and will be less sensitive to other potential sources. This set of auxiliary response parameters will be denoted as primary auxiliary response parameters. The remaining auxiliary response parameters are denoted as secondary. The selection of *primary auxiliary response parameters* for each of the source simulation vectors is as follows:

1. **Airborne Propeller** – The microphone on the aircraft exterior center windshield, AE1. Microphones on the pilot's and copilot's doors (AE2 and AE3) are considered secondary since exhaust noise may be present at these positions.

2. **Airborne Exhaust** – The microphone directly downstream from the exhaust, AE4.

3. **Airborne Engine** – The microphone mounted mid center on the firewall, EC14.

4. **Structure-borne Engine** – Accelerometers mounted on the engine, namely EC1, EC2, and EC3.

There are *auxiliary parameters* for a given source simulation vector that may be *of no interest at all*. For example:

1. **Airborne Propeller** – The accelerometers on the engine, engine mount, etc., (EC1 through EC11). The accelerometers are mounted on rather massive structure, which would be difficult to excite with an airborne noise source. The microphone downstream from the exhaust, AE4, may be dominated by engine exhaust and, therefore, not considered active.

2. **Airborne Exhaust** – The accelerometers on the engine, engine mount, etc.

3. **Airborne Engine** – The accelerometers on the engine, engine mount, etc.

4. **Structure-borne Engine** – Microphones on the aircraft exterior (AE1 through AE4). The firewall microphone may be of interest due to secondary radiation.

The selection of primary (P) and secondary (S) auxiliary response parameters for each of the simulation vectors is given in Table 2.18. Those auxiliary response parameters, which are considered to be of no interest for a given simulation vector are left blank.

Predicted results using only the primary auxiliary response parameters were quite poor; however, including the secondary auxiliary response parameters resulted in a significant improvement in the predicted source trends, as can be seen by the results shown in Table 2.19. In the previous evaluation, the distribution of cabin noise levels at the 80 Hz tone resulted in nearly a uniform sound pressure level distribution or one with higher noise levels in the forward cabin (AC1 and AC2), while the measured results showed the aft cabin noise levels to be dominant. In the present analysis, using only the selected primary and secondary auxiliary parameters, the distribution of cabin noise levels exhibits much improved correlation. The cabin response at 400 Hz is still not well represented by any of the ground simulation vectors. Improved correlation with the measured in-flight cabin noise levels is important to gain confidence in making judgments on which noise source/path dominates a particular spectral response.

Separation of Airborne and Structure-Borne Contributions

While effects of engine induced structure-borne noise transmission on the cabin noise levels appears to be negligible, the contribution of SBN to other secondary response parameters used to estimate the levels of airborne noise transmission should be removed. This was accomplished by employing only the responses from the auxiliary accelerometers mounted on the engine, engine mounts, and support truss, namely, EC1 through EC11 to estimate the level of SBN transmission. These locations represent the more massive components of the aircraft, which are likely to exhibit little or no response to airborne excitation. The effects of SBN transmission were then removed from all other auxiliary responses prior to estimating the airborne source contributions. Mathematically, we have:

$$\{ \,\tilde{}\mathbf{a}^f_{EC1\text{-}11} \,\} = [\, \mathbf{A}^{GSB}_{EC1\text{-}11} \,]\, \{ \,\alpha_{EC1\text{-}11} \,\}, \tag{2.18}$$

where, $\{ \,\tilde{}\mathbf{a}^f_{EC1\text{-}11}\}$ - is the in-flight measured responses at EC1 through EC11

$[\, \mathbf{A}^{GSB}_{EC1\text{-}11} \,]$ **-** is the structure-borne engine simulation vector (11 x 1),

and $\quad \{ \,\alpha_{EC1\text{-}11} \,\}$ - the structure-borne source simulation weight.

This being the case, we may then estimate the in-flight structure-borne noise components from

$$\{ \,\tilde{}\mathbf{p}_{SB\text{-}Eng} \,\} = [\, \mathbf{P}^G_{SB\text{-}Eng} \,]\, \{ \,\alpha_{EC1\text{-}11} \,\}, \tag{2.19}$$

where, $\{ \,\tilde{}\mathbf{p}_{SB\text{-}Eng} \,\}$ - is an estimate of the in-flight structure-borne cabin response vector,

$[\, \mathbf{P}^G_{SB\text{-}Eng} \,]$ - is the cabin ground test response vector (4 x 1), consistent with $\{ \,\alpha_{EC1\text{-}11} \,\}$ and

$\{ \,\alpha_{EC1\text{-}11} \,\}$ - is the structure-borne source simulation weight.

The estimated responses at all other auxiliary parameter locations, denoted as AC-AE and consisting of AC5 through AC12, EC12 through EC14, and AE1 through AE5 are computed using the structure-borne source simulation weight:

$$\{ \,\tilde{}\mathbf{a}^f_{AC\text{-}AE/EC1\text{-}11} \,\} = [\, \mathbf{A}^{GSB}_{AC\text{-}AE} \,]\, \{ \,\alpha_{EC1\text{-}11} \,\} \tag{2.20}$$

where, $\{ \,\tilde{}\mathbf{a}^f_{AC\text{-}AE/EC1\text{-}11}\}$ - is the estimated in-flight responses at AC-AE

$[\, \mathbf{A}^{GSB}_{AC\text{-}AE} \,]$ **-** is the structure-borne engine simulation vector (N x 1) at auxiliary locations AC-AE,

and $\quad \{ \,\alpha_{EC1\text{-}11} \,\}$ - is the structure-borne source simulation weight.

The engine structure-borne contributions are removed from the in-flight measured responses as:

$$\{ \,\mathbf{a}^f_{AC\text{-}AE} \,\} = \{ \,\mathbf{a}^f \,\} \textbf{-} \{ \,\mathbf{a}^f_{AC\text{-}AE/EC1\text{-}11} \,\}. \tag{2.21}$$

The airborne only simulation vectors are then used to estimate the cabin responses using the reduced set of auxiliary response parameters, AC-AE. Computing the contribution of engine structure-borne noise transmission independently and then removing the source from all remaining auxiliary response parameters resulted in the predictions given in Table 2.20. Here we see somewhat further reduced structure-borne noise levels as given by the responses under the heading "SB-Eng Removed." The levels given under the heading "AB Combined" are for the airborne predictions only. The combined predictions for the propeller tones 1P and 2P appear reasonable; however, the engine firing tone 1F is overpredicted and the 5P tone remains low in the forward cabin.

Independent Estimates From Like Parameter Sets

The simulation results in Table 2.20 were encouraging. However, further evaluation of the sensitivity of certain individual parameters to the predicted results showed that the microphone auxiliary parameters were controlling the predicted responses and the accelerometers were not significant when included with the microphone auxiliaries. In fact,

there appeared to be no contribution from the accelerometer responses in weighting the airborne simulation vectors. After detailed evaluation of the mathematics associated with the pseudo inverse used in the solution of the simulation weight vector, α, it was found that the relative magnitude scaling between the microphone responses and accelerometer responses introduced a very biased weighting towards the microphone auxiliary parameter responses. Recall that microphone responses were normalized with respect to the standard reference pressure, 2×10^{-5} *Pa*, and the accelerometer responses with respect to gravity units, $g=386$ in/sec^2. This resulted in orders of magnitude differences in the elements of the simulation vectors for the accelerometers when using a pressure reference. The pseudo inverse routine is basically a least squares solution technique, which results in virtually eliminating any contribution from the relatively small elements corresponding to accelerometer responses in the coefficient matrix, $\mathbf{A^G}$.

To circumvent this problem, the microphone and accelerometer auxiliary parameters for the airborne simulation vectors were separated and independent cabin response estimates were made using each of the auxiliary parameter sets. The results from these independent parameter estimates are given in Tables 2.21 and 2.22, respectively, for the microphone and accelerometer auxiliary parameters. In the tables, the in-flight levels and combined levels are highlighted under various tones to indicate acceptable analysis results. The major contributing airborne sources are in bold print. The tones at 80 Hz, 160 Hz, 400 Hz, and 480 Hz are best represented employing the external microphone auxiliary response parameters, as indicated in Table 2.21. The 120 and 240 Hz tones are best represented by employing the accelerometer auxiliary response parameters, as indicated in Table 2.22.

2.6   Combined CRA Analyses

The combined analysis results employing the microphone and accelerometer auxiliary parameter sets are given in Table 2.23 and are used to identify the source/paths for the various spectral tones. The combination of airborne propeller and airborne engine noise at the 80 Hz tone is most interesting. The vector plots of the contributing sources at each cabin microphone is given in Figure 2.37. The vector plots show the source contributions in the forward cabin to be mainly out of phase and, therefore, destructively combining, while the aft cabin microphones are somewhat more in phase. Physically it appears that the propeller airborne noise radiation from the windshield and the engine airborne noise transmitted from the firewall destructively combine in the forward cabin. The propeller and engine airborne sources were analyzed independently and the results for the 80 Hz tone are given in Table 2.24. The independent sources resulted in higher noise levels in the forward cabin, a trend opposite to the measured data, yet when jointly employed, they predict the proper trends.

Summary of CRA Procedure

Based on the above evaluations, the procedure that is recommended for conditioned response analysis for noise source identification is as follows:

1.   Compute the engine induced structure-borne noise transmission contribution to interior noise using only those selected accelerometer auxiliary parameter measurements taken on the more massive airframe components, such as the engine, engine mounts, and support structure.

2. Remove the resulting engine induced structure-borne vibration responses from all other auxiliary parameter measurements.

3. Separate the microphone and accelerometer auxiliary parameter sets to form two independent estimates for the airborne noise transmission.

4. Select the results for a given tone from the independent parameter set which best match the amplitude distribution of the measured cabin noise levels.

5. Combine the estimates from the independent analyses and identify the potential noise sources from the relative levels of the contributing sources.

CRA Results for All Flight Conditions

CRA analysis results for the remaining flight conditions are given in Tables 2.25 through 2.28. In these tables, the contributions from the judged to be major sources are printed in bold numbers. A summary of the major airborne noise source contributions for all flight conditions is given in Table 2.29. The indicated sources appear to be consistent across the various flight conditions with few exceptions. It is to be noted that the cabin response levels at 400 Hz for the best rate of climb, normal rate of climb, and cruise descent flight conditions were not significant and, therefore, not included in the analysis summary of Table 2.29.

Table 2.1 Cessna Model 182E Dimensions.

Dimensions, External:	
Wing span	36 ft 2 in (11.02 m)
Length Overall	27 ft 4 in (8.33 m)
Height Overall	9 ft 0 in (2.74 m)
Tailplane Span	10 ft 10 in (3.30 m)

Table 2.2 Aircraft Cabin Instrumentation Layout.

Channel	Type – Nomenclature	Description
1	Microphone – AC1	Reference Mic above pilot's control column
2	Microphone – AC2	Reference Mic above copilot's control column
3	Microphone – AC3	Reference Mic near right rear seat passenger's head
4	Microphone – AC4	Reference Mic near left rear seat passenger's head
5	Accelerometer – AC5	Instrument panel right side
6	Accelerometer – AC6	Instrument panel left side
7	Accelerometer – AC7	Windshield right side
8	Accelerometer – AC8	Windshield left side
9	Accelerometer – AC9	Pilot's side window center
10	Accelerometer – AC10	Copilot's side window center
11	Accelerometer – AC11	Right rear passenger's window center
12	Accelerometer – AC12	Left rear passenger's window center

Table 2.3 Engine Cowling Instrumentation Layout.

Channel	Type – Nomenclature	Description
13	Accelerometer – EC1	Engine axial vibration
14	Accelerometer – EC2	Engine lateral vibration
15	Accelerometer – EC3	Engine vertical vibration
16	Accelerometer – EC4	Front engine mount engine side transverse
17	Accelerometer – EC5	Front engine mount engine side axial
18	Accelerometer – EC6	Engine truss lower left upper member axial
19	Accelerometer – EC7	Engine truss lower left lower member axial
20	Accelerometer – EC8	Front engine mount airframe side transverse
21	Accelerometer – EC9	Front engine mount airframe side axial
22	Accelerometer – EC10	Engine truss upper left member axial
23	Accelerometer – EC11	Engine truss upper right member axial
24	Accelerometer – EC12	Firewall normal acceleration – mid center
25	Accelerometer – EC13	Firewall normal acceleration – upper center
26	Microphone – EC14	Firewall sound pressure level – upper center

Table 2.4 Aircraft Exterior Instrumentation Layout.

Channel	Type – Nomenclature	Description
27	Microphone – AE1	Center windshield - pressure excitation
28	Microphone – AE2	Pilot's door center - pressure excitation
29	Microphone – AE3	Copilot's door center - pressure excitation
30	Microphone – AE4	On fuselage downstream from engine exhaust
31	Accelerometer – AE5	Fuselage vibration downstream from exhaust

Table 2.5 Cessna Model 182E Overall Response Levels.

Inst.	Description	Flight Test Condition - Overall Response out to 1,000 Hz				
		NCL	BRC	C65	C75	DES
AC1	Reference Mic above pilot's control column	105.3dB 94.7dBA	106.1 dB 94.8dBA	104.0dB 92.IdBA	104.5dB 92.9dBA	103.8dB 91.9dBA
AC2	Reference Mic above copilot's control column	104.8dB 93.5dBA	104.OdB 93.4dBA	103.3dB 91.3dBA	104.7dB 93.2dBA	103.5dB 90.9dBA
AC3	Reference Mic near right rear seat passenger's head	106.6dB 92.4dBA	106.2dB 91.6dBA	106.6dB 91.1dBA	109.5dB 93.2dBA	106.2dB 90.0dBA
AC4	Reference Mic near left rear seat passenger's head	105.5dB 90.8dBA	106.1 dB 89.9dBA	105.3dB 89.7dBA	108.3dB 91.0dBA	104.7dB 90.1dBA
AC5	Instrument panel right side	0.46 g_{rms}	0.50 g_{rms}	0.59 g_{rms}	0.55 g_{rms}	0.51 g_{rms}
AC6	Instrument panel left side	0.12 g_{rms}	0.11 g_{rms}	0.13 g_{rms}	0.13 g_{rms}	0.11 g_{rms}
AC7	Windshield right side	0.49 g_{rms}	0.51 g_{rms}	0.42 g_{rms}	0.60 g_{rms}	0.48 g_{rms}
AC8	Windshield left side	0.55 g_{rms}	0-55 g_{rms}	0.53 g_{rms}	0.43 g_{rms}	0.46 g_{rms}
AC9	Pilot's side window center	0.86 g_{rms}	0-87 g_{rms}	1.47 g_{rms}	1.80 g_{rms}	1.24 g_{rms}
AC10	Copilot's side window center	0.60 g_{rms}	0.40 g_{rms}	0.67 g_{rms}	0.77 g_{rms}	0.67 g_{rms}
AC 11	Right rear passenger's window center	0.46 g_{rms}	0.50 g_{rms}	0.68 g_{rms}	0.70 g_{rms}	0.55 g_{rms}
AC12	Left rear passenger's window center	0.62 g_{rms}	0.68 g_{rms}	0.76 g_{rms}	0.85 g_{rms}	0.74 g_{rms}
EC1	Engine axial vibration	1.75 g_{rms}	1. 12 g_{rms}	1.01 g_{rms}	1.07 g_{rms}	1.38 g_{rms}
EC2	Engine lateral vibration	1.82 g_{rms}	1.76 g_{rms}	1.89 g_{rms}	1.89 g_{rms}	1.79 g_{rms}
EC3	Engine vertical vibration	1.64 g_{rms}	1.45 g_{rms}	1.26 g_{rms}	1.26 g_{rms}	1.40 g_{rms}
EC4	Front engine mount engine side transverse	4.23 g_{rms}	3.92 g_{rms}	4.10 g_{rms}	4.10 g_{rms}	3.92 g_{rms}
EC5	Front engine mount engine side axial	3.64 g_{rms}	3.04 g_{rms}	3.13 g_{rms}	3.13 g_{rms}	3.33 g_{rms}
EC6	Engine truss lower left upper member axial	0.90 g_{rms}	0.86 g_{rms}	0.84 g_{rms}	0.84g	0.73 g_{rms}
EC7	Engine truss lower left lower member axial	0.80 g_{rms}	0.82 g_{rms}	0.73 g_{rms}	0.73g	0.68 g_{rms}
EC8	Front engine mount airframe side transverse	2.67 g_{rms}	2.84 g_{rms}	2.59 g_{rms}	2.59 g_{rms}	2.52 g_{rms}
EC9	Front engine mount airframe side axial	2.15 g_{rms}	2.22 g_{rms}	2.03 g_{rms}	2.03 g_{rms}	1.93 g_{rms}
EC10	Engine truss upper left member axial	0.83 g_{rms}	0.83 g_{rms}	0.83 g_{rms}	0.83 g_{rms}	0.84 g_{rms}
EC11	Engine truss upper right member axial	0.66 g_{rms}	0.67 g_{rms}	0.68 g_{rms}	0.72 g_{rms}	0.71 g_{rms}
EC12	Firewall normal acceleration - mid center	2.84 g_{rms}	2.6 g_{rms}	2.68 g_{rms}	2.87 g_{rms}	2.13 g_{rms}
EC 13	Firewall normal acceleration - upper center	1.64 g_{rms}	1.65 g_{rms}	1.50 g_{rms}	1.61 g_{rms}	1.42 g_{rms}
EC14	Engine SPL - firewall mid center	133.8dB 122.8dBA	134.7dB 122.IdBA	132.2dB 122.7dBA	131.8dB 122.3dBA	130.3dB 120.8dBA
AE1	Center windshield pressure excitation	132.6dB 116.1dBA	132.1dB 114.5dBA	132.8dB 116.5dBA	133.OdB 117.OdBA	133.OdB 118.OdBA
AE2	Pilot's door center pressure excitation	129.9dB 114.7dBA	129.OdB 113.9dBA	13 1. 1dB 115.2dBA	131.1dB I 15.6dB A	130.4dB 116.0dBA
AE3	Copilot's door center pressure excitation	l30.0dB 112.7dBA	128.4dB 111.2dBA	127.4dB 112.4dBA	127.9dB 113.1dBA	129.6dB 113.8dBA
AE4	On fuselage downstream from engine exhaust	134.5dB 122.4dBA	134.2dB 121.5dBA	134.8dB 123.1dBA	134.9dB 123.2dBA	134.2dB 122.9dBA
AE5	Fuselage vibration downstream from exhaust	0.43 g_{rms}	0.34 g_{rms}	0.64 g_{rms}	0.60 g_{rms}	0.56 g_{rms}

Table 2.6 75% Power Cruise – Response Levels at Engine Harmonics.

Freq Hz	Tone	AC1 dBA	AC2 dBA	AC3 dBA	AC4 dBA	AC5 g$_{rms}$	AC6 g$_{rms}$	AC7 g$_{rms}$	AC8 g$_{rms}$	AC9 g$_{rms}$	AC10 g$_{rms}$	AC11 g$_{rms}$	AC12 g$_{rms}$	EC1 g$_{rms}$	EC2 g$_{rms}$	EC3 g$_{rms}$	EC4 g$_{rms}$
40	1E	58.8	60.1	59.7	60.7	0.036	0.013	0.007	0.010	0.265	0.025	0.014	0.012	0.076	0.088	0.071	0.131
80	1P	69.9	70.4	83.3	82.6	0.094	0.061	0.214	0.130	1.126	0.506	0.427	0.571	0.218	0.177	0.160	0.222
120	1F	80.4	78.1	81.9	76.0	0.118	0.005	0.058	0.035	0.086	0.217	0.125	0.033	0.148	0.058	0.103	0.165
160	2P	76.2	82.8	81.1	79.5	0.090	0.006	0.346	0.185	0.056	0.051	0.078	0.050	0.098	0.064	0.071	0.195
200	5E	73.1	72.1	66.0	67.8	0.112	0.005	0.060	0.017	0.174	0.017	0.042	0.110	0.207	0.074	0.040	0.105
240	2F-3P	75.9	69.5	85.6	75.4	0.067	0.009	0.094	0.080	0.257	0.126	0.075	0.118	0.183	0.076	0.081	0.146
280	7E	65.2	64.8	66.1	65.5	0.041	0.005	0.041	0.023	0.063	0.021	0.042	0.036	0.146	0.156	0.153	0.162
320	4P	73.4	69.0	73.0	67.1	0.031	0.003	0.052	0.051	0.515	0.050	0.050	0.049	0.049	0.053	0.076	0.059
360	3F	65.3	66.5	66.3	66.2	0.040	0.004	0.024	0.023	0.032	0.028	0.031	0.040	0.063	0.035	0.119	0.077
400	5P	79.4	80.5	64.8	66.4	0.015	0.003	0.017	0.043	0.029	0.027	0.051	0.026	0.125	0.032	0.062	0.039
440	11E	67.2	70.3	67.2	64.9	0.029	0.003	0.025	0.028	0.044	0.021	0.021	0.021	0.032	0.055	0.112	0.116
480	4F-6P	82.8	81.1	72.2	74.8	0.024	0.003	0.031	0.053	0.054	0.040	0.056	0.030	0.128	0.026	0.107	0.089
520	13E	75.2	75.2	71.6	72.8	0.061	0.002	0.078	0.061	0.031	0.054	0.031	0.023	0.183	0.064	0.089	0.242
560	7P	72.0	72.5	67.6	66.3	0.048	0.002	0.016	0.022	0.029	0.020	0.022	0.031	0.112	0.045	0.056	0.741
600	5F	72.0	76.3	64.9	64.4	0.047	0.002	0.011	0.024	0.018	0.015	0.015	0.014	0.079	0.053	0.154	1.103
640	8P	66.2	70.7	64.8	62.0	0.014	0.002	0.026	0.033	0.011	0.011	0.014	0.021	0.104	0.063	0.089	0.239
680	17E	64.2	65.4	63.6	60.6	0.016	0.002	0.008	0.012	0.011	0.027	0.011	0.012	0.087	0.057	0.139	0.173
720	6F-9P	67.5	66.0	56.6	58.5	0.031	0.005	0.023	0.012	0.023	0.057	0.019	0.015	0.101	0.169	0.200	0.111
760	19E	71.4	68.2	62.4	56.7	0.023	0.003	0.015	0.011	0.014	0.021	0.015	0.012	0.150	0.178	0.086	0.047
800	10P	70.4	70.9	66.2	60.4	0.018	0.003	0.012	0.009	0.009	0.016	0.018	0.010	0.053	0.083	0.043	0.104
840	7F	62.8	75.0	66.9	60.7	0.016	0.003	0.010	0.010	0.014	0.012	0.010	0.009	0.064	0.152	0.154	0.115
880	11P	73.5	74.2	63.8	62.3	0.015	0.004	0.007	0.017	0.005	0.010	0.013	0.010	0.103	0.386	0.114	0.185
920	23E	60.0	72.7	57.2	55.7	0.029	0.004	0.012	0.013	0.007	0.008	0.008	0.008	0.096	0.221	0.156	0.136
960	8F-12P	67.7	66.4	55.7	54.7	0.026	0.004	0.013	0.011	0.012	0.010	0.008	0.006	0.027	0.269	0.073	0.183
1000	25E	72.5	71.4	60.7	66.7	0.015	0.005	0.010	0.011	0.007	0.007	0.009	0.007	0.035	0.336	0.151	0.105
Overall		92.9	93.2	93.2	91.0	0.550	0.130	0.600	0.430	1.800	0.770	0.700	0.850	1.070	1.890	1.260	4.100

Table 2.6 (continued) 75% Power Cruise – Response Levels at Engine Harmonics.

Freq	Tone	EC5	EC6	EC7	EC8	EC9	EC10	EC11	EC12	EC13	EC14	AE1	AE2	AE3	AE4	AE5
Hz		g_{rms}	g_{rms}	g_{rms}	g_{rms}	g_{rms}	g_{rms}	g_{rms}	g_{rms}	g_{rms}	dBA	dBA	dBA	dBA	dBA	g_{rms}
40	1E	0.152	0.058	0.009	0.071	0.071	0.012	0.013	0.030	0.068	80.2	77.6	82.1	74.1	75.0	0.003
80	1P	0.242	0.089	0.020	0.348	0.093	0.077	0.010	0.160	0.147	98.9	107.5	103.2	98.3	95.3	0.028
120	1F	0.051	0.060	0.030	0.728	0.065	0.018	0.022	0.055	0.545	108.7	94.8	93.6	99.5	114.4	0.018
160	2P	0.044	0.054	0.019	0.342	0.196	0.061	0.058	0.117	0.306	105.7	98.7	94.1	92.4	99.5	0.023
200	5E	0.042	0.037	0.057	0.264	0.052	0.025	0.012	0.188	0.118	87.2	97.1	93.4	89.9	99.0	0.013
240	2F-3P	0.099	0.048	0.049	0.323	0.012	0.053	0.045	0.433	0.209	99.9	101.5	96.9	97.5	99.4	0.018
280	7E	0.144	0.017	0.019	0.147	0.031	0.130	0.077	0.254	0.072	87.5	95.8	91.5	89.4	98.7	0.020
320	4P	0.054	0.013	0.021	0.013	0.059	0.027	0.010	0.240	0.079	94.5	100.7	95.3	91.4	101.2	0.019
360	3F	0.022	0.025	0.024	0.047	0.095	0.062	0.022	0.173	0.048	101.9	97.3	89.7	88.7	106.9	0.026
400	5P	0.047	0.020	0.012	0.038	0.102	0.042	0.093	0.172	0.037	103.3	93.4	92.1	96.4	99.5	0.060
440	11E	0.092	0.031	0.016	0.098	0.168	0.062	0.024	0.334	0.035	109.6	91.5	89.0	87.5	98.3	0.054
480	4F-6P	0.154	0.190	0.235	0.157	0.663	0.176	0.068	0.256	0.329	109.7	93.6	90.9	91.4	98.9	0.155
520	13E	0.414	0.267	0.203	0.099	0.405	0.256	0.211	1.332	0.159	101.1	90.9	89.2	86.7	97.8	0.057
560	7P	0.372	0.074	0.039	0.258	0.092	0.104	0.047	0.152	0.102	99.3	90.1	89.0	86.3	97.3	0.056
600	5F	0.689	0.124	0.105	0.551	0.363	0.048	0.065	0.047	0.220	95.6	90.7	88.8	86.2	98.2	0.072
640	8P	0.168	0.037	0.028	0.152	0.104	0.051	0.041	0.089	0.084	96.3	88.5	89.1	86.8	96.9	0.038
680	17E	0.349	0.019	0.014	0.046	0.132	0.027	0.029	0.140	0.136	100.4	87.8	87.9	84.8	96.0	0.035
720	6F-9P	0.328	0.015	0.032	0.089	0.119	0.024	0.042	0.113	0.055	104.0	86.9	89.1	84.6	95.7	0.025
760	19E	0.233	0.052	0.021	0.083	0.176	0.038	0.017	0.179	0.072	99.5	86.4	88.0	83.9	95.6	0.030
800	10P	0.178	0.031	0.035	0.096	0.081	0.011	0.048	0.095	0.067	95.1	85.3	88.2	83.9	94.8	0.024
840	7F	0.242	0.047	0.016	0.327	0.142	0.050	0.023	0.077	0.081	99.3	85.3	87.6	83.1	94.3	0.020
880	11P	0.244	0.042	0.048	0.055	0.053	0.051	0.023	0.121	0.068	96.1	84.3	86.9	81.5	94.0	0.026
920	23E	0.246	0.029	0.021	0.103	0.059	0.100	0.104	0.083	0.069	95.8	83.7	86.2	81.2	93.2	0.022
960	8F-12P	0.158	0.022	0.012	0.090	0.051	0.049	0.045	0.175	0.079	102.8	83.3	87.1	81.8	92.8	0.019
1000	25E	0.188	0.005	0.006	0.044	0.033	0.016	0.023	0.077	0.071	104.2	83.0	85.4	78.6	92.6	0.021
Overall		3.130	0.840	0.730	2.590	2.030	0.830	0.720	2.870	1.610	122.3	117.0	115.6	113.1	123.2	0.600

Table 2.7 Normal Climb – Normalized Singular Values at Engine Harmonics.

Frequency Hz	Engine Harmonic	Normalized Singular Values				
		1	2	3	4	Scale Factor
40	1E	1.00	0.027	0.000	0.000	7.17E+09
80	1P	1.00	0.088	0.000	0.000	3.14E+10
120	1F	1.00	0.019	0.000	0.000	3.16E+10
160	2P	1.00	0.094	0.025	0.000	1.66E+10
200	5E	1.00	0.543	0.210	0.076	2.80E+08
240	2F-3P	1.00	0.082	0.014	0.000	8.25E+09
280	7E	1.00	0.157	0.091	0.031	1.99E+08
320	4P	1.00	0.107	0.021	0.016	7.80E+08
360	3F	1.00	0.363	0.138	0.088	6.29E+07
400	5P	1.00	0.551	0.051	0.038	2.78E+08
440	11E	1.00	0.077	0.055	0.015	2.42E+08
480	4F-6P	1.00	0.319	0.048	0.018	4.02E+08
520	13E	1.00	0.397	0.126	0.036	1.13E+08
560	7P	1.00	0.057	0.010	0.000	1.15E+09
600	5F	1.00	0.141	0.012	0.000	3.43E+08
640	8P	1.00	0.162	0.061	0.026	6.96E+07
680	17E	1.00	0.269	0.172	0.075	1.44E+07
720	6F-9P	1.00	0.344	0.081	0.030	3.29E+07
760	19E	1.00	0.397	0.051	0.021	3.02E+07
800	10P	1.00	0.139	0.050	0.014	4.79E+07
840	7F	1.00	0.326	0.033	0.013	7.42E+07
880	11P	1.00	0.096	0.031	0.000	3.76E+07
920	23E	1.00	0.161	0.038	0.024	1.27E+07
960	8F-12P	1.00	0.074	0.018	0.000	2.50E+07
1000	25E	1.00	0.087	0.052	0.013	5.23E+07

Table 2.8 Best Rate of Climb – Normalized Singular Values at Engine Harmonics.

Frequency Hz	Engine Harmonic	Normalized Singular Values				
		1	2	3	4	Scale Factor
40	1E	1.00	0.419	0.000	0.000	1.52E+09
80	1P	1.00	0.024	0.000	0.000	6.71E+10
120	1F	1.00	0.022	0.000	0.000	2.47E+10
160	2P	1.00	0.093	0.013	0.000	8.22E+09
200	5E	1.00	0.728	0.186	0.095	1.72E+08
240	2F-3P	1.00	0.140	0.000	0.000	6.05E+09
280	7E	1.00	0.308	0.059	0.024	2.29E+08
320	4P	1.00	0.176	0.063	0.036	3.27E+08
360	3F	1.00	0.449	0.072	0.064	7.48E+07
400	5P	1.00	0.174	0.028	0.021	2.74E+08
440	11E	1.00	0.217	0.037	0.018	1.39E+08
480	4F-6P	1.00	0.068	0.023	0.000	1.14E+09
520	13E	1.00	0.164	0.029	0.013	2.66E+08
560	7P	1.00	0.015	0.000	0.000	1.54E+09
600	5F	1.00	0.238	0.013	0.000	1.72E+08
640	8P	1.00	0.085	0.028	0.024	1.35E+08
680	17E	1.00	0.227	0.112	0.074	1.46E+07
720	6F-9P	1.00	0.372	0.086	0.049	1.99E+07
760	19E	1.00	0.193	0.036	0.022	3.22E+07
800	10P	1.00	0.267	0.063	0.016	5.11E+07
840	7F	1.00	0.039	0.020	0.000	2.31E+08
880	11P	1.00	0.028	0.000	0.000	1.90E+08
920	23E	1.00	0.191	0.022	0.000	2.80E+07
960	8F-12P	1.00	0.026	0.000	0.000	1.80E+08
1000	25E	1.00	0.078	0.024	0.000	3.84E+07

Table 2.9 65% Power Cruise – Normalized Singular Values at Engine Harmonics.

Frequency Hz	Engine Harmonic	Normalized Singular Values				
		1	2	3	4	Scale Factor
40	1E	1.00	0.028	0.000	0.000	1.16E+10
80	1P	1.00	0.000	0.000	0.000	4.01E+10
120	1F	1.00	0.000	0.000	0.000	2.47E+10
160	2P	1.00	0.031	0.000	0.000	1.01E+10
200	5E	1.00	0.154	0.077	0.051	4.79E+08
240	2F-3P	1.00	0.037	0.012	0.000	2.50E+09
280	7E	1.00	0.120	0.073	0.042	1.37E+08
320	4P	1.00	0.080	0.040	0.026	2.37E+08
360	3F	1.00	0.302	0.195	0.115	2.80E+07
400	5P	1.00	0.021	0.000	0.000	5.89E+08
440	11E	1.00	0.133	0.034	0.023	1.10E+08
480	4F-6P	1.00	0.040	0.014	0.000	6.16E+08
520	13E	1.00	0.206	0.082	0.056	7.42E+07
560	7P	1.00	0.104	0.063	0.031	7.43E+07
600	5F	1.00	0.103	0.025	0.010	1.87E+08
640	8P	1.00	0.234	0.142	0.086	2.00E+07
680	17E	1.00	0.175	0.125	0.076	1.55E+07
720	6F-9P	1.00	0.246	0.106	0.064	1.15E+07
760	19E	1.00	0.159	0.035	0.017	2.77E+07
800	10P	1.00	0.102	0.059	0.026	2.58E+07
840	7F	1.00	0.102	0.022	0.000	3.37E+07
880	11P	1.00	0.192	0.027	0.011	4.10E+07
920	23E	1.00	0.061	0.025	0.015	2.10E+07
960	8F-12P	1.00	0.120	0.045	0.023	9.14E+06
1000	25E	1.00	0.100	0.032	0.017	1.53E+07

Table 2.10 75% Power Cruise – Normalized Singular Values at Engine Harmonics.

Frequency Hz	Engine Harmonic	Normalized Singular Values				
		1	2	3	4	Scale Factor
40	1E	1.00	0.000	0.000	0.000	1.62E+10
80	1P	1.00	0.000	0.000	0.000	1.08E+11
120	1F	1.00	0.000	0.000	0.000	2.58E+10
160	2P	1.00	0.019	0.000	0.000	1.39E+10
200	5E	1.00	0.146	0.070	0.039	6.72E+08
240	2F-3P	1.00	0.048	0.000	0.000	5.10E+09
280	7E	1.00	0.438	0.204	0.091	7.16E+07
320	4P	1.00	0.090	0.049	0.015	3.23E+08
360	3F	1.00	0.312	0.137	0.095	5.86E+07
400	5P	1.00	0.013	0.000	0.000	9.33E+08
440	11E	1.00	0.180	0.080	0.057	7.39E+07
480	4F-6P	1.00	0.060	0.012	0.000	1.18E+09
520	13E	1.00	0.119	0.038	0.015	2.64E+08
560	7P	1.00	0.140	0.058	0.025	9.97E+07
600	5F	1.00	0.197	0.049	0.025	1.30E+08
640	8P	1.00	0.150	0.104	0.083	3.60E+07
680	17E	1.00	0.466	0.247	0.133	1.12E+07
720	6F-9P	1.00	0.286	0.079	0.049	1.58E+07
760	19E	1.00	0.134	0.036	0.019	3.66E+07
800	10P	1.00	0.102	0.034	0.018	4.55E+07
840	7F	1.00	0.033	0.017	0.000	6.58E+07
880	11P	1.00	0.038	0.000	0.000	8.36E+07
920	23E	1.00	0.050	0.023	0.018	2.98E+07
960	8F-12P	1.00	0.062	0.041	0.018	1.53E+07
1000	25E	1.00	0.018	0.013	0.000	5.39E+07

Table 2.11 Cruise Descent – Normalized Singular Values at Engine Harmonics.

Frequency Hz	Engine Harmonic	Normalized Singular Values				
		1	2	3	4	Scale Factor
40	1E	1.00	0.013	0.000	0.000	1.14E+10
80	1P	1.00	0.021	0.000	0.000	3.40E+10
120	1F	1.00	0.000	0.000	0.000	2.47E+10
160	2P	1.00	0.109	0.027	0.018	3.16E+09
200	5E	1.00	0.220	0.134	0.074	3.32E+08
240	2F-3P	1.00	0.043	0.014	0.000	2.86E+09
280	7E	1.00	0.110	0.080	0.025	2.09E+08
320	4P	1.00	0.106	0.061	0.034	2.08E+08
360	3F	1.00	0.187	0.125	0.058	6.20E+07
400	5P	1.00	0.055	0.030	0.022	2.40E+08
440	11E	1.00	0.088	0.038	0.023	1.58E+08
480	4F-6P	1.00	0.065	0.030	0.000	4.04E+08
520	13E	1.00	0.072	0.041	0.018	2.11E+08
560	7P	1.00	0.102	0.051	0.040	9.40E+07
600	5F	1.00	0.114	0.079	0.027	9.92E+07
640	8P	1.00	0.515	0.420	0.271	9.92E+06
680	17E	1.00	0.345	0.274	0.154	1.21E+07
720	6F-9P	1.00	0.303	0.141	0.067	1.63E+07
760	19E	1.00	0.529	0.119	0.087	8.89E+06
800	10P	1.00	0.362	0.166	0.083	1.16E+07
840	7F	1.00	0.082	0.034	0.026	2.37E+07
880	11P	1.00	0.191	0.072	0.056	1.12E+07
920	23E	1.00	0.195	0.132	0.089	6.17E+06
960	8F-12P	1.00	0.215	0.080	0.042	8.18E+06
1000	25E	1.00	0.077	0.040	0.024	1.65E+07

Table 2.12 Normal Climb (500 fpm) – Singular Vector Contributions for Selected Engine Harmonics.

	Reference SPL @ Pilot's Position - AC1	Frequency/Harmonic/Eigenvector							
		73.1dBA	79.2dBA	84.6dBA	71.2dBA	80.5dBA	75.8dBA	77.2dBA	72.9dBA
Loc.	Description	80/1P/1	120/1F/1	160/2P/1	200/5E/1	240/2F-3P/1	400/5P/1	480/4F-6P/1	520/13E/1
AC5	Dash face right side	0.071	0.121	0.028	0.062	0.065	0.022	0.001	0.031
AC6	Dash face left side	0.048	0.001	0.006	0.004	0.005	0.002	0.002	0.002
AC7	Windshield right side	0.262	0.077	0.098	0.017	0.073	0.029	0.028	0.043
AC8	Windshield left side	0.258	0.028	0.199	0.010	0.097	0.035	0.028	0.034
AC9	Pilot's side window center	0.670	0.059	0.061	0.010	0.061	0.028	0.012	0.007
AC10	Copilot's side window center	0.322	0.264	0.016	0.007	0.060	0.009	0.019	0.014
AC 11	Right rear passenger's window center	0.076	0.165	0.049	0.012	0.102	0.044	0.033	0.025
AC12	Left rear passenger's window center	0.466	0.008	0.114	0.013	0.077	0.014	0.017	0.009
EC1	Engine axial vibration	0.292	0.185	0.071	0.196	0.247	0.086	0.081	0.177
EC2	Engine lateral vibration	0. 232	0.083	0.054	0.109	0.119	0.030	0.005	0.085
EC3	Engine vertical vibration	0.189	0.168	0.078	0.034	0.115	0.044	0.066	0.072
EC4	Front engine mount engine side transverse	0.231	0.249	0.269	0.109	0.185	0.064	0.026	0.170
EC5	Front engine mount engine side axial	0.308	0.097	0.125	0.074	0.122	0.029	0.081	0.326
EC6	Engine truss lower left upper member axial	0.096	0.087	0.067	0.041	0.101	0.012	0.097	0.266
EC7	Engine truss lower left lower member axial	0.012	0.046	0.033	0.052	0.080	0.005	0.122	0.204
EC8	Front engine mount airframe side transverse	0.395	1.153	0.368	0.236	0.461	0.026	0.068	0.100
EC9	Front engine mount airframe side axial	0.104	0.096	0.213	0.032	0.027	0.083	0.308	0.571
EC10	Engine truss upper left member axial	0.077	0.020	0.057	0.026	0.110	0.042	0.073	0.151
EC11	Engine truss upper right member axial	0.039	0.037	0.040	0.020	0.043	0.051	0.028	0.131
EC12	Firewall normal acceleration - mid center	0.325	0.035	0.270	0.198	0.474	0.092	0.246	0.857
EC 13	Firewall normal acceleration - upper center	0.159	0.773	0.167	0.065	0.158	0.018	0.213	0.110
EC14	Engine SPL - firewall mid center	128.3	127.7	100.8	100.1	79.6	108.1	107.9	95.3
AE1	Center windshield pressure excitation	128.4	114.0	115.4	100.6	99.6	89.1	68.7	67.8
AE2	Pilots door center pressure excitation	123.3	113.1	110.8	85.7	98.1	91.3	76.9	74.5
AE3	Copilots door center pressure excitation	123.0	118.3	100.9	81.9	101.1	100.0	93.0	75.3
AE4	On fuselage downstream from engine exhaust	119.7	128.0	108.3	105.1	113.4	89.7	90.2	77.3
AE5	Fuselage vibration downstream from exhaust	0.032	0.026	0.010	0.004	0.018	0.027	0.066	0.034

Table 2.13 Best Rate of Climb – Singular Vector Contributions for Selected Engine Harmonics.

	Reference SPL @ Pilot's Position - AC1	Frequency/Harmonic/Eigenvector							
		78.2dBA	79.4dBA	82.1dBA	68.6dBA	79.8dBA	73.4dBA	82.0dBA	76.5dBA
Loc.	Descriptio n	80/1P/1	120/1F/1	160/2P/1	200/5E/1	240/2F-3P/1	400/5P/1	480/4F-6P/1	520/13E/1
AC5	Dash face right side	0.247	0.138	0.030	0.072	0.043	0.005	0.013	0.045
AC6	Dash face left side	0.041	0.006	0.008	0.005	0.004	0.002	0.001	0.003
AC7	Windshield right side	0.289	0.041	0.203	0.010	0.044	0.012	0.016	0.065
AC8	Windshield left side	0.299	0.070	0.191	0.017	0.086	0.015	0.016	0.060
AC9	Pilot's side window center	0.788	0.061	0.016	0.013	0.066	0.013	0.004	0.011
AC10	Copilot's side window center	0.138	0.249	0.050	0.006	0.041	0.009	0.028	0.006
AC 11	Right rear passenger's window center	0.312	0.161	0.055	0.019	0.120	0.040	0.031	0.037
AC12	Left rear passenger's window center	0.592	0.021	0.111	0.014	0.075	0.011	0.021	0.005
EC1	Engine axial vibration	0.306	0.201	0.061	0.198	0.237	0.031	0.048	0.289
EC2	Engine lateral vibration	0.247	0.078	0.032	0.112	0.113	0.011	0.001	0.133
EC3	Engine vertical vibration	0.232	0.178	0.032	0.030	0.114	0.013	0.037	0.105
EC4	Front engine mount engine side transverse	0.299	0.272	0.133	0.127	0.181	0.026	0.043	0.300
EC5	Front engine mount engine side axial	0.335	0.140	0.041	0.072	0.109	0.010	0.038	0.391
EC6	Engine truss lower left upper member axial	0.072	0.084	0.036	0.046	0.104	0.007	0.052	0.373
EC7	Engine truss lower left lower member axial	0.015	0.053	0.011	0.059	0.089	0.002	0.075	0.329
EC8	Front engine mount airframe side transverse	0.473	1.332	0.249	0.243	0.448	0.010	0.044	0.215
EC9	Front engine mount airframe side axial	0.090	0.097	0.174	0.025	0.038	0.028	0.206	0.883
EC10	Engine truss upper left member axial	0.074	0.044	0.032	0.031	0.108	0.012	0.047	0.264
EC11	Engine truss upper right member axial	0.046	0.056	0.038	0.018	0.045	0.023	0.023	0.157
EC12	Firewall normal acceleration - mid center	0.515	0.178	0.133	0.136	0.459	0.053	0.107	0.856
EC 13	Firewall normal acceleration - upper center	0.124	0.936	0.100	0.105	0.220	0.012	0.112	0.233
EC14	Engine SPL - firewall mid center	131.1	128.7	116.8	96.6	100.8	94.2	103.8	92.9
AE1	Center windshield pressure excitation	129.3	112.7	110.8	102.9	103.8	87.6	81.3	71.7
AE2	Pilots door center pressure excitation	124.1	113.5	110.4	87.8	105.3	94.9	96.3	86.3
AE3	Copilots door center pressure excitation	123.6	119.5	110.4	86.9	104.5	95.6	91.3	72.0
AE4	On fuselage downstream from engine exhaust	120.6	125.8	107.7	111.4	108.6	93.4	84.9	87.4
AE5	Fuselage vibration downstream from exhaust	0.038	0.052	0.029	0.009	0.033	0.022	0.030	0.037

Table 2.14 65% Power Cruise – Singular Vector Contributions for Selected Engine Harmonics.

	Reference SPL @ Pilot's Position - AC1	Frequency/Harmonic/Eigenvector							
		69.5dBA	79.7dBA	79.7dBA	73.4dBA	78.9dBA	77.1dBA	79.5dBA	70.3dBA
Loc.	Description	80/1P/1	120/1F/1	160/2P/1	200/5E/1	240/2F-3P/1	400/5P/1	480/4F-6P/1	520/13E/1
AC5	Dash face right side	0.288	0.129	0.092	0.061	0.026	0.019	0.021	0.026
AC6	Dash face left side	0.064	0.008	0.006	0.001	0.012	0.007	0.004	0.002
AC7	Windshield right side	0.226	0.049	0.155	0.028	0.137	0.017	0.042	0.061
AC8	Windshield left side	0.169	0.058	0.380	0.024	0.085	0.041	0.038	0.055
AC9	Pilot's side window center	1.202	0.058	0.077	0.107	0.079	0.009	0.012	0.022
AC10	Copilot's side window center	0.497	0.292	0.086	0.014	0.099	0.024	0.030	0.027
AC 11	Right rear passenger's window center	0.501	0.176	0.084	0.031	0.108	0.067	0.060	0.022
AC12	Left rear passenger's window center	0.635	0.011	0.062	0.073	0.046	0.012	0.040	0.018
EC1	Engine axial vibration	0.265	0.156	0.100	0.200	0.219	0.107	0.148	0.160
EC2	Engine lateral vibration	0.216	0.071	0.077	0.077	0.091	0.034	0.024	0.065
EC3	Engine vertical vibration	0.195	0.125	0.085	0.042	0.097	0.065	0.114	0.094
EC4	Front engine mount engine side transverse	0.270	0.202	0.235	0.109	0.175	0.038	0.082	0.259
EC5	Front engine mount engine side axial	0.293	0.059	0.052	0.042	0.119	0.049	0.169	0.448
EC6	Engine truss lower left upper member axial	0.108	0.073	0.065	0.040	0.056	0.020	0.208	0.295
EC7	Engine truss lower left lower member axial	0.024	0.037	0.022	0.061	0.059	0.006	0.258	0.225
EC8	Front engine mount airframe side transverse	0.424	0.889	0.409	0.279	0.388	0.039	0.168	0.097
EC9	Front engine mount airframe side axial	0.114	0.079	0.235	0.053	0.009	0.109	0.721	0.428
EC10	Engine truss upper left member axial	0.094	0.022	0.073	0.026	0.062	0.042	0.186	0.283
EC11	Engine truss upper right member axial	0.004	0.023	0.060	0.015	0.066	0.059	0.060	0.213
EC12	Firewall normal acceleration - mid center	0.222	0.045	0.095	0.290	0.514	0.195	0.396	1.177
EC 13	Firewall normal acceleration - upper center	0.169	0.725	0.300	0.095	0.263	0.088	0.273	0.152
EC14	Engine SPL - firewall mid center	125.0	127.6	118.7	97.9	108.1	113.1	111.9	95.1
AE1	Center windshield pressure excitation	131.0	112.4	114.1	100.4	109.1	96.4	95.9	81.2
AE2	Pilots door center pressure excitation	127.0	112.0	108.7	90.8	100.7	94.3	91.1	84.2
AE3	Copilots door center pressure excitation	119.8	118.8	105.8	83.5	87.5	97.7	88.3	65.5
AE4	On fuselage downstream from engine exhaust	118.1	132.6	111.5	106.3	114.1	100.1	106.5	89.8
AE5	Fuselage vibration downstream from exhaust	0.030	0.013	0.031	0.010	0.032	0.028	0.126	0.014

Table 2.15 75% Power Cruise – Singular Vector Contributions for Selected Engine Harmonics.

	Reference SPL @ Pilot's Position - AC1	Frequency/Harmonic/Eigenvector							
		69.9dBA	80.4dBA	76.2dBA	73.1dBA	75.9dBA	79.4dBA	82.8dBA	75.2dBA
Loc.	Description	80/1P/1	120/1F/1	160/2P/1	200/5E/1	240/2F-3P/1	400/5P/1	480/4F-6P/1	520/13E/1
AC5	Dash face right side	0.111	0.143	0.105	0.122	0.078	0.012	0.008	0.061
AC6	Dash face left side	0.074	0.005	0.007	0.005	0.010	0.001	0.003	0.002
AC7	Windshield right side	0.260	0.070	0.418	0.069	0.106	0.012	0.021	0.091
AC8	Windshield left side	0.156	0.041	0.201	0.014	0.095	0.048	0.060	0.069
AC9	Pilot's side window center	1.370	0.098	0.057	0.181	0.290	0.019	0.051	0.030
AC10	Copilot's side window center	0.619	0.265	0.055	0.014	0.145	0.030	0.039	0.060
AC 11	Right rear passenger's window center	0.521	0.147	0.087	0.041	0.082	0.049	0.062	0.033
AC12	Left rear passenger's window center	0.693	0.032	0.045	0.110	0.133	0.002	0.012	0.018
EC1	Engine axial vibration	0.263	0.180	0.116	0.228	0.220	0.125	0.128	0.212
EC2	Engine lateral vibration	0.205	0.105	0.087	0.086	0.093	0.042	0.042	0.105
EC3	Engine vertical vibration	0.193	0.142	0.096	0.050	0.132	0.059	0.088	0.109
EC4	Front engine mount engine side transverse	0.268	0.223	0.260	0.099	0.216	0.069	0.054	0.335
EC5	Front engine mount engine side axial	0.277	0.051	0.054	0.063	0.123	0.050	0.102	0.583
EC6	Engine truss lower left upper member axial	0.105	0.071	0.064	0.054	0.082	0.009	0.172	0.473
EC7	Engine truss lower left lower member axial	0.023	0.038	0.025	0.055	0.079	0.017	0.229	0.341
EC8	Front engine mount airframe side transverse	0.433	0.855	0.493	0.229	0.488	0.055	0.170	0.188
EC9	Front engine mount airframe side axial	0.106	0.082	0.283	0.031	0.036	0.140	0.660	0.836
EC10	Engine truss upper left member axial	0.095	0.013	0.083	0.028	0.073	0.032	0.183	0.384
EC11	Engine truss upper right member axial	0.011	0.027	0.068	0.013	0.054	0.092	0.065	0.245
EC12	Firewall normal acceleration - mid center	0.193	0.059	0.119	0.167	0.519	0.062	0.262	1.556
EC 13	Firewall normal acceleration - upper center	0.178	0.665	0.366	0.125	0.252	0.018	0.319	0.152
EC14	Engine SPL - firewall mid center	122.7	127.2	120.5	93.7	110.4	107.4	113.5	104.7
AE1	Center windshield pressure excitation	131.6	111.5	112.7	107.2	111.1	94.7	95.8	87.9
AE2	Pilots door center pressure excitation	127.2	108.9	101.7	100.1	104.1	95.1	91.4	83.2
AE3	Copilots door center pressure excitation	122.3	117.7	104.5	95.5	107.7	102.3	94.4	62.9
AE4	On fuselage downstream from engine exhaust	118.9	132.8	111.6	107.0	106.8	97.0	98.3	88.4
AE5	Fuselage vibration downstream from exhaust	0.034	0.021	0.026	0.012	0.020	0.021	0.155	0.046

Table 2.16 Cruise Descent – Singular Vector Contributions for Selected Engine Harmonics.

	Reference SPL @ Pilot's Position - AC1	Frequency/Harmonic/Eigenvector							
		67.4dBA	80.1dBA	76.2dBA	70.0dBA	78.7dBA	74.7dBA	78.7dBA	75.9dBA
Loc.	Description	80/1P/1	120/1F/1	160/2P/1	200/5E/1	240/2F-3P/1	400/5P/1	480/4F-6P/1	520/13E/1
AC5	Dash face right side	0.075	0.164	0.062	0.143	0.086	0.025	0.009	0.028
AC6	Dash face left side	0.005	0.005	0.002	0.004	0.007	0.002	0.004	0.001
AC7	Windshield right side	0.201	0.041	0.277	0.048	0.046	0.010	0.080	0.065
AC8	Windshield left side	0.157	0.060	0.267	0.038	0.063	0.044	0.011	0.038
AC9	Pilot's side window center	0.953	0.062	0.096	0.103	0.170	0.025	0.005	0.010
AC10	Copilot's side window center	0.487	0.251	0.092	0.021	0.136	0.013	0.043	0.021
AC 11	Right rear passenger's window center	0.227	0.221	0.057	0.016	0.061	0.020	0.028	0.029
AC12	Left rear passenger's window center	0.552	0.036	0.077	0.089	0.086	0.024	0.041	0.018
EC1	Engine axial vibration	0.238	0.125	0.088	0.172	0.193	0.090	0.135	0.162
EC2	Engine lateral vibration	0.215	0.072	0.064	0.085	0.080	0.041	0.023	0.057
EC3	Engine vertical vibration	0.214	0.107	0.090	0.025	0.081	0.053	0.086	0.124
EC4	Front engine mount engine side transverse	0.258	0.176	0.234	0.157	0.159	0.024	0.091	0.234
EC5	Front engine mount engine side axial	0.252	0.047	0.086	0.055	0.142	0.022	0.138	0.426
EC6	Engine truss lower left upper member axial	0.040	0.019	0.021	0.038	0.081	0.014	0.168	0.237
EC7	Engine truss lower left lower member axial	0.029	0.037	0.010	0.068	0.068	0.010	0.214	0.221
EC8	Front engine mount airframe side transverse	0.412	0.703	0.394	0.332	0.387	0.020	0.162	0.178
EC9	Front engine mount airframe side axial	0.128	0.068	0.241	0.064	0.018	0.077	0.644	0.341
EC10	Engine truss upper left member axial	0.011	0.007	0.061	0.023	0.085	0.048	0.201	0.326
EC11	Engine truss upper right member axial	0.049	0.011	0.045	0.026	0.004	0.029	0.072	0.231
EC12	Firewall normal acceleration - mid center	0.141	0.411	0.116	0.093	0.168	0.320	0.304	0.700
EC 13	Firewall normal acceleration - upper center	0.010	0.579	0.043	0.054	0.128	0.062	0.230	0.420
EC14	Engine SPL - firewall mid center	118.5	126.2	117.3	96.9	104.4	109.7	111.6	92.0
AE1	Center windshield pressure excitation	130.9	99.9	117.8	103.2	110.0	103.8	94.6	90.7
AE2	Pilots door center pressure excitation	124.6	105.9	112.6	99.3	87.6	92.8	86.1	87.1
AE3	Copilots door center pressure excitation	125.0	117.1	106.4	98.1	100.1	90.1	79.6	44.9
AE4	On fuselage downstream from engine exhaust	124.3	129.7	119.3	107.3	122.0	100.1	98.2	99.3
AE5	Fuselage vibration downstream from exhaust	0.009	0.024	0.019	0.002	0.015	0.035	0.089	0.009

**Table 2.17 Brute Force CRA Analysis – All Auxiliary Parameters Active
Cruise at 75% Power.**

Spectral Tone	Cabin Sensor	In-Flight Levels dBA	Predicted Responses - dBA				
			Combined	AB-Prop Contribution	AB-Exhst Contribution	AB-Eng Contribution	SB-Eng Contribution
80Hz 1P	AC1	69.9	80.0	88.3	0	87.4	78.4
	AC2	70.4	80.2	86.4	0	88.0	79.9
	AC3	83.3	80.3	84.3	0	80.2	76
	AC4	82.6	75.6	81.8	0	79.9	80.8
120 Hz 1F	AC1	80.4	94.7	0	90.8	97.7	70.8
	AC2	78.1	95.7	0	90.9	97.8	75.6
	AC3	81.9	95.0	0	96.4	91.6	73.7
	AC4	76.0	93.8	0	85.5	91.0	68.4
160 Hz 2P	AC1	76.2	80.8	60.3	0	82.1	59.9
	AC2	82.8	72.0	65.5	0	73.5	54.2
	AC3	81.1	81.1	68.3	0	83.1	56.7
	AC4	79.5	78.3	69.9	0	76.1	56.7
240 Hz 2F-3P	AC1	75.9	85.3	77.1	65.6	87.0	67.9
	AC2	69.5	83.0	74.7	58.1	82.6	67.1
	AC3	85.6	86.3	85.3	62.2	79.3	71.2
	AC4	75.4	85.5	86.0	61.4	78.0	77.5
400 Hz 5P	AC1	79.4	68.7	60.7	0	69.4	40.2
	AC2	80.5	39.8	52.1	0	54.1	59.3
	AC3	64.8	69.0	63.2	0	64.7	47.3
	AC4	66.4	70.1	41.5	0	67.8	59.8
480 Hz 4F-6P	AC1	82.8	80.4	70.3	61.1	77.0	57.2
	AC2	81.1	85.8	51.3	58.6	85.7	55.5
	AC3	72.2	81.9	60.0	65.6	79.2	56.4
	AC4	74.8	67.2	63.3	62.9	70.6	52.3

Table 2.18 Primary and Secondary Auxiliary Response Parameter Selection.

Loc.	Description	AB Prop	AB Exhst	AB Eng	SB Eng
	Reference Signal				
	Description				
AC5	Dash face right side	S	S	S	S
AC6	Dash face left side	S	S	S	S
AC7	Windshield right side	S	S	S	S
AC8	Windshield left side	S	S	S	S
AC9	Pilot's side window center	S	S	S	S
AC10	Copilot's side window center	S	S	S	S
AC 11	Right rear passenger's window center	S	S	S	S
AC12	Left rear passenger's window center	S	S	S	S
EC1	Engine axial vibration	--	--	--	P
EC2	Engine lateral vibration	--	--	--	P
EC3	Engine vertical vibration	--	--	--	P
EC4	Front engine mount engine side transverse	--	--	--	S
EC5	Front engine mount engine side axial	--	--	--	S
EC6	Engine truss lower left upper member axial	--	--	--	S
EC7	Engine truss lower left lower member axial	--	--	--	S
EC8	Front engine mount airframe side transverse	--	--	--	S
EC9	Front engine mount airframe side axial	--	--	--	S
EC10	Engine truss upper left member axial	--	--	--	S
EC11	Engine truss upper right member axial	--	--	--	S
EC12	Firewall normal acceleration - mid center	S	S	S	S
EC 13	Firewall normal acceleration - upper center	S	S	S	S
EC14	Engine SPL - firewall mid center	S	S	P	S
AE1	Center windshield pressure excitation	P	S	S	--
AE2	Pilots door center pressure excitation	S	S	S	--
AE3	Copilots door center pressure excitation	S	S	S	--
AE4	Fuselage pressure downstream from exhaust	--	P	S	--
AE5	Fuselage vibration downstream from exhaust	--	S	S	S

**Table 2.19 CRA Analysis – Primary and Secondary Auxiliary Parameters Active
Cruise at 75% Power.**

Spectral Tone	Cabin Sensor	In-Flight Levels dBA	Predicted Responses - dBA				
			AB Combined	AB-Prop Contribution	AB-Exhst Contribution	AB-Eng Contribution	SB-Eng Removed
80Hz 1P	AC1	69.9	72.4	92.3	0	91.2	65.4
	AC2	70.4	76.6	90.5	0	91.9	66.9
	AC3	83.3	88.0	88.3	0	84.1	63.0
	AC4	82.6	78.2	85.8	0	83.8	67.8
120 Hz 1F	AC1	80.4	95.2	0	90.8	97.7	54.1
	AC2	78.1	96.6	0	90.9	97.8	58.9
	AC3	81.9	95.2	0	96.4	91.6	57.0
	AC4	76.0	94.1	0	85.5	91.0	51.8
160 Hz 2P	AC1	76.2	81.8	62.3	0	82.6	50.1
	AC2	82.8	72.1	67.4	0	74.0	44.5
	AC3	81.1	81.6	70.2	0	83.5	46.9
	AC4	79.5	79.8	71.9	0	76.6	46.9
240 Hz 2F-3P	AC1	75.9	87.0	77.3	71.0	86.8	56.6
	AC2	69.5	83.6	74.9	63.5	82.5	55.8
	AC3	85.6	88.0	85.5	67.6	79.2	59.8
	AC4	75.4	81.1	86.1	66.8	77.9	66.1
400 Hz 5P	AC1	79.4	68.1	57.2	0	69.2	28.7
	AC2	80.5	56.5	48.6	0	53.9	47.8
	AC3	64.8	67.4	59.7	0	64.5	35.8
	AC4	66.4	68.4	38.1	0	67.7	48.3
480 Hz 4F-6P	AC1	82.8	80.9	71.9	55.6	77.0	46.4
	AC2	81.1	85.8	52.9	53.0	85.7	44.6
	AC3	72.2	81.0	61.6	60.1	79.2	45.6
	AC4	74.8	70.3	64.9	57.4	70.6	41.5

Table 2.20 CRA Analysis – Structure-Borne Components Removed
Cruise at 75% Power.

Spectral Tone	Cabin Sensor	In-Flight Levels dBA	Predicted Responses - dBA				
			AB Combined	AB-Prop Contribution	AB-Exhst Contribution	AB-Eng Contribution	SB-Eng Removed
80Hz 1P	AC1	69.9	74.6	92.3	0	91.2	58.3
	AC2	70.4	77.1	90.5	0	91.9	59.8
	AC3	83.3	88.5	88.3	0	84.1	55.8
	AC4	82.6	80.5	85.8	0	83.8	60.7
120 Hz 1F	AC1	80.4	95.2	0	90.8	97.7	61.7
	AC2	78.1	96.5	0	90.9	97.8	66.4
	AC3	81.9	95.2	0	96.4	91.6	64.5
	AC4	76.0	94.0	0	85.5	91.0	59.3
160 Hz 2P	AC1	76.2	81.9	62.3	0	82.6	48.1
	AC2	82.8	71.8	67.4	0	74.0	42.4
	AC3	81.1	81.5	70.2	0	83.5	44.8
	AC4	79.5	80.0	71.9	0	76.6	44.8
240 Hz 2F-3P	AC1	75.9	87.2	77.3	71.0	86.8	42.5
	AC2	69.5	83.7	74.9	63.5	82.5	41.7
	AC3	85.6	88.1	85.5	67.6	79.2	45.8
	AC4	75.4	80.5	86.1	66.8	77.9	52.1
400 Hz 5P	AC1	79.4	68.1	57.2	0	69.2	29.5
	AC2	80.5	57.6	48.6	0	53.9	48.7
	AC3	64.8	67.3	59.7	0	64.5	36.7
	AC4	66.4	67.6	38.1	0	67.7	49.2
480 Hz 4F-6P	AC1	82.8	80.8	71.9	55.6	77.0	51.2
	AC2	81.1	85.8	52.9	53.0	85.7	49.4
	AC3	72.2	80.8	61.6	60.1	79.2	50.3
	AC4	74.8	70.6	64.9	57.4	70.6	46.3

Table 2.21 CRA Analysis – Structure-Borne Components Removed – Microphone Auxiliary Parameters Only – Cruise at 75% Power.

Spectral Tone	Cabin Sensor	In-Flight Levels dBA	Predicted Responses - dBA				
			AB Combined	AB-Prop Contribution	AB-Exhst Contribution	AB-Eng Contribution	SB-Eng Removed
80Hz 1P	AC1	69.9	74.6	**92.3**	0	**91.2**	58.3
	AC2	70.4	77.1	**90.5**	0	**91.9**	59.8
	AC3	83.3	88.5	**88.3**	0	**84.1**	55.8
	AC4	82.6	80.5	**85.8**	0	**83.8**	60.7
120 Hz 1F	AC1	80.4	95.2	0	90.8	97.7	61.7
	AC2	78.1	96.5	0	90.9	97.8	66.4
	AC3	81.9	95.2	0	96.4	91.6	64.5
	AC4	76.0	94.0	0	85.5	91.0	59.3
160 Hz 2P	AC1	76.2	81.9	62.3	0	**82.6**	48.1
	AC2	82.8	71.8	67.4	0	**74.0**	42.4
	AC3	81.1	81.5	70.2	0	**83.5**	44.8
	AC4	79.5	80.0	71.9	0	**76.6**	44.8
240 Hz 2F-3P	AC1	75.9	87.2	77.3	71.0	86.8	42.5
	AC2	69.5	83.7	74.9	63.5	82.5	41.7
	AC3	85.6	88.1	85.5	67.6	79.2	45.8
	AC4	75.4	80.5	86.1	66.8	77.9	52.1
400 Hz 5P	AC1	79.4	68.1	57.2	0	**69.2**	29.5
	AC2	80.5	57.6	48.6	0	**53.9**	48.7
	AC3	64.8	67.3	59.7	0	**64.5**	36.7
	AC4	66.4	67.6	38.1	0	**67.7**	49.2
480 Hz 4F-6P	AC1	82.8	80.8	71.9	55.6	**77.0**	51.2
	AC2	81.1	85.8	52.9	53	**85.7**	49.4
	AC3	72.2	80.8	61.6	60.1	**79.2**	50.3
	AC4	74.8	70.6	64.9	57.4	**70.6**	46.3

Table 2.22 CRA Analysis – Structure-Borne Components Removed - Accelerometer Auxiliary Parameters Only – Cruise at 75% Power.

Spectral Tone	Cabin Sensor	In-Flight Levels dBA	Predicted Responses - dBA				
			AB Combined	AB-Prop Contribution	AB-Exhst Contribution	AB-Eng Contribution	SB-Eng Removed
80Hz 1P	AC1	69.9	79.6	79.4	0	55.0	58.3
	AC2	70.4	77.8	77.6	0	55.6	59.8
	AC3	83.3	75.2	75.5	0	47.8	55.8
	AC4	82.6	72.8	72.9	0	47.5	60.7
120 Hz 1F	AC1	80.4	82.3	0	73.3	80.2	61.7
	AC2	78.1	81.8	0	73.4	80.3	66.4
	AC3	81.9	80.8	0	78.9	74.1	64.5
	AC4	76.0	68.9	0	68.1	73.5	59.3
160 Hz 2P	AC1	76.2	53.0	63.1	0	64.1	48.1
	AC2	82.8	66.1	68.3	0	55.5	42.4
	AC3	81.1	70.2	71.1	0	65.0	44.8
	AC4	79.5	72.8	72.7	0	58.0	44.8
240 Hz 2F-3P	AC1	75.9	85.6	74.8	84.6	75.9	42.5
	AC2	69.5	70.6	72.4	77.1	71.6	41.7
	AC3	85.6	87.8	83.0	81.1	68.3	45.8
	AC4	75.4	85.1	83.6	80.4	67.0	52.1
400 Hz 5P	AC1	79.4	63.3	62.6	0	49.9	29.5
	AC2	80.5	53.0	54.0	0	34.6	48.7
	AC3	64.8	65.0	65.1	0	45.2	36.7
	AC4	66.4	49.7	43.4	0	48.4	49.2
480 Hz 4F-6P	AC1	82.8	75.7	77.5	61.3	58.0	51.2
	AC2	81.1	69.2	58.6	58.7	66.7	49.4
	AC3	72.2	70.3	67.2	65.8	60.2	50.3
	AC4	74.8	69.4	70.5	63.1	51.6	46.3

Table 2.23 Combined CRA Analysis – Cruise at 75% Power.

Spectral Tone	Cabin Sensor	In-Flight Levels dBA	Predicted Responses - dBA				
			AB Combined	AB-Prop Contribution	AB-Exhst Contribution	AB-Eng Contribution	SB-Eng Removed
80Hz 1P	AC1	69.9	74.6	**92.3**	0	**91.2**	58.3
	AC2	70.4	77.1	**90.5**	0	**91.9**	59.8
	AC3	83.3	88.5	**88.3**	0	**84.1**	55.8
	AC4	82.6	80.5	**85.8**	0	**83.8**	60.7
120 Hz 1F	AC1	80.4	82.3	0	**73.3**	**80.2**	61.7
	AC2	78.1	81.8	0	**73.4**	**80.3**	66.4
	AC3	81.9	80.8	0	**78.9**	**74.1**	64.5
	AC4	76.0	68.9	0	**68.1**	**73.5**	59.3
160 Hz 2P	AC1	76.2	81.9	62.3	0	**82.6**	48.1
	AC2	82.8	71.8	67.4	0	**74.0**	42.4
	AC3	81.1	81.5	70.2	0	**83.5**	44.8
	AC4	79.5	80.0	71.9	0	**76.6**	44.8
240 Hz 2F-3P	AC1	75.9	85.6	**74.8**	84.6	75.9	42.5
	AC2	69.5	70.6	**72.4**	77.1	71.6	41.7
	AC3	85.6	87.8	**83.0**	81.1	68.3	45.8
	AC4	75.4	85.1	**83.6**	80.4	67.0	52.1
400 Hz 5P	AC1	79.4	68.1	57.2	0	**69.2**	29.5
	AC2	80.5	57.6	48.6	0	**53.9**	48.7
	AC3	64.8	67.3	59.7	0	**64.5**	36.7
	AC4	66.4	67.6	38.1	0	**67.7**	49.2
480 Hz 4F-6P	AC1	82.8	80.8	71.9	55.6	**77.0**	51.2
	AC2	81.1	85.8	52.9	53	**85.7**	49.4
	AC3	72.2	80.8	61.6	60.1	**79.2**	50.3
	AC4	74.8	70.6	64.9	57.4	**70.6**	46.3

**Table 2.24 Independent AB Propeller and Engine Predictions –
Cruise at 75% Power.**

Spectral Tone	Cabin Sensor	In-Flight Levels dBA	Predicted Responses - dBA			
			AB Combined	AB-Prop Only	AB-Eng Only	SB-Eng Removed
80Hz 1P	AC1	69.9	74.6	76.7	74.9	58.3
	AC2	70.4	77.1	74.9	75.6	59.8
	AC3	83.3	88.5	72.8	67.7	55.8
	AC4	82.6	80.5	70.2	67.5	60.7

Table 2.25 Combined CRA Analysis – Cruise at 65% Power.

Spectral Tone	Cabin Sensor	In-Flight Levels dBA	Predicted Responses - dBA				
			AB Combined	AB-Prop Contribution	AB-Exhst Contribution	AB-Eng Contribution	SB-Eng Removed
80Hz 1P	AC1	69.5	69.6	**91.3**	0	**91.3**	58.3
	AC2	69.9	80.9	**89.4**	0	**92.0**	59.8
	AC3	78.8	87.8	**87.3**	0	**84.2**	55.9
	AC4	77.9	79.8	**84.8**	0	**83.9**	60.7
120 Hz 1F	AC1	79.7	82.6	0	**74.1**	**79.9**	61.8
	AC2	77.2	82.1	0	**74.1**	**80.0**	66.5
	AC3	82.1	81.6	0	**79.7**	**73.8**	64.6
	AC4	76.6	69.0	0	**68.8**	**73.2**	59.4
160 Hz 2P	AC1	79.7	81.7	**66.9**	0	**82.8**	46.3
	AC2	80.5	72.4	**72.1**	0	**74.2**	40.7
	AC3	77.4	80.0	**74.8**	0	**83.7**	43.1
	AC4	78.5	82.1	**76.5**	0	**76.7**	43.1
240 Hz 2F-3P	AC1	78.9	82.6	**67.7**	**80.6**	**72.4**	43.8
	AC2	74.3	62.6	**65.3**	**73.1**	**68.1**	43
	AC3	79.8	83.6	**75.9**	**77.2**	**64.8**	47
	AC4	73.1	75.4	**76.5**	**76.4**	**63.4**	53.3
400 Hz 5P	AC1	77.1	59.4	**57.6**	0	**61.9**	31.3
	AC2	78.5	48.1	**49.1**	0	**46.7**	50.5
	AC3	65.5	64.3	**60.1**	0	**57.3**	38.5
	AC4	68.8	59.8	**38.5**	0	**60.4**	51
480 Hz 4F-6P	AC1	79.5	81.9	**81.7**	59.8	61.0	57.7
	AC2	71.9	62.0	**62.7**	57.2	69.7	55.9
	AC3	78.2	74.3	**71.4**	64.3	63.2	56.8
	AC4	73.0	73.8	**74.7**	61.6	54.6	52.8

Table 2.26 Combined CRA Analysis – Best Rate of Climb.

Spectral Tone	Cabin Sensor	In-Flight Levels dBA	Predicted Responses - dBA				
			AB Combined	AB-Prop Contribution	AB-Exhst Contribution	AB-Eng Contribution	SB-Eng Removed
80Hz 1P	AC1	78.2	78.5	**78.3**	0	55.1	59.9
	AC2	75.7	76.8	**76.4**	0	55.8	61.4
	AC3	77.6	74.7	**74.3**	0	48	57.5
	AC4	80.3	72.2	**71.7**	0	47.7	62.3
120 Hz 1F	AC1	79.4	84.7	0	**72.6**	**82.5**	65.3
	AC2	77.1	84.5	0	**72.6**	**82.6**	70
	AC3	82.4	82.7	0	**78.1**	**76.4**	68.1
	AC4	76.8	74.8	0	**67.3**	**75.8**	62.9
160 Hz 2P	AC1	82.1	68.2	**66.2**	0	**69.6**	42.4
	AC2	73.2	69.5	**71.4**	0	**61.0**	36.8
	AC3	79.4	76.7	**74.1**	0	**70.5**	39.2
	AC4	70.5	74.3	**75.8**	0	**63.5**	39.2
240 Hz 2F-3P	AC1	79.8	80.1	**67.9**	**77.8**	**74.7**	46.8
	AC2	81.8	63.1	**65.5**	**70.3**	**70.4**	45.9
	AC3	83.8	80	**76.1**	**74.4**	**67.1**	50
	AC4	79.8	80.2	**76.8**	**73.6**	**65.8**	56.3
480 Hz 4F-6P	AC1	82.0	60.8	61.3	29.0	**66.6**	47.6
	AC2	81.6	75.3	42.4	26.5	**75.4**	45.9
	AC3	72.8	67.8	51.0	33.5	**68.8**	46.8
	AC4	74.9	61.3	54.3	30.9	**60.2**	42.8

Table 2.27 Combined CRA Analysis – Normal Rate of Climb.

Spectral Tone	Cabin Sensor	In-Flight Levels dBA	Predicted Responses - dBA				
			AB Combined	AB-Prop Contribution	AB-Exhst Contribution	AB-Eng Contribution	SB-Eng Removed
80Hz 1P	AC1	73.1	81.9	**80.2**	0	**83.6**	58.8
	AC2	74.8	82.8	**78.3**	0	**84.2**	60.3
	AC3	75.2	81.3	**76.2**	0	**76.4**	56.4
	AC4	76.9	77.7	**73.7**	0	**76.2**	61.2
120 Hz 1F	AC1	79.2	83.3	0	**72.3**	**80.7**	64.1
	AC2	76.8	83.1	0	**72.3**	**80.8**	68.9
	AC3	83.9	81.8	0	**77.8**	**74.6**	67.0
	AC4	79.0	73.2	0	**67.0**	**74.0**	61.7
160 Hz 2P	AC1	84.6	73.5	**67.4**	0	**76.7**	46.1
	AC2	82.0	68.4	**72.6**	0	**68.1**	40.4
	AC3	79.3	71.2	**75.3**	0	**77.6**	42.9
	AC4	77.4	79.5	**77.0**	0	**70.6**	42.8
240 Hz 2F-3P	AC1	80.5	80.4	**66.2**	**82.2**	**73.1**	47.9
	AC2	82.0	76.5	**63.8**	**74.7**	**68.8**	47.1
	AC3	85.2	81.7	**74.4**	**78.7**	**65.4**	51.1
	AC4	81.8	77.7	**75.1**	**780**	**64.1**	57.5
480 Hz 4F-6P	AC1	77.2	72.4	60.2	39.4	**70.9**	51.4
	AC2	77.8	79.6	41.2	36.8	**79.7**	49.7
	AC3	74.4	72.7	49.9	43.9	**73.1**	50.6
	AC4	72.8	67.0	53.2	41.2	**64.5**	46.5

Table 2.28 Combined CRA Analysis – Cruise Descent.

Spectral Tone	Cabin Sensor	In-Flight Levels dBA	Predicted Responses - dBA				
			AB Combined	AB-Prop Contribution	AB-Exhst Contribution	AB-Eng Contribution	SB-Eng Removed
80Hz 1P	AC1	67.4	77.5	**78.1**	0	64.7	58.5
	AC2	71.1	75.4	**76.2**	0	65.4	60.0
	AC3	78.5	72.8	**74.1**	0	57.5	56.0
	AC4	76.4	70.2	**71.6**	0	57.3	60.9
120 Hz 1F	AC1	80.1	80.6	0	**73.2**	**78.3**	59.7
	AC2	78.9	80.0	0	**73.2**	**78.4**	64.4
	AC3	81.0	79.9	0	**78.7**	**72.2**	62.5
	AC4	76.8	65.0	0	**67.9**	**71.6**	57.3
160 Hz 2P	AC1	76.2	79.8	**71.9**	0	**82.7**	45.5
	AC2	69.1	66.7	**77.1**	0	**74.1**	39.9
	AC3	74.7	82.4	**79.9**	0	**83.6**	42.3
	AC4	75.4	83.0	**81.5**	0	**76.7**	42.3
240 Hz 2F-3P	AC1	78.7	75.2	**67.1**	**76.8**	62.5	42.5
	AC2	71.1	68.2	**64.7**	**69.3**	58.2	41.7
	AC3	79.2	80.4	**75.3**	**73.4**	54.9	45.7
	AC4	79.1	76.5	**76.0**	**72.6**	53.6	52.0
480 Hz 4F-6P	AC1	78.7	76.6	**75.3**	56.8	**67.8**	57.2
	AC2	73.9	76.1	**56.3**	54.2	**76.5**	55.4
	AC3	73.5	65.7	**65.0**	61.3	**70.0**	56.4
	AC4	68.5	72.4	**68.3**	58.6	**61.4**	52.3

Table 2.29 Summary of Significant Airborne Noise Sources.

Spectral Tone	Flight Condition	Airborne Source		
		Propeller	Exhaust	Engine
80 Hz 1P	C75	√		√
	C65	√		√
	BRC	√		
	NCL	√		√
	DES	√		
120 Hz 1F	C75		√	√
	C65		√	√
	BRC		√	√
	NCL		√	√
	DES		√	√
160 Hz 2P	C75			√
	C65	√		√
	BRC	√		√
	NCL	√		√
	DES	√		√
240 Hz 2F-3P	C75	√	√	√
	C65	√	√	√
	BRC	√	√	√
	NCL	√	√	√
	DES	√	√	
400 Hz 5P	C75			√
	C65	√		√
	BRC			
	NCL			
	DES			
480 Hz 4F-6P	C75			√
	C65	√		
	BRC			√
	NCL			√
	DES	√		√

Figure 2.1 Cessna Model 182E Test Aircraft.

■ **Accelerometer**　　　● **Microphone**
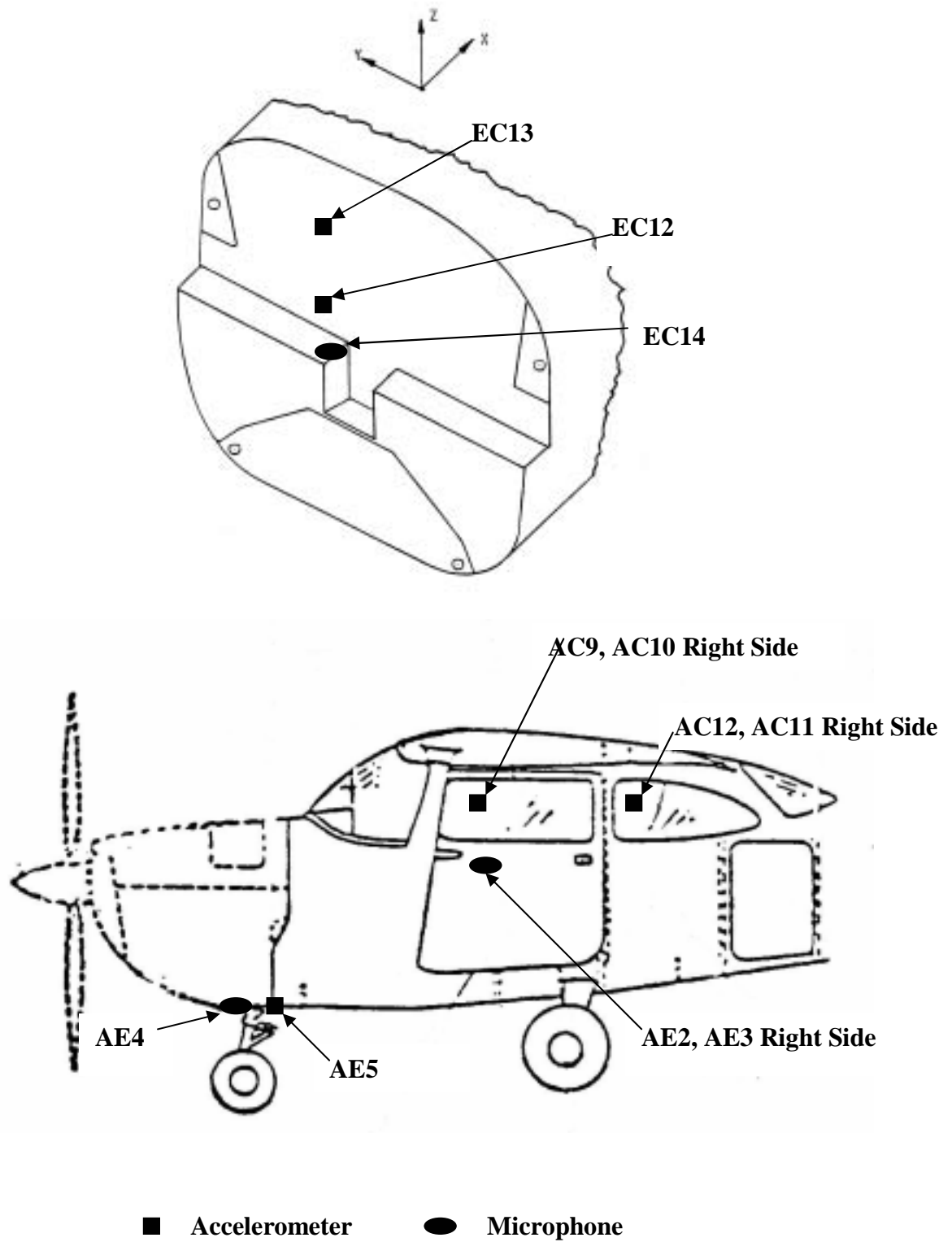
Figure 2.2 Instrumentation Layout.
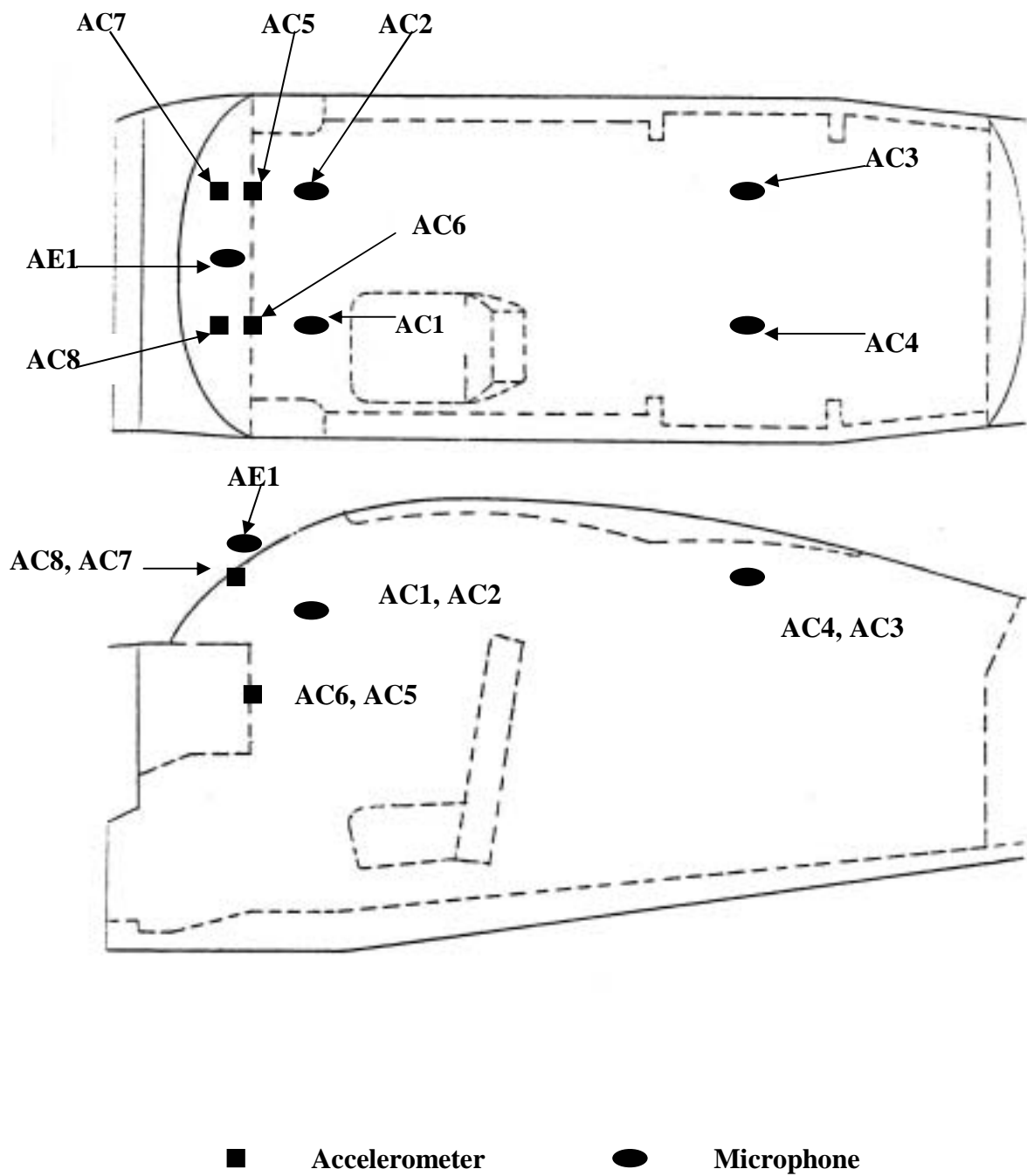
Figure 2.2 (continued) Instrumentation Layout.
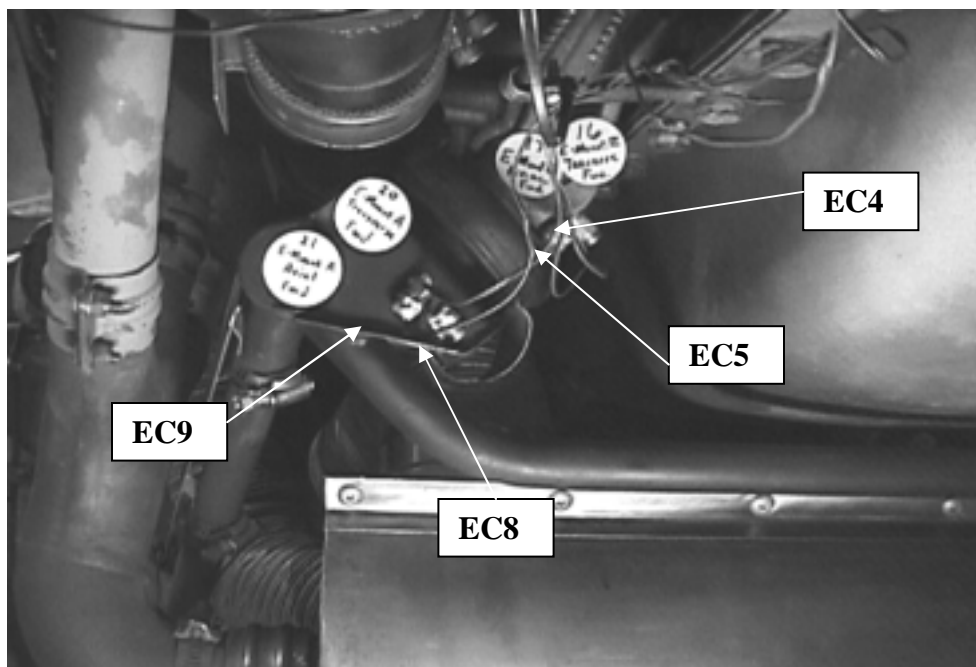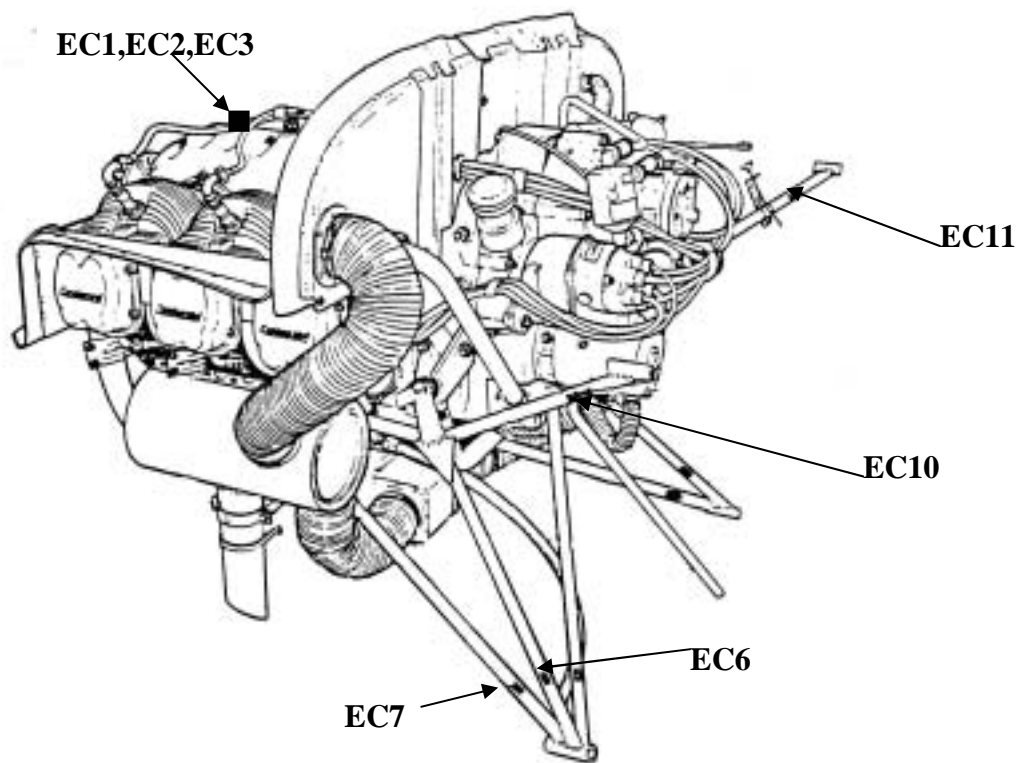
Figure 2.2 (continued) Instrumentation Layout.
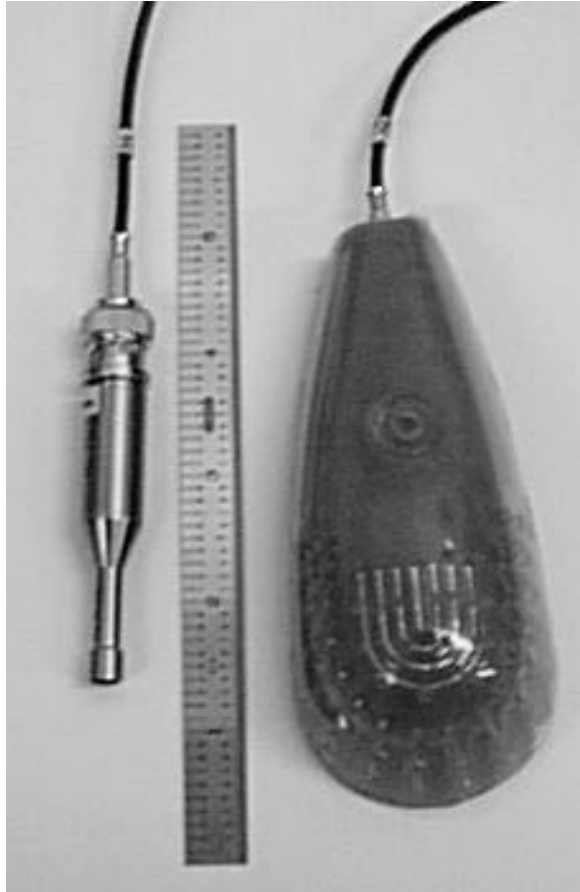
Figure 2.3 External Microphone Mounting Arrangement.

Cessna 182E 75% Power Cruise
Cabin Microphone AC1

Legend:
AC1-Lin: 104.46 dB
AC1-Awt: 92.93 dBA

a) Pilot's Position

Cessna 182E 75% Power Cruise
Cabin Microphone AC2

Legend:
AC2-Lin: 104.66 dB
AC2-Awt: 93.18 dBA
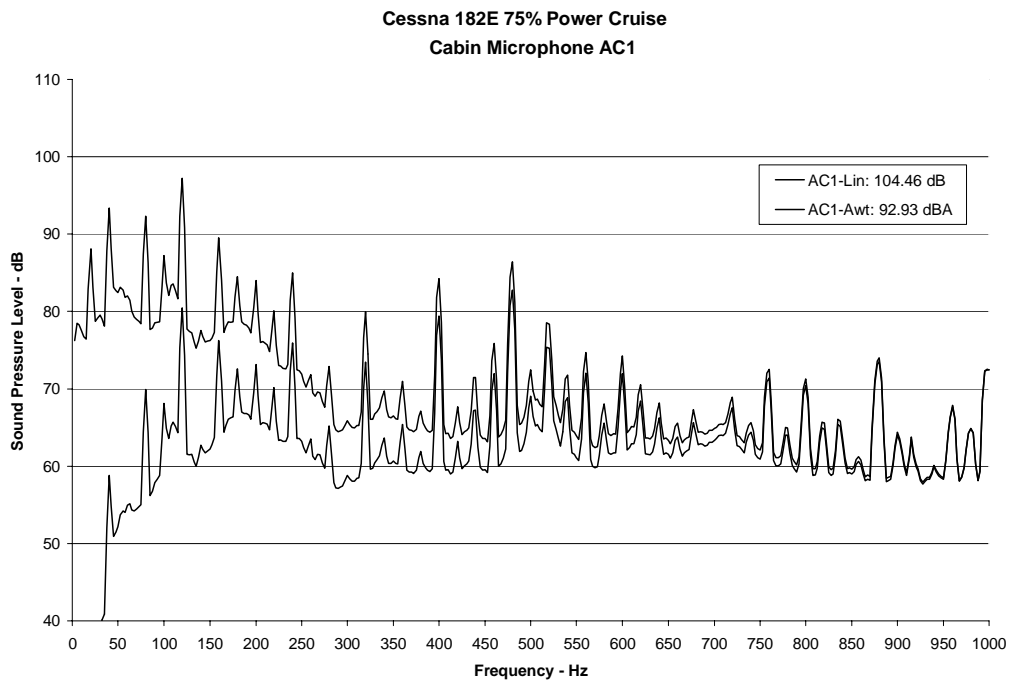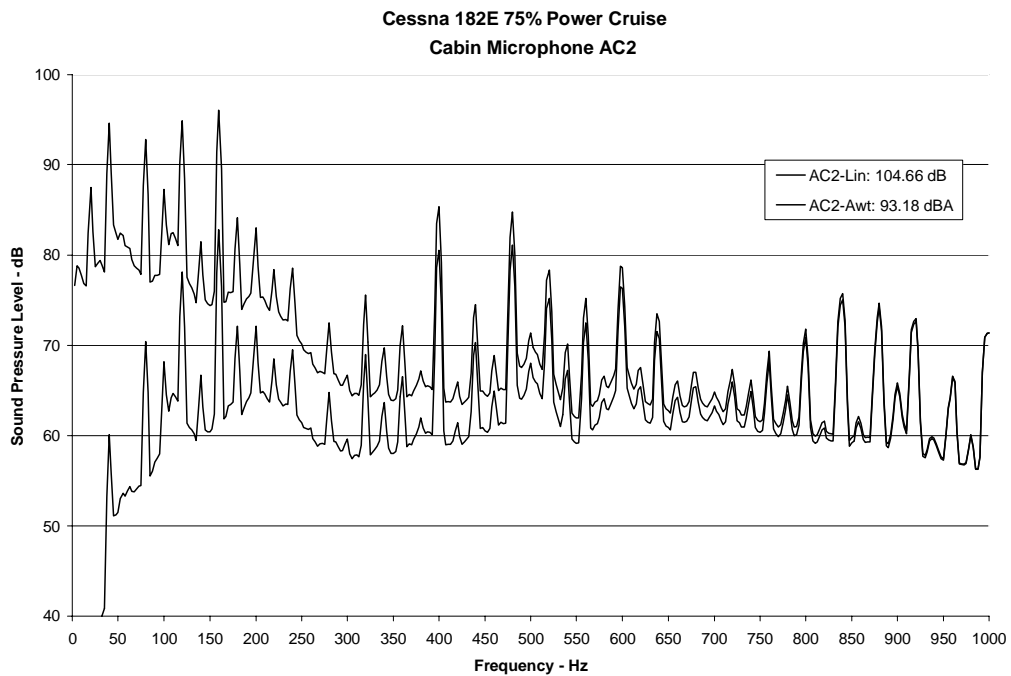
b) Copilot's Position

Figure 2.4 Forward Cabin SPL Spectra.

Cessna 182E 75% Power Cruise
Cabin Microphone AC3

a) Right Passenger

Cessna 182E 75% Power Cruise
Cabin Microphone AC4
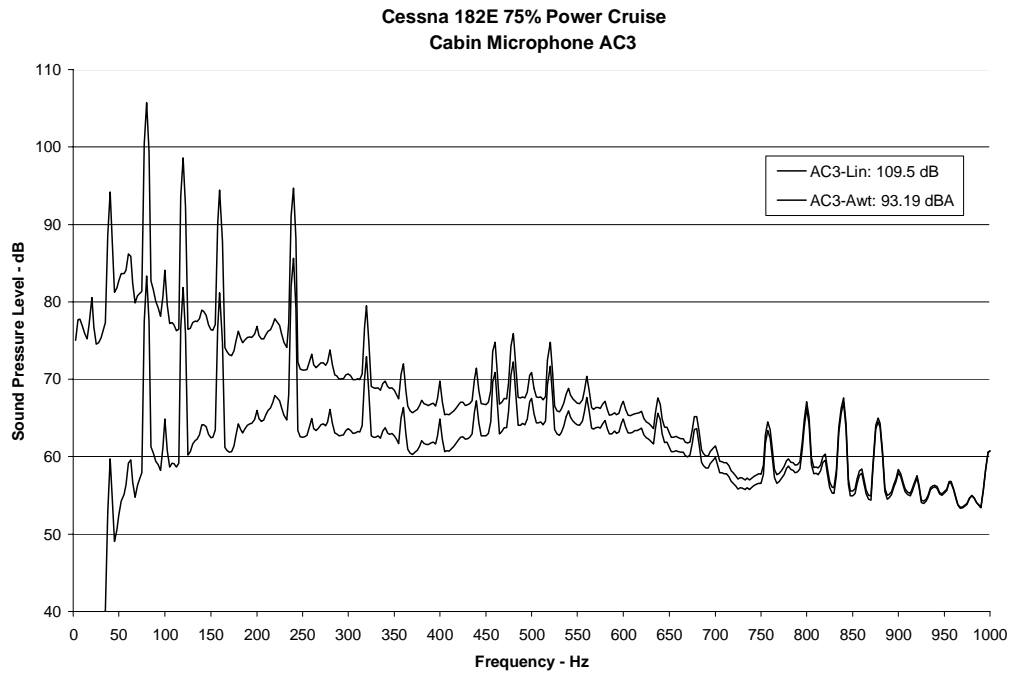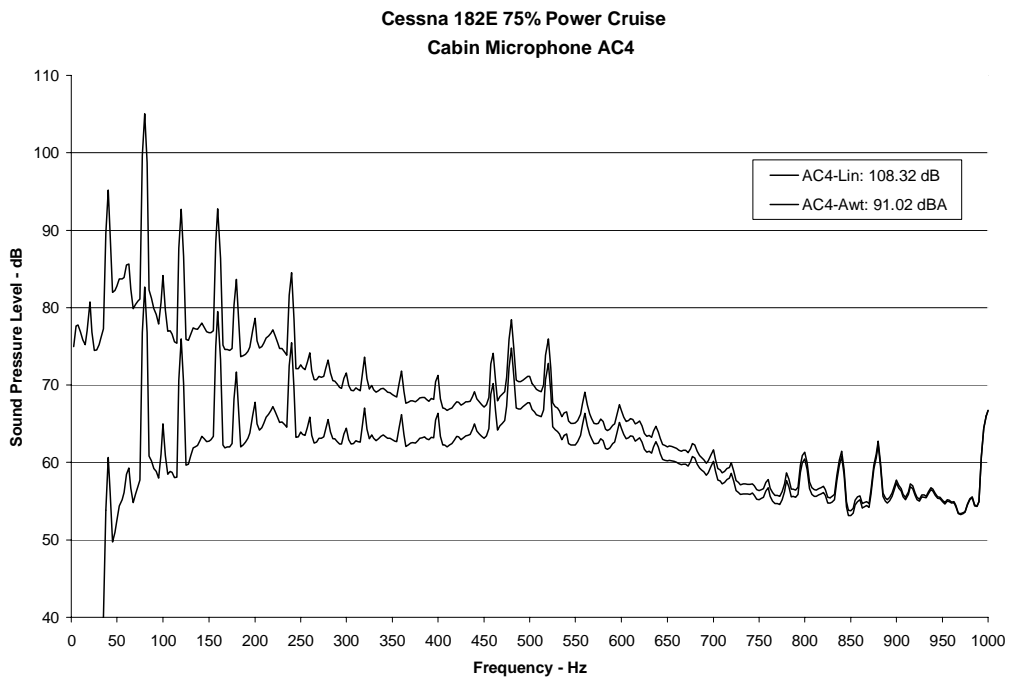
b) Left Passenger

Figure 2.5 Aft Cabin SPL Spectra.

Cessna 182E 75% Power Cruise

Cabin Accelerometer AC5

a) Right Side

Cessna 182E 75% Power Cruise

Cabin Accelerometer AC6
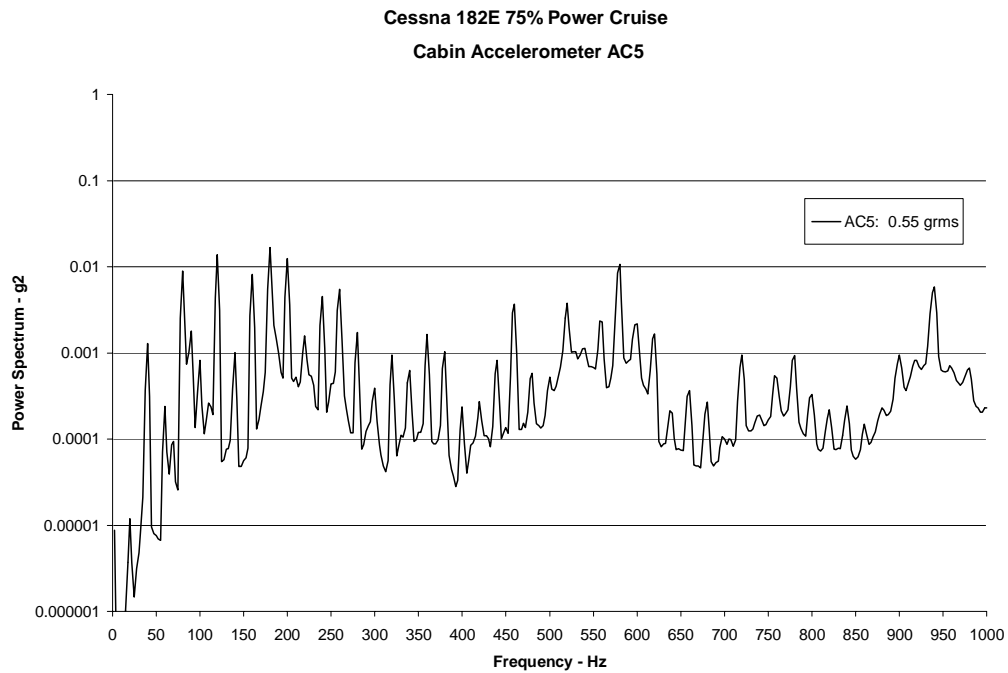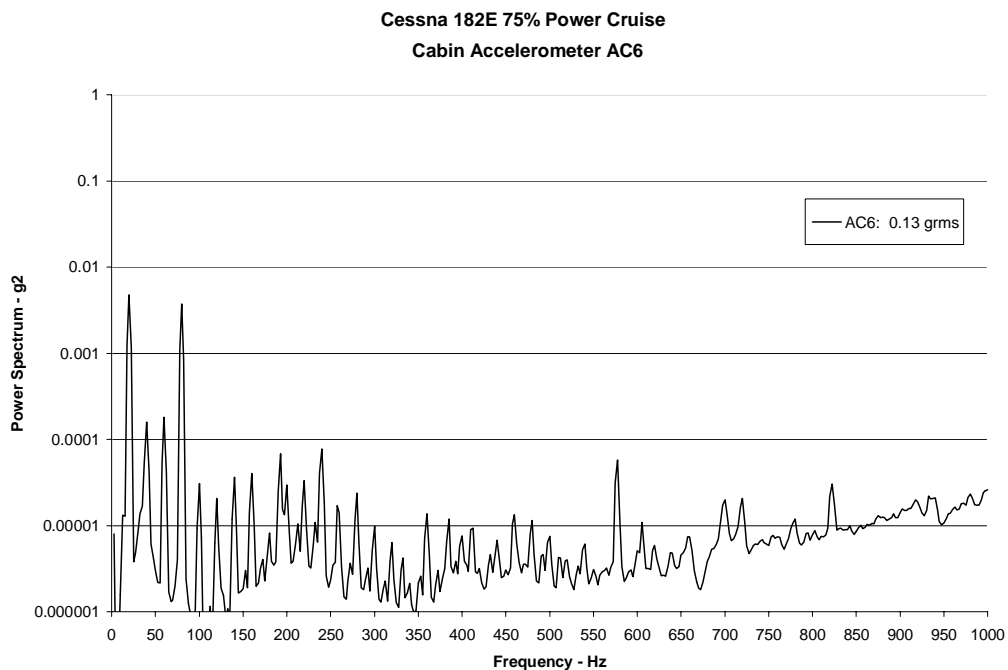
b) Left Side

Figure 2.6 Instrument Panel Vibration Spectra.

Cessna 182E 75% Power Cruise

Cabin Accelerometer AC7

a) **Right Side**

Cessna 182E 75% Power Cruise

Cabin Accelerometer AC8
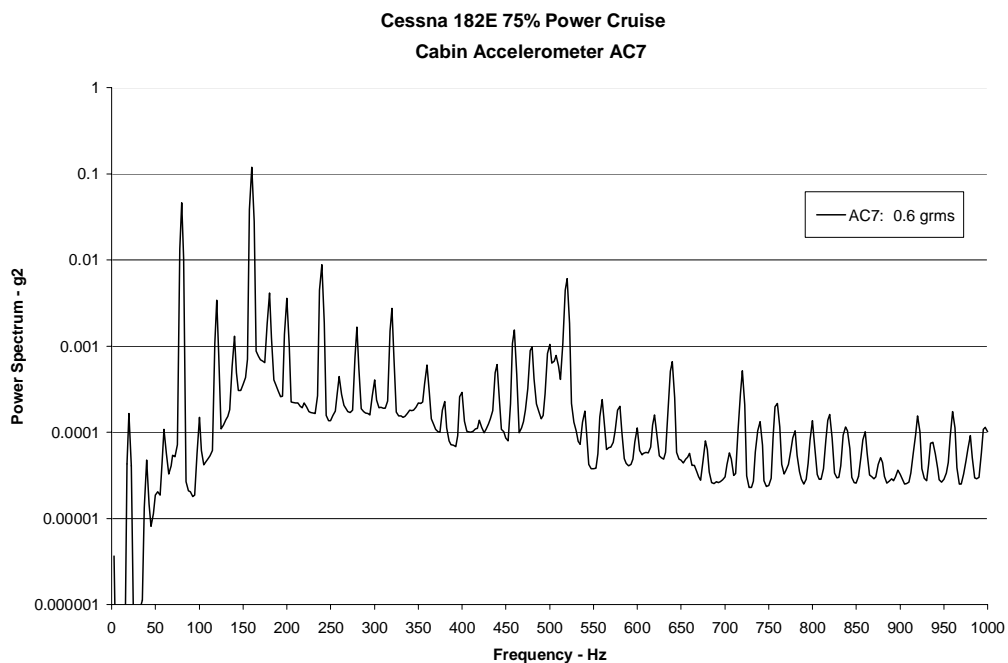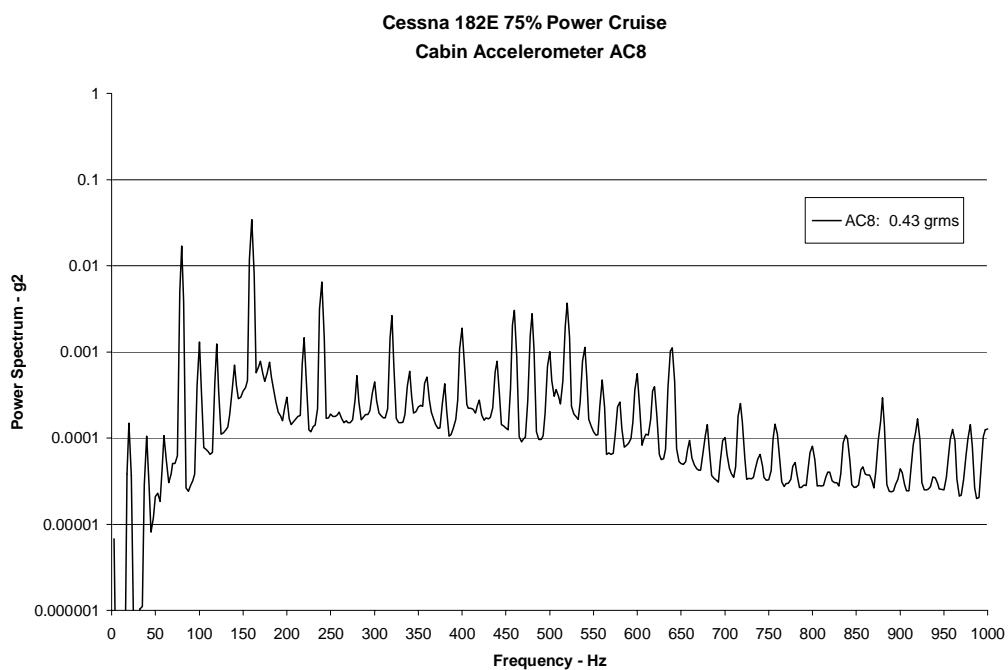
b) **Left Side**

Figure 2.7 Windshield Vibration Spectra.

Cessna 182E 75% Power Cruise
Cabin Accelerometer AC9

a) Pilot's Side

Cessna 182E 75% Power Cruise
Cabin Accelerometer AC10
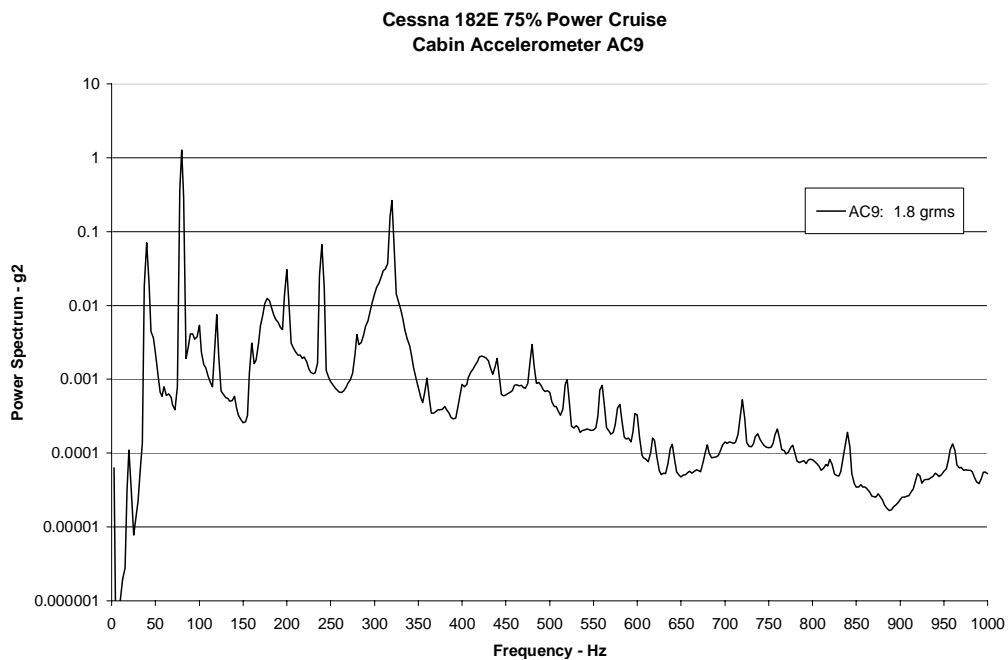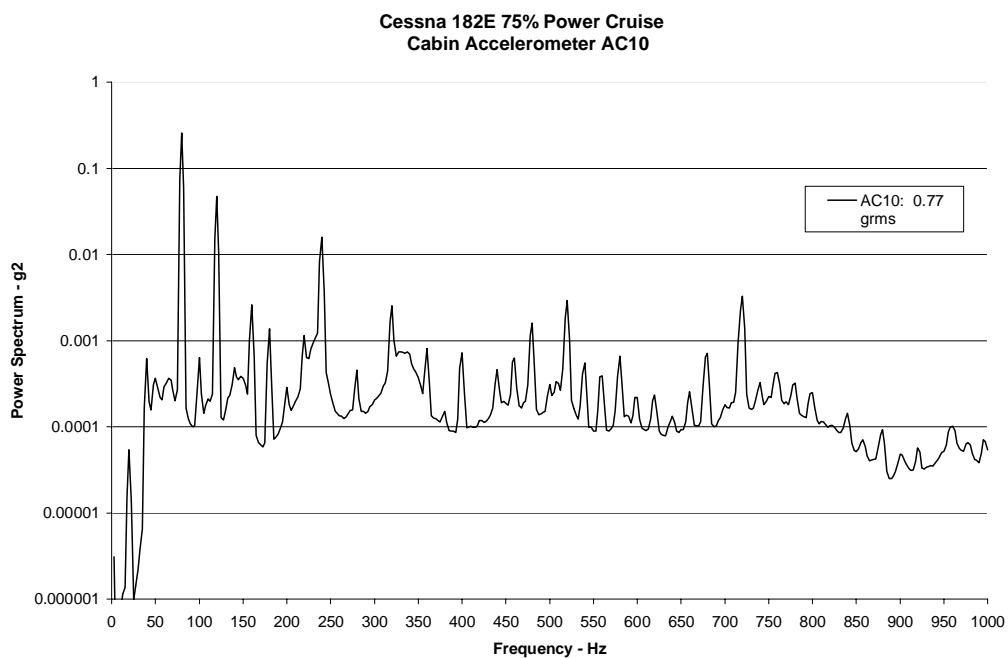
b) Copilot's Side

Figure 2.8 Forward Cabin Window Vibration Spectra.

Cessna 182E 75% Power Cruise
Cabin Accelerometer AC11

a) Right Side

Cessna 182E 75% Power Cruise
Cabin Accelerometer AC12
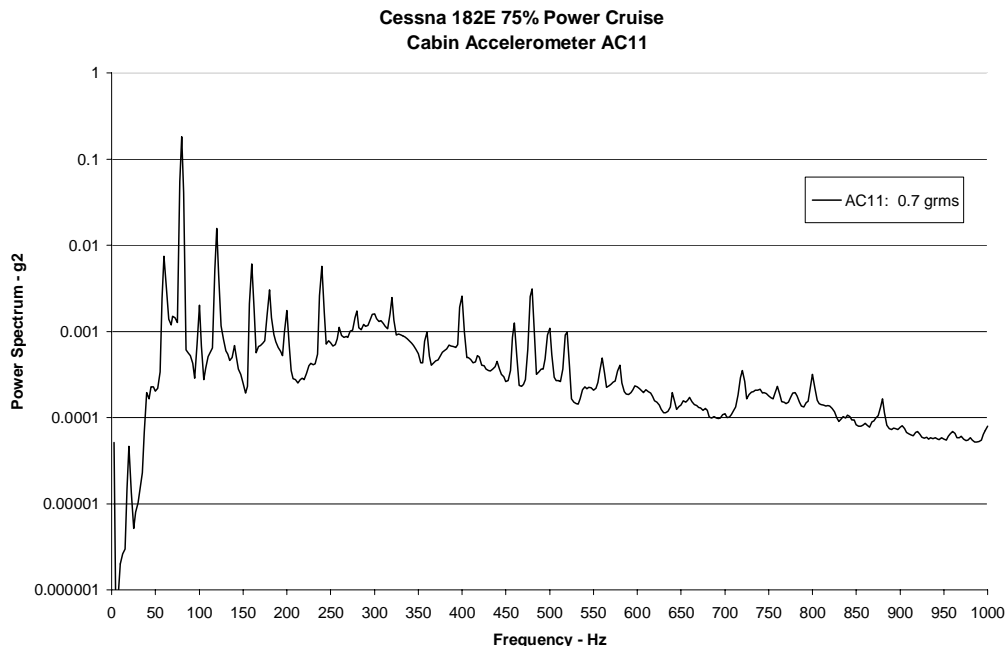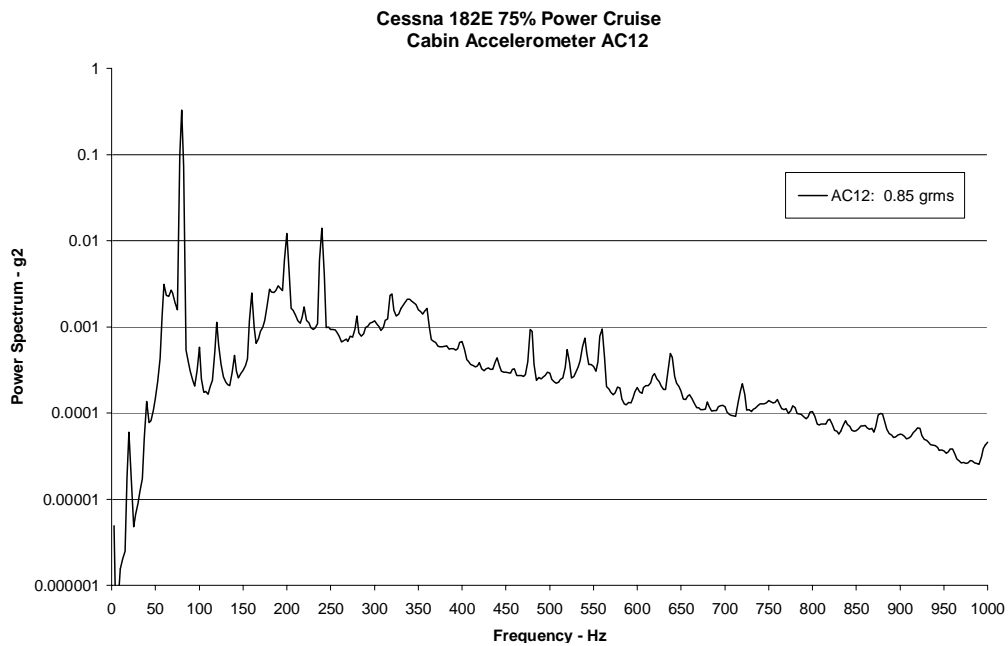
b) Left Side

Figure 2.9 Aft Cabin Window Vibration Spectra.

Cessna 182E 75% Power Cruise
Engine Accelerometer EC1

a) Axial

Cessna 182E 75% Power Cruise
Engine Accelerometer EC2
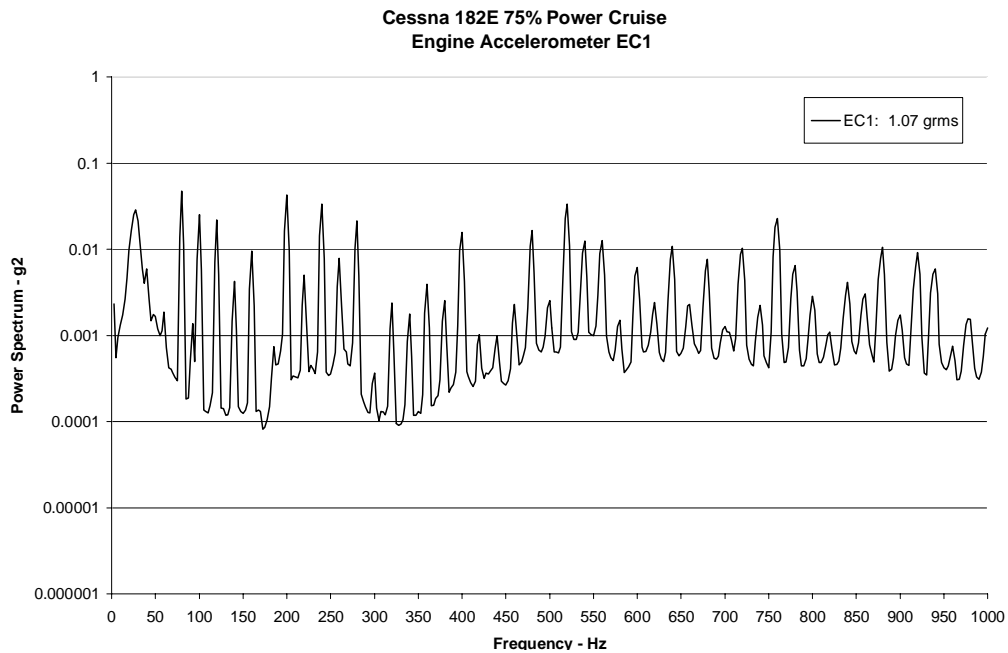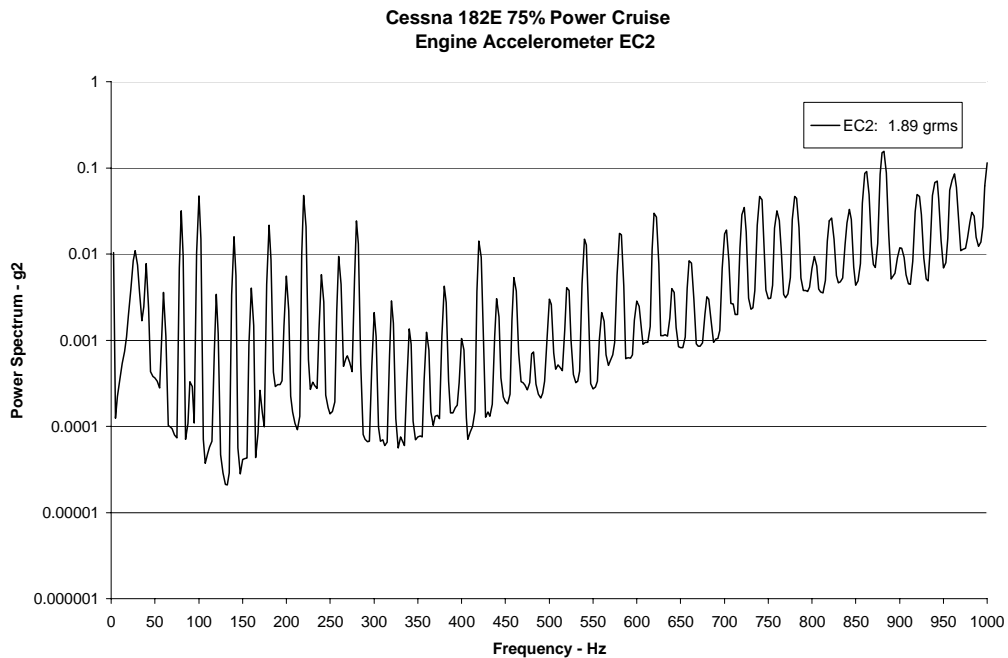
b) Lateral

Figure 2.10 Engine Vibration Spectra.

Cessna 182E 75% Power Cruise
Engine Accelerometer EC3
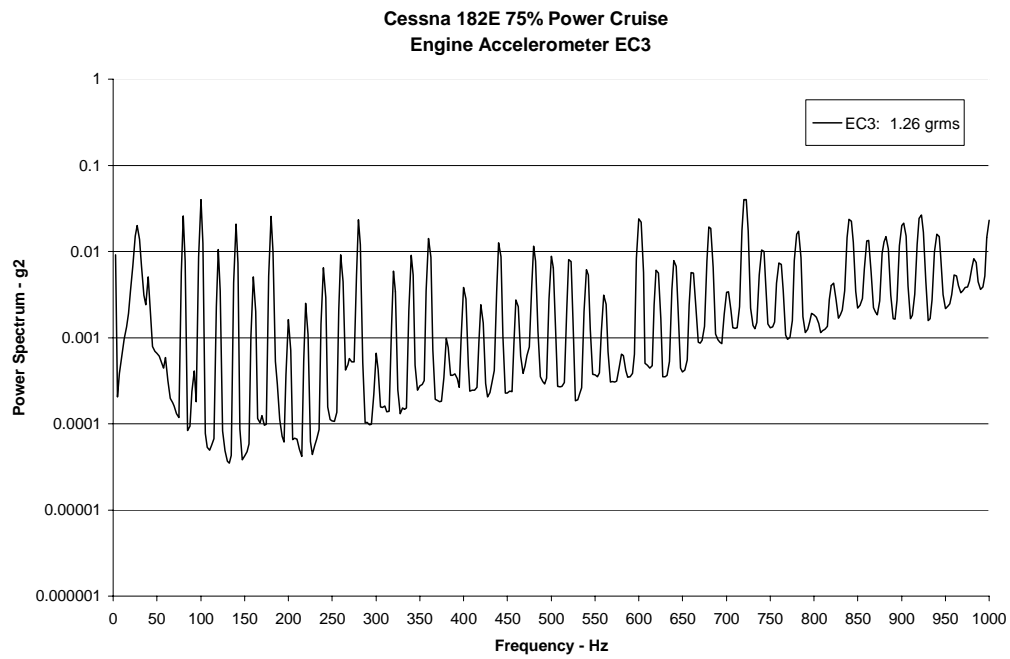
c) **Vertical**

Figure 2.10 (continued) Engine Vibration Spectra.

Cessna 182E 75% Power Cruise
Engine Accelerometer EC4

a) Transverse

Cessna 182E 75% Power Cruise
Engine Accelerometer EC5
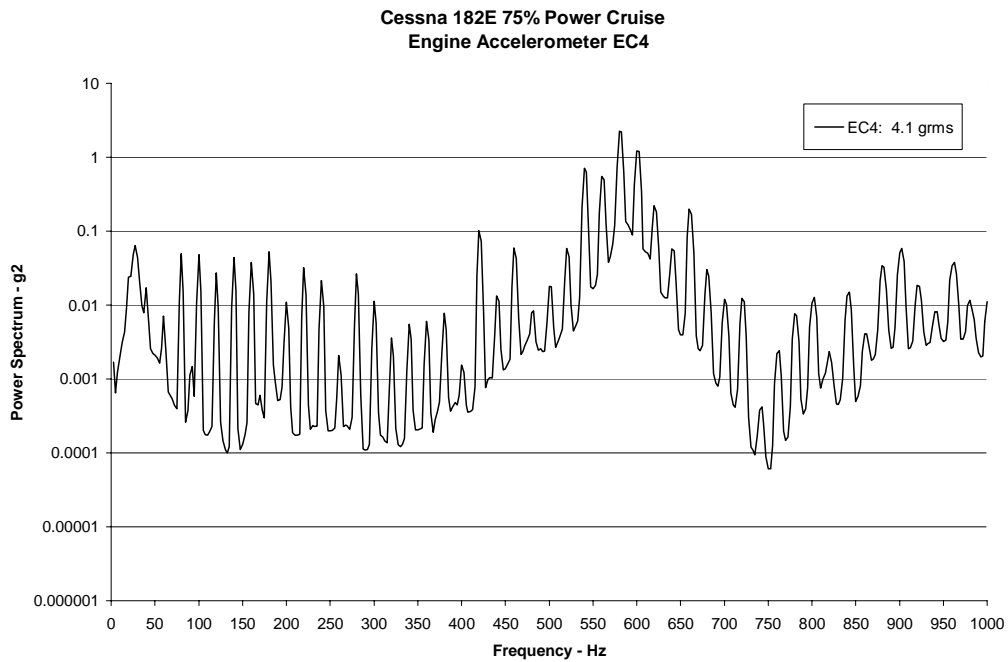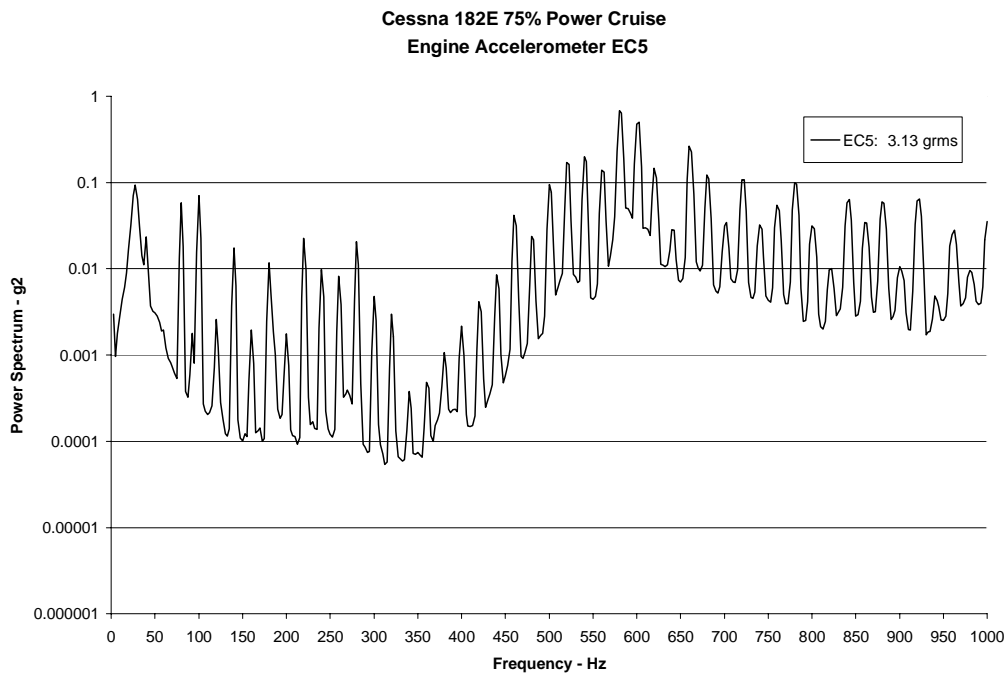
b) Axial

Figure 2.11 Engine Mount Engine Side Vibration Spectra.

Cessna 182E 75% Power Cruise
Engine Accelerometer EC6

a) Upper Member

Cessna 182E 75% Power Cruise
Engine Accelerometer EC7
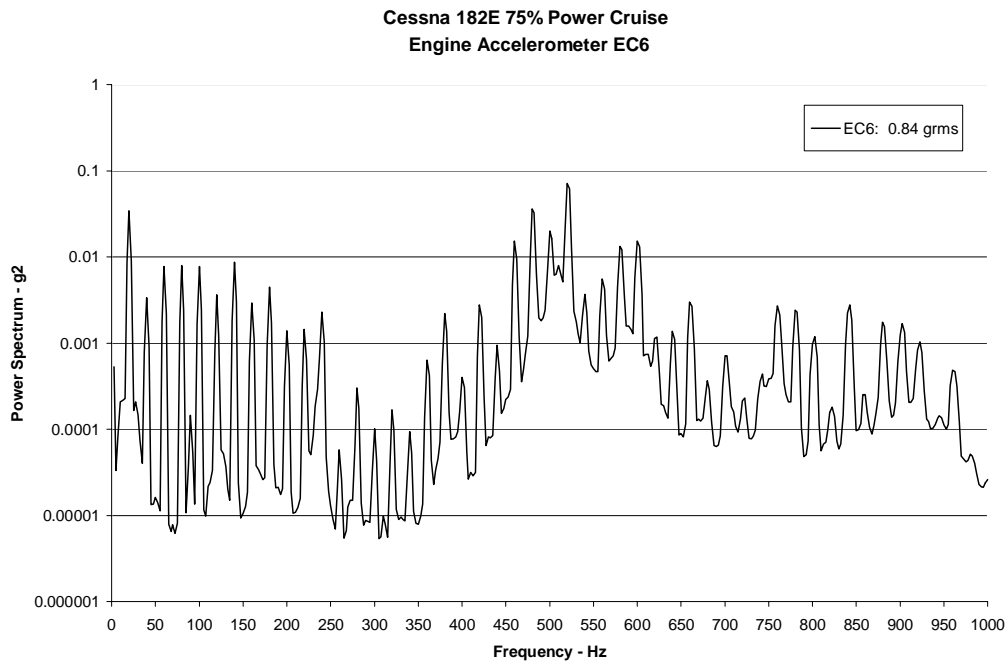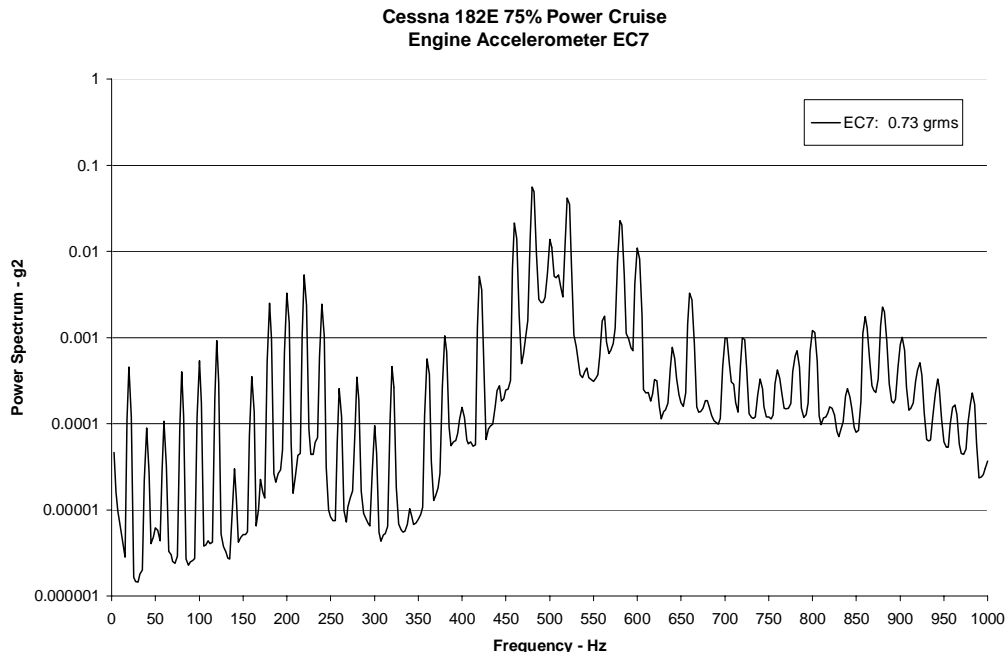
b) Lower Member

Figure 2.12 Engine Lower Left Truss Axial Vibration Spectra.

Cessna 182E 75% Power Cruise
Engine Mount Isolation EC8/EC4

a) Transverse

Cessna 182E 75% Power Cruise
Engine Mount Isolation EC9/EC5
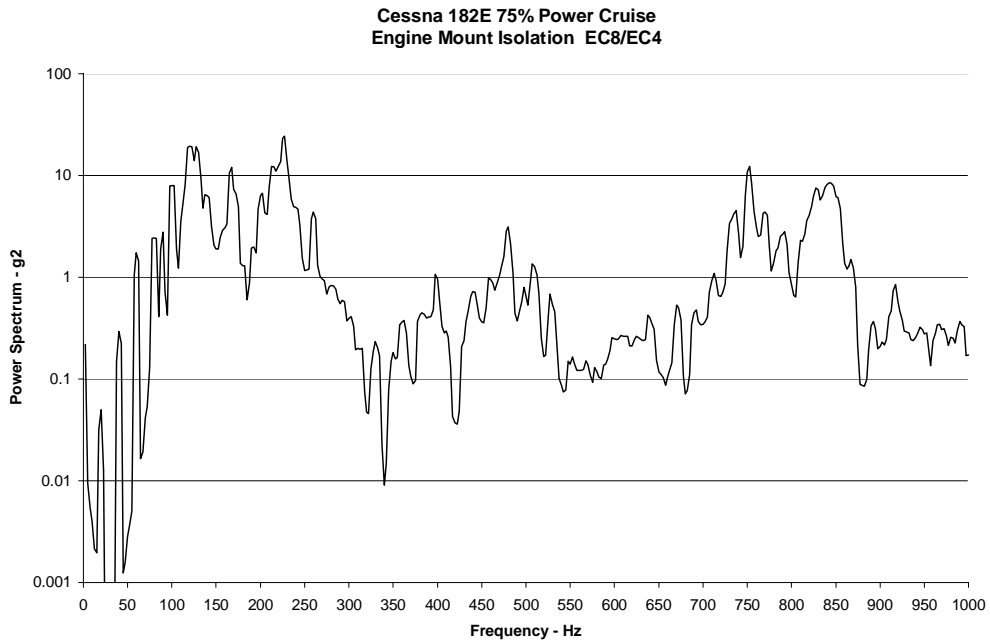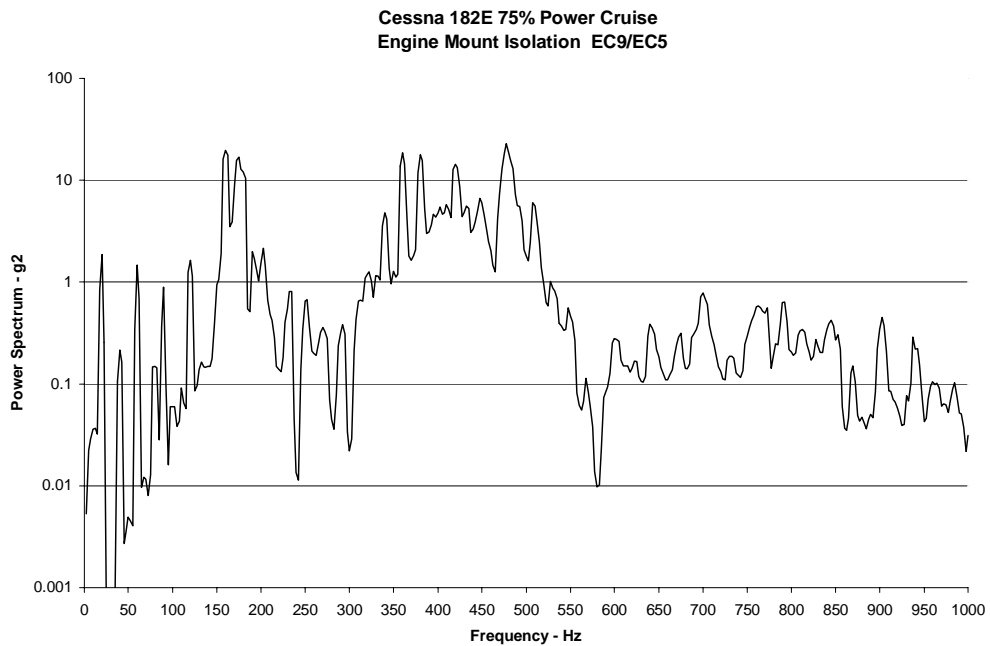
b) Axial

Figure 2.13 Engine Mount Isolation.

Cessna 182E 75% Power Cruise
Engine Accelerometer EC10

a) Left Member

Cessna 182E 75% Power Cruise
Engine Accelerometer EC11
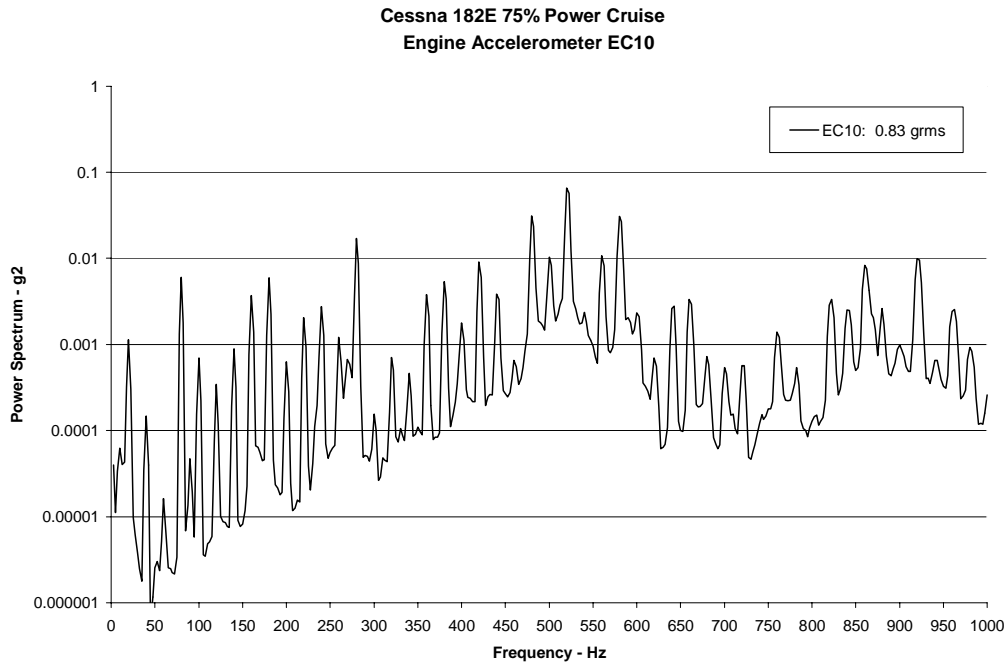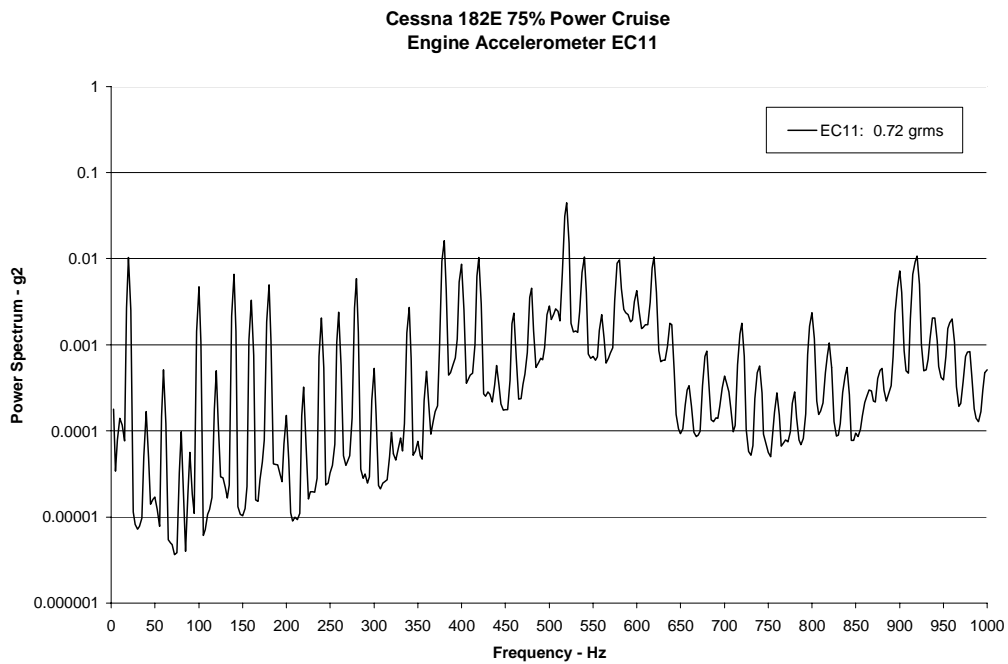
b) Right Member

Figure 2.14 Engine Upper Truss Axial Vibration Spectra.

Cessna 182E 75% Power Cruise
Engine Accelerometer EC12

a) Mid Center

Cessna 182E 75% Power Cruise
Engine Accelerometer EC13
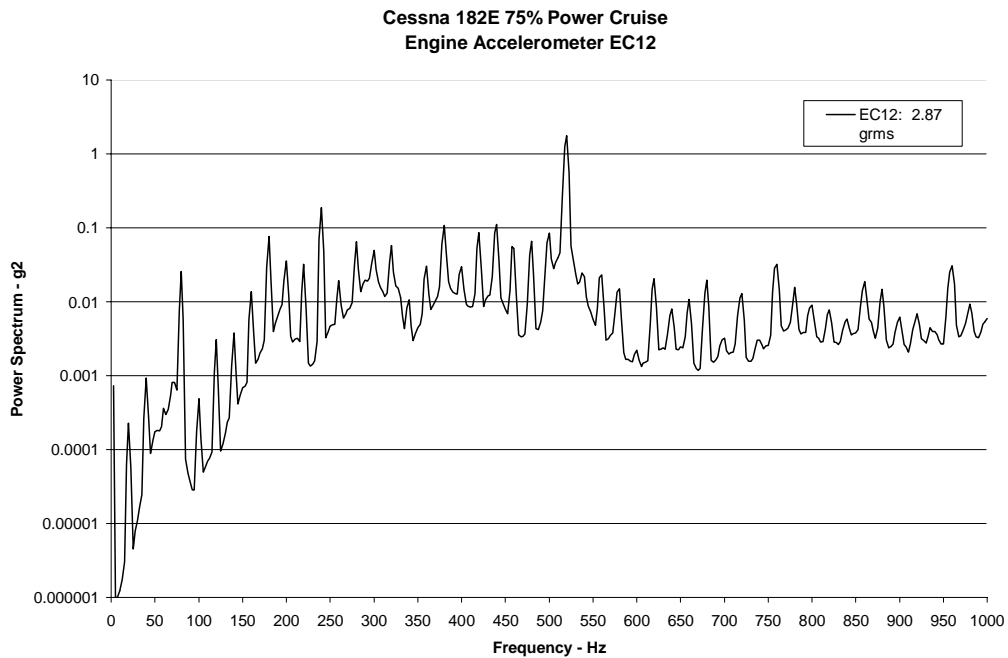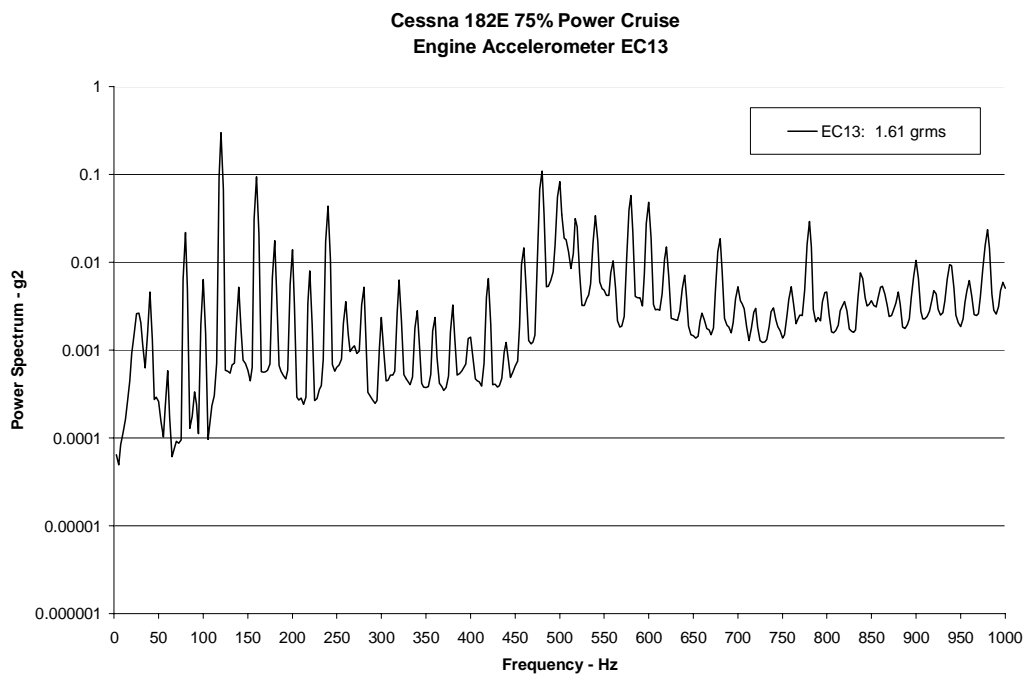
c) Upper Center

Figure 2.15 Firewall Vibration Spectra.

Cessna 182E 75% Power Cruise
Engine Microphone EC14
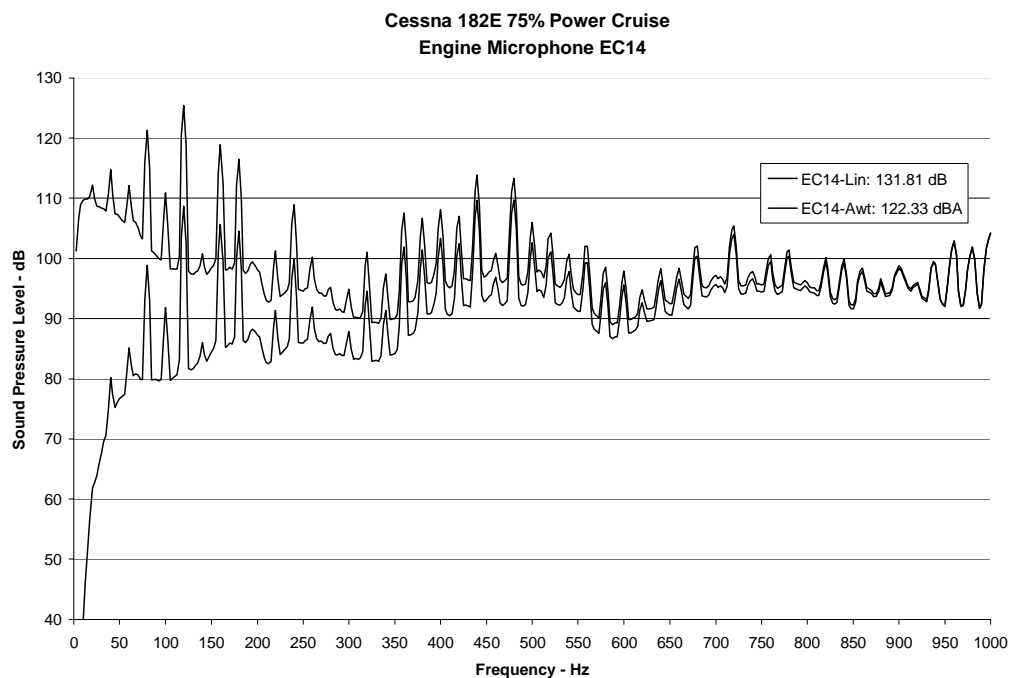
Figure 2.16 Engine SPL Spectra – Firewall Mid Center.

Cessna 182E 75% Power Cruise
Exterior Microphone AE1

AE1-Lin: 133.03 dB
AE1-Awt: 116.99 dBA

a)   Center Windshield

Cessna 182E 75% Power Cruise
Exterior Microphone AE2

AE2-Lin: 131.09 dB
AE2-Awt: 115.6 dBA
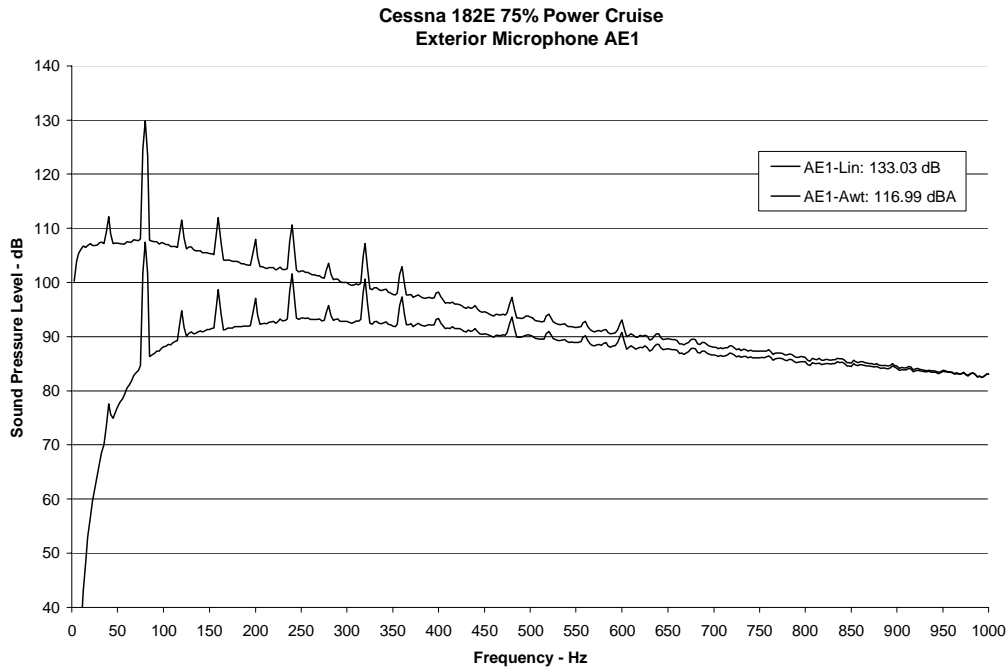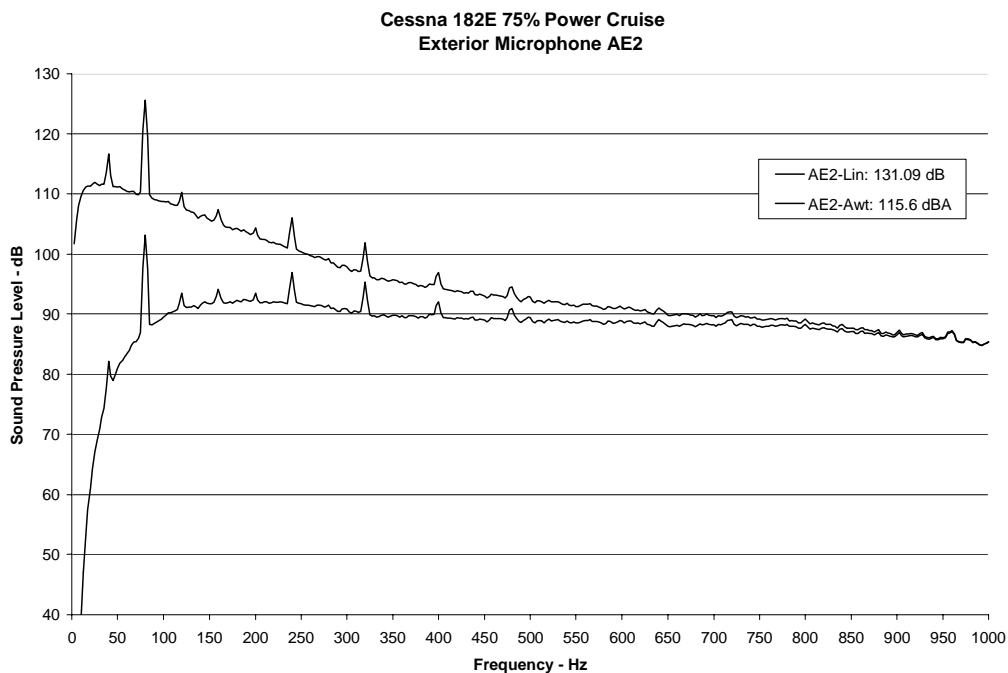
b) Pilot's Door – Center

Figure 2.17 Fuselage Exterior SPL Spectra.

Cessna 182E 75% Power Cruise
Exterior Microphone AE3

Legend:
AE3-Lin: 127.86 dB
AE3-Awt: 113.07 dBA

Y-axis: Sound Pressure Level - dB
X-axis: Frequency - Hz

c) Copilot's Door – Center

Cessna 182E 75% Power Cruise
Exterior Microphone AE4

Legend:
AE4-Lin: 134.94 dB
AE4-Awt: 123.2 dBA

Y-axis: Sound Pressure Level - dB
X-axis: Frequency - Hz
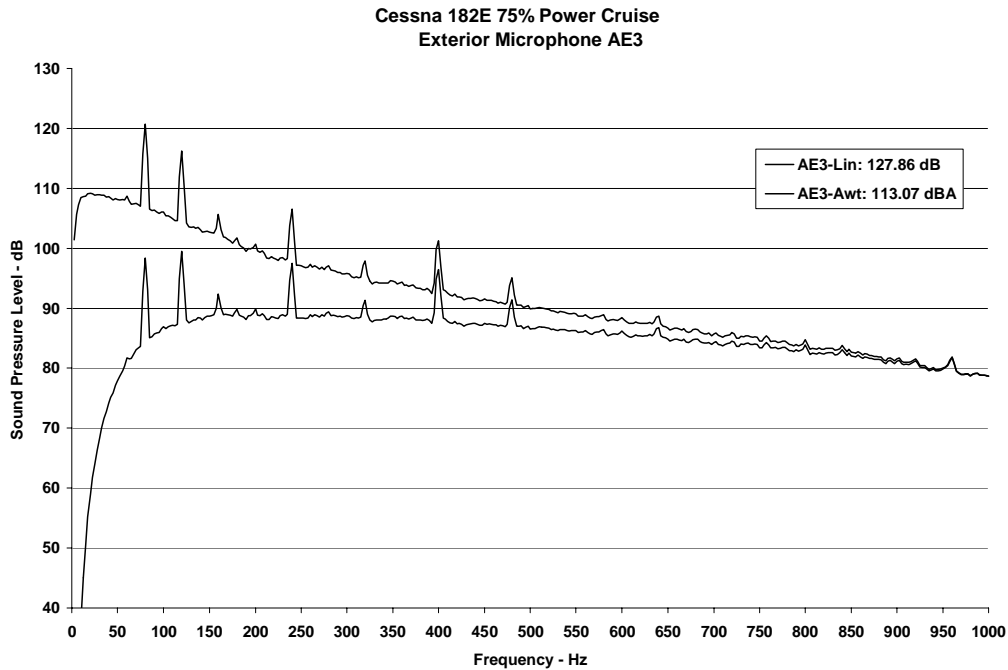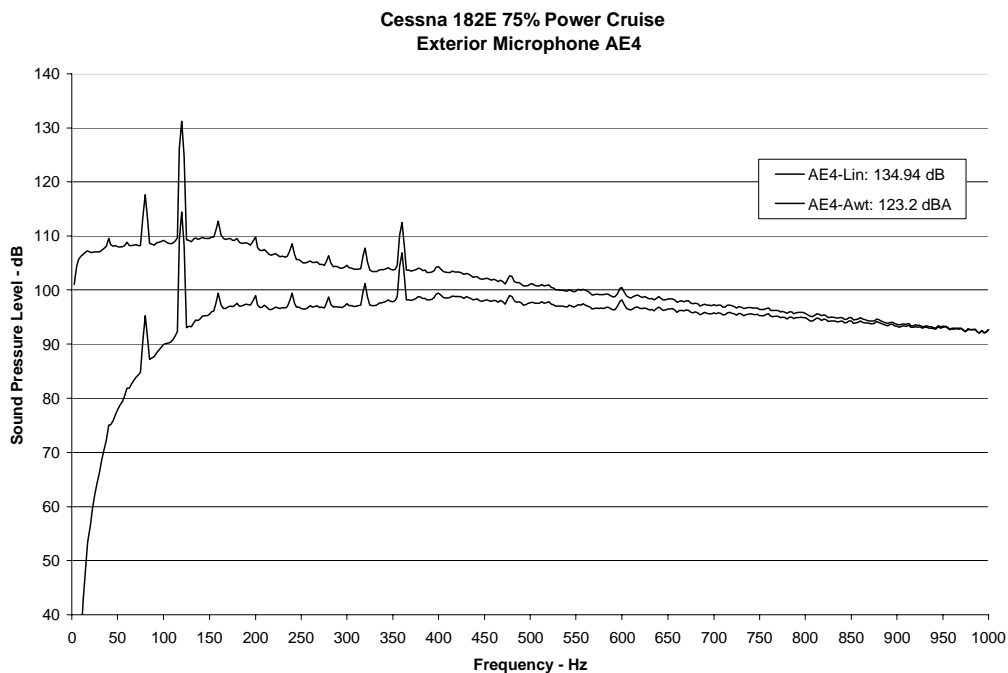
d) Downstream From Exhaust

Figure 2.17 (continued) Fuselage Exterior SPL Spectra.

Cessna 182E 75% Power Cruise
Exterior Accelerometer AE5
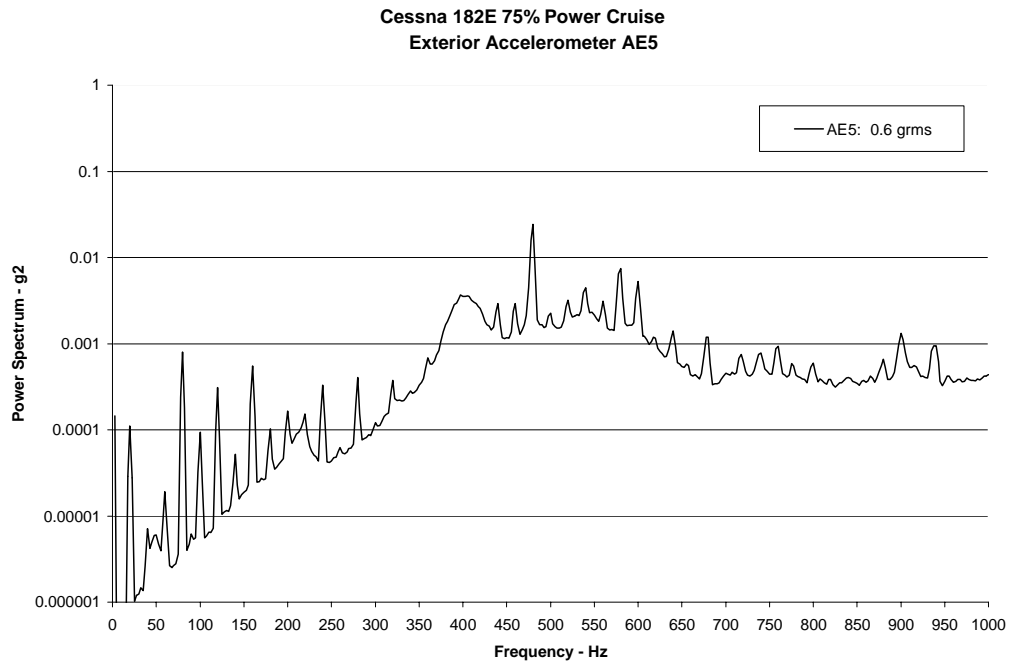
Figure 2.18 Fuselage Vibration Spectra Downstream of Exhaust.

Figure 2.19 Cessna Model 182E in Ground Test Configuration.

Figure 2.20 Speaker Array Used to Simulate Propeller Airborne Noise.
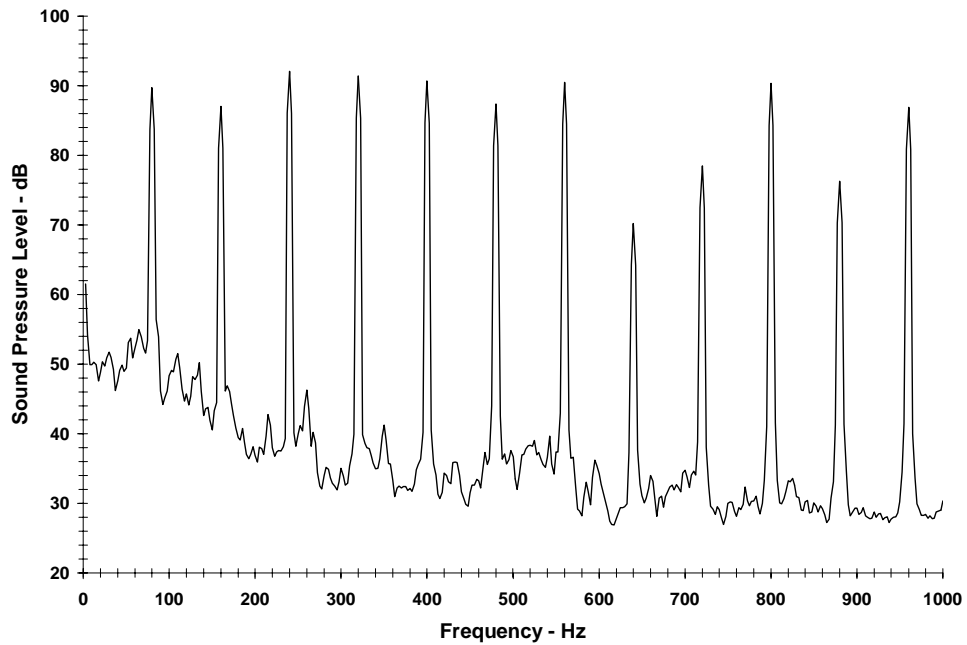
Figure 2.21 Response of Windshield Microphone, AE1, to Propeller Simulation.
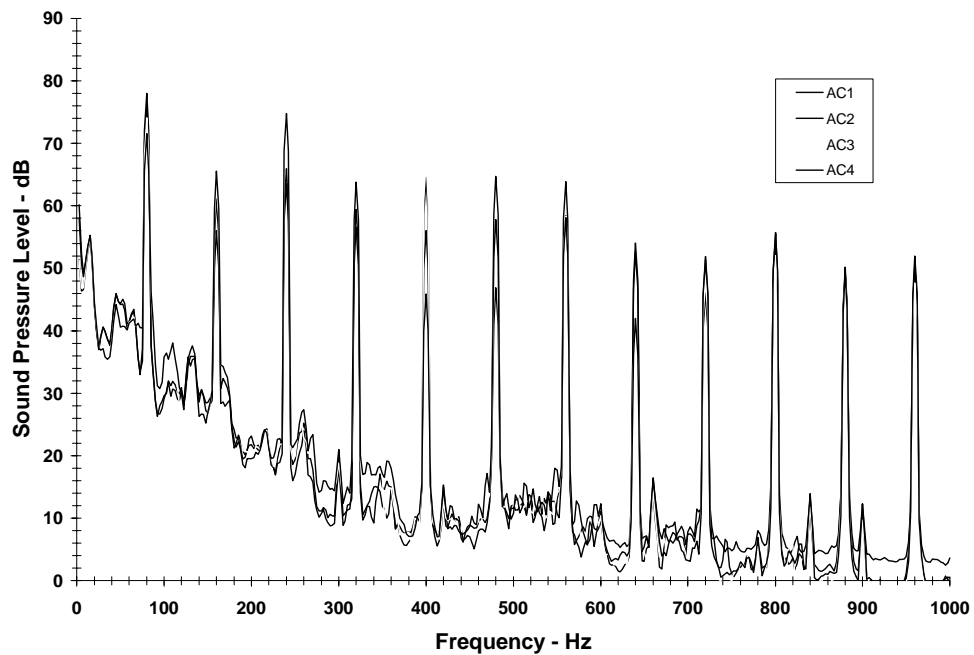
Figure 2.22 Response of Cabin Microphones to Propeller Simulation.

Figure 2.23 Speaker Used for Engine Exhaust Airborne Noise Simulation.
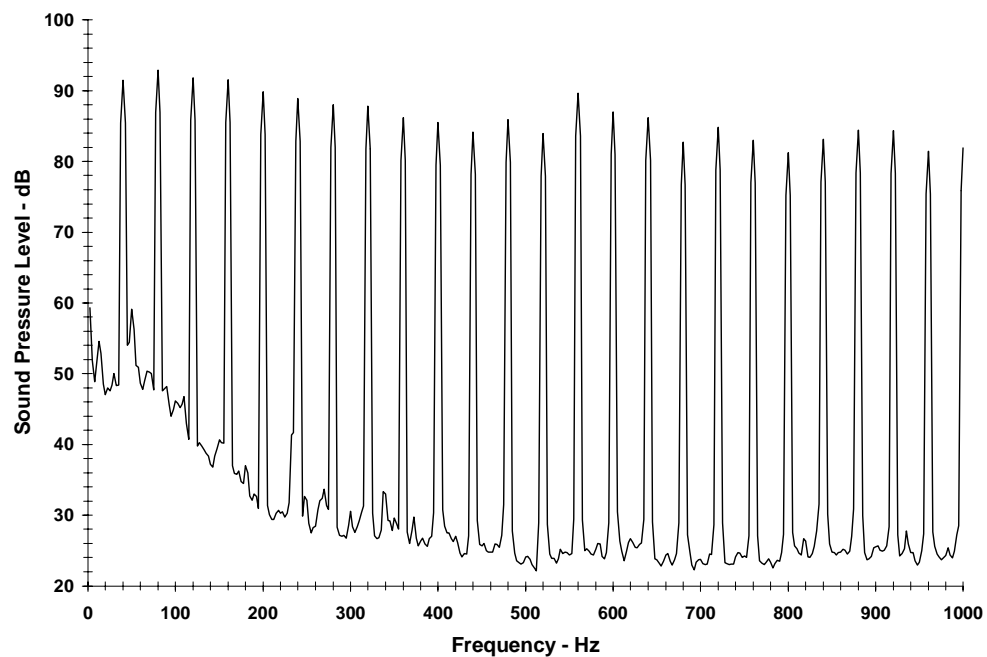
Figure 2.24 Response of Downstream Microphone AE4 to Exhaust Simulation.
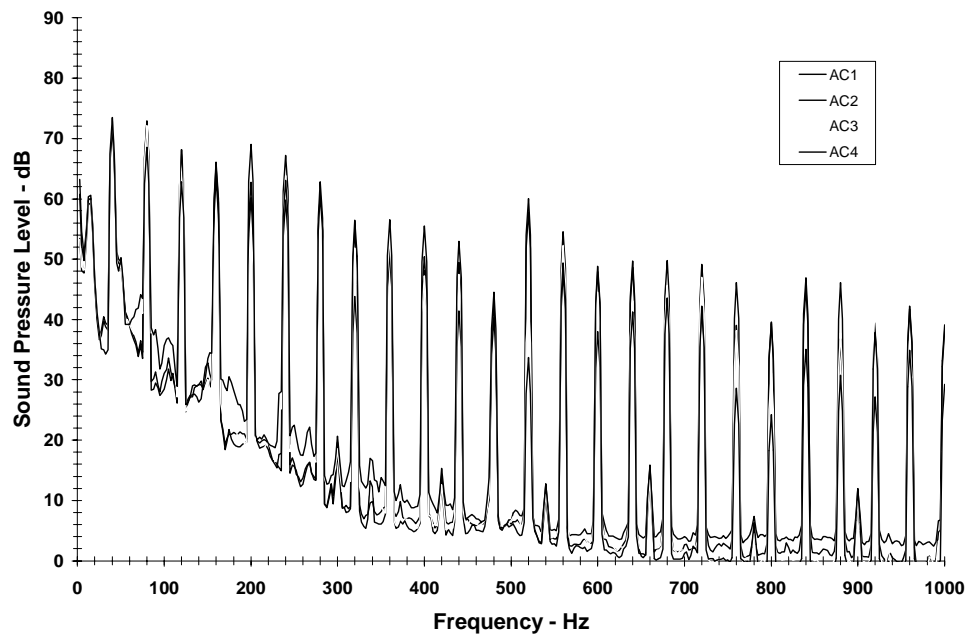
Figure 2.25 Response of Cabin Microphones to Exhaust Simulation.
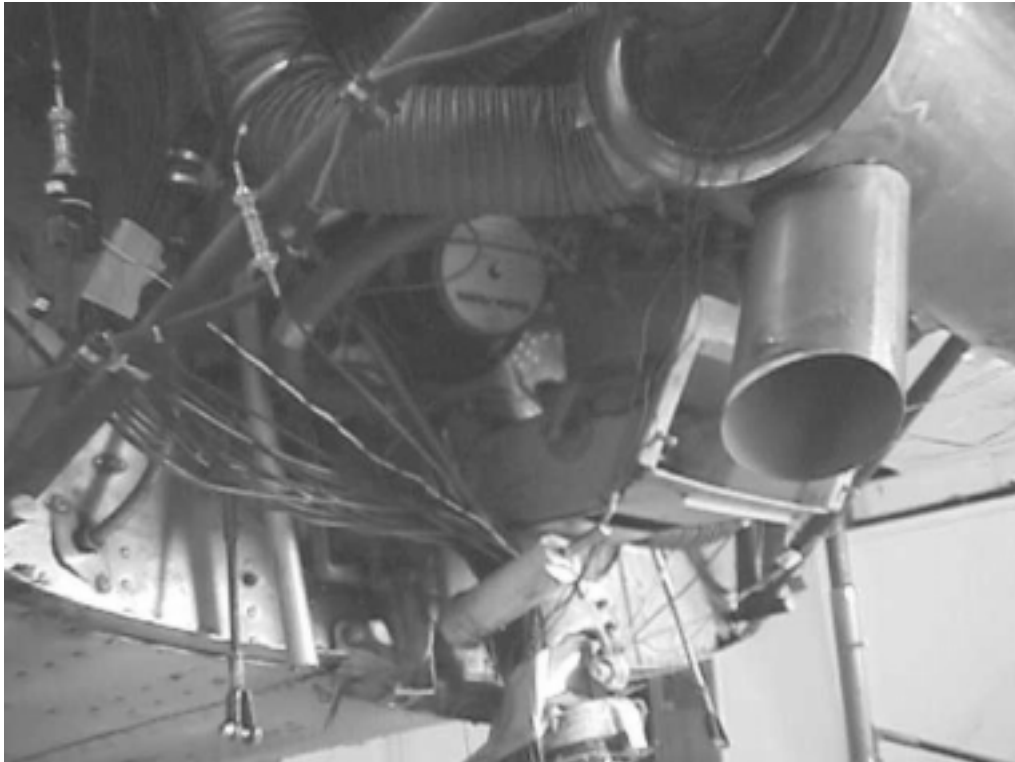
Figure 2.26 Speaker Used to Simulate Engine Case Radiation.
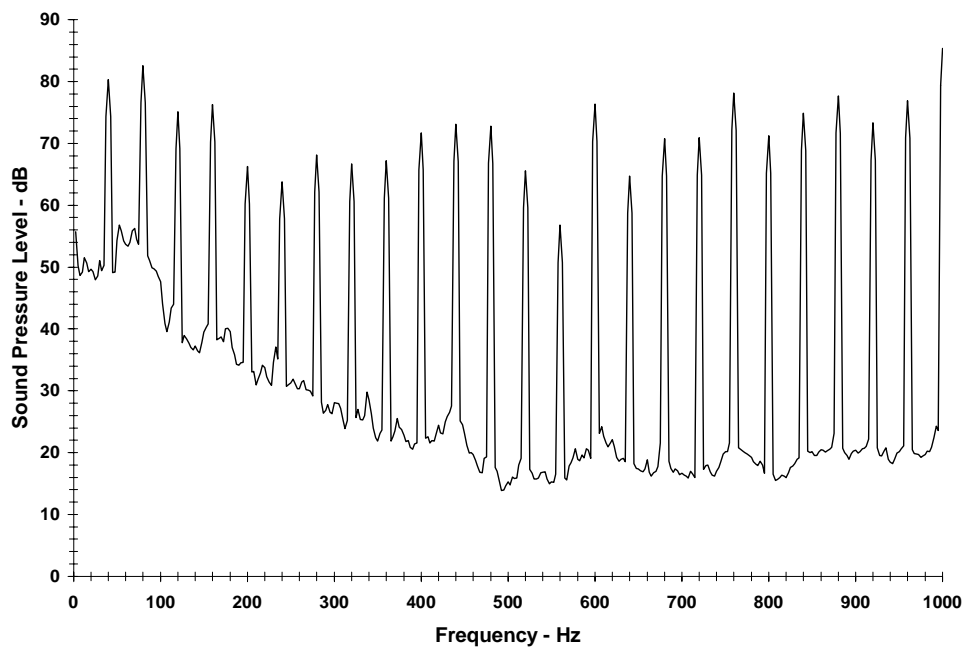
Figure 2.27 Response of Firewall Microphone EC14 to Simulated Engine Noise.
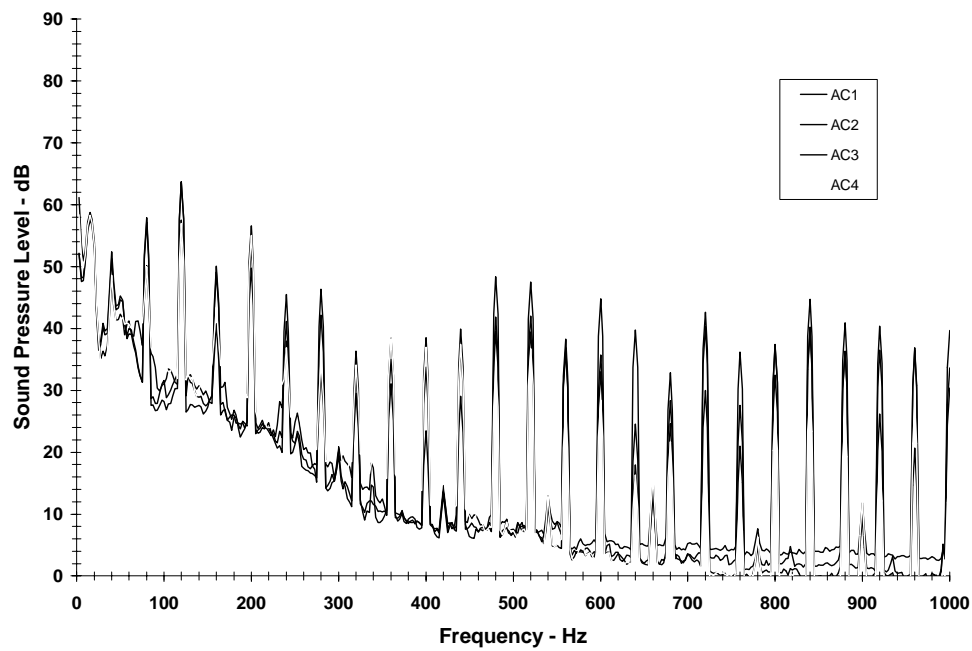
Figure 2.28 Response of Cabin Microphones to Simulated Engine Noise.
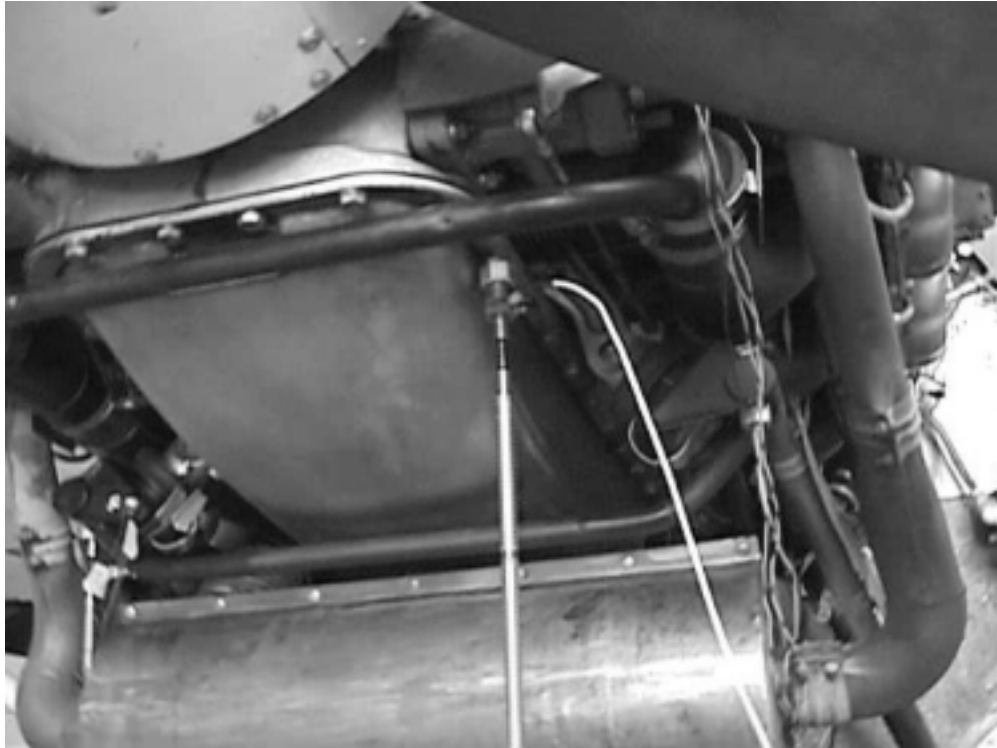
Figure 2.29 Shaker Sting Attachment During Structure-Borne Noise Simulation.
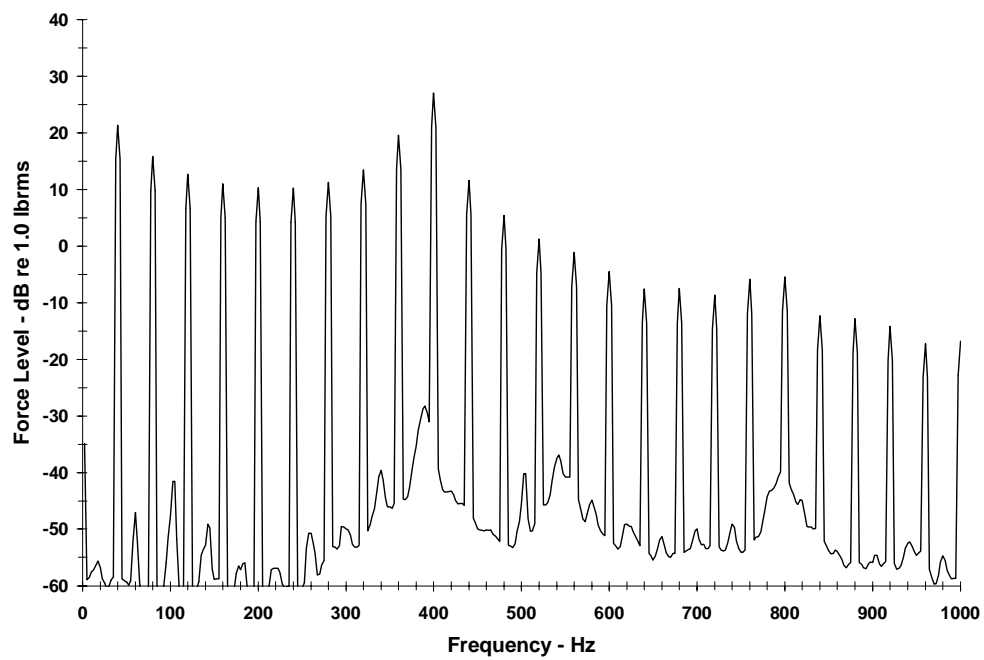
Figure 2.30 Shaker Force Level Spectra.
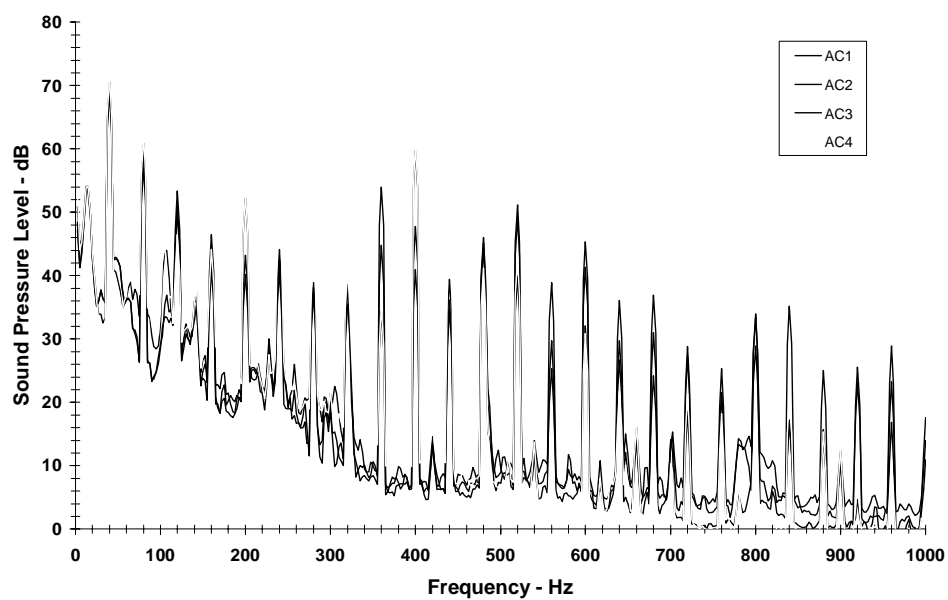
Figure 2.31 Cabin Response During Structure-Borne Noise Simulation.

Figure 2.32 Test Setup During Structure-Borne Noise Simulation.
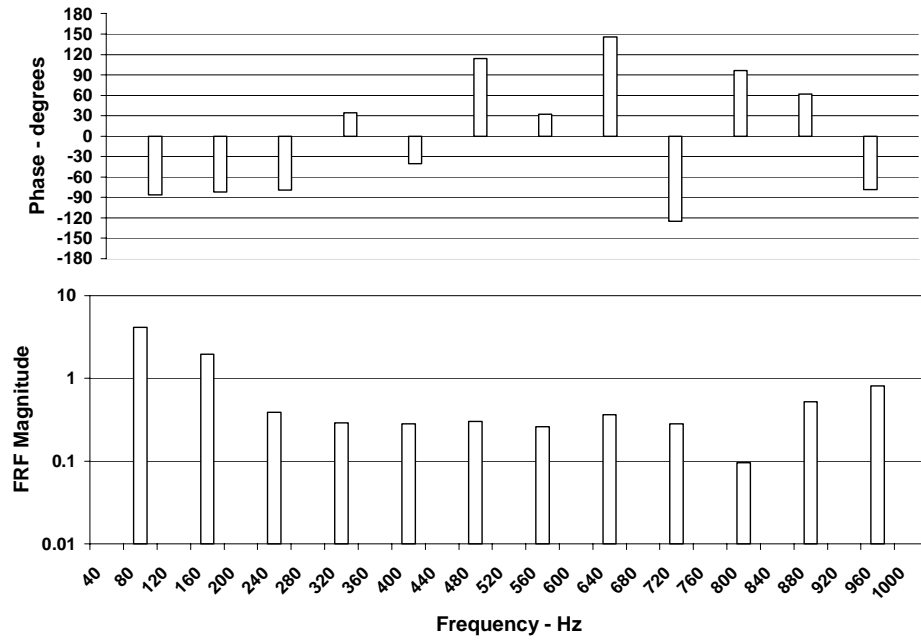
a) Microphone EC14 – Firewall Mid Center
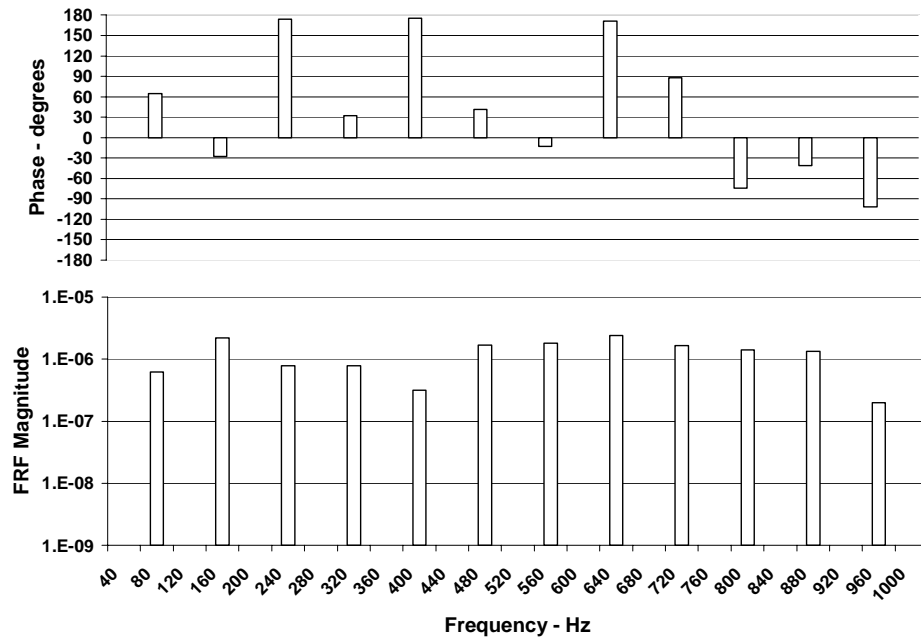
b) Accelerometer EC13 – Firewall Upper Center

Figure 2.33 Simulated Propeller Excitation FRF's.
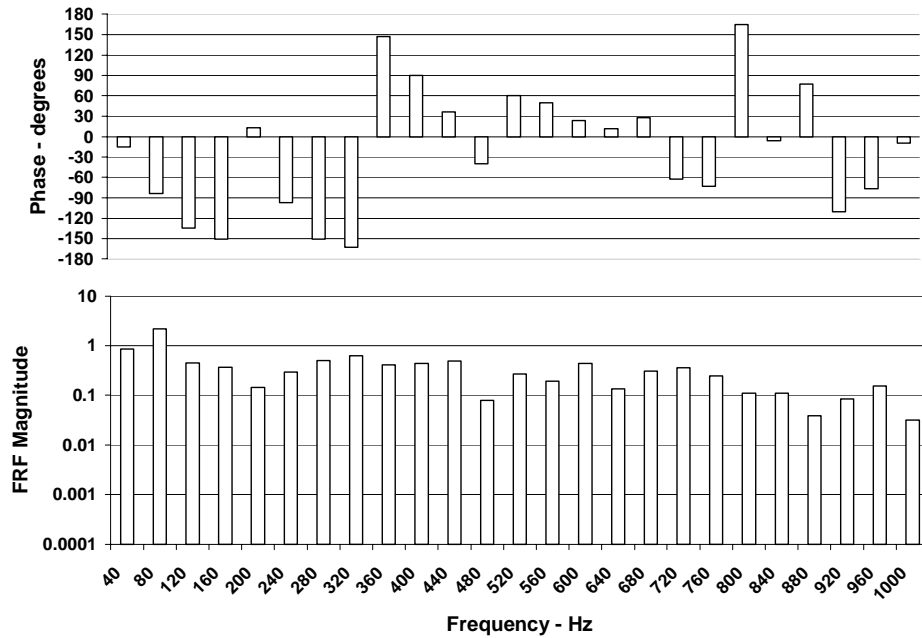
a) Microphone EC14 – Firewall Mid Center
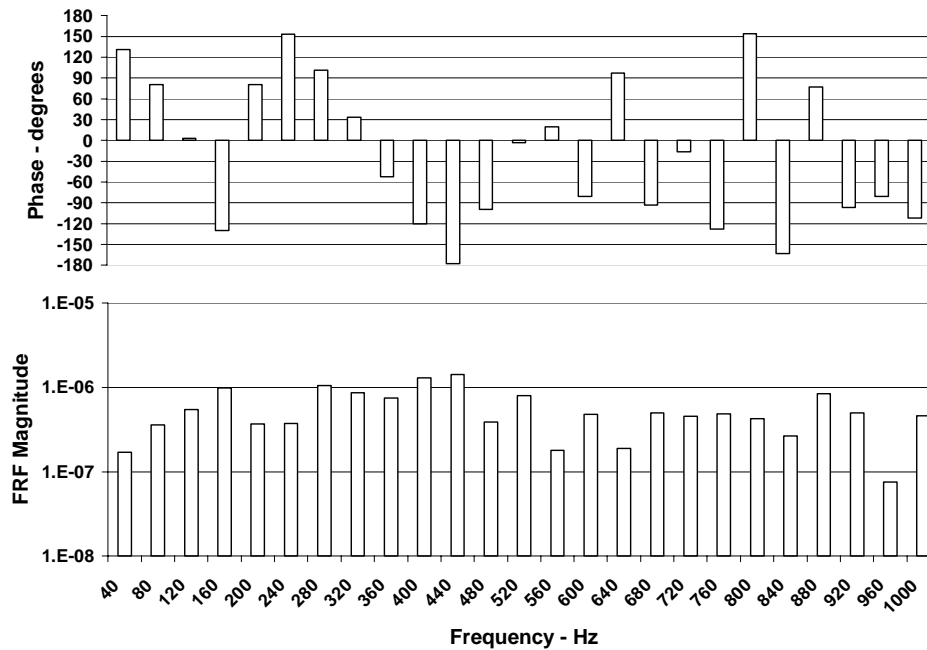
b) Accelerometer EC13 – Firewall Upper Center

Figure 2.34 Simulated Exhaust Excitation FRF's.
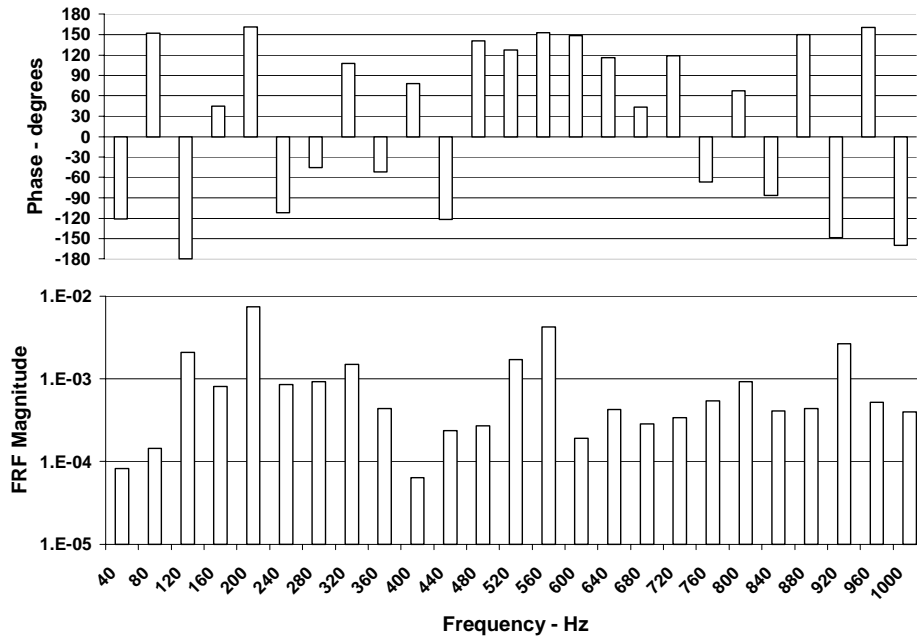
a) Accelerometer AC5 – Instrument Panel Right Side
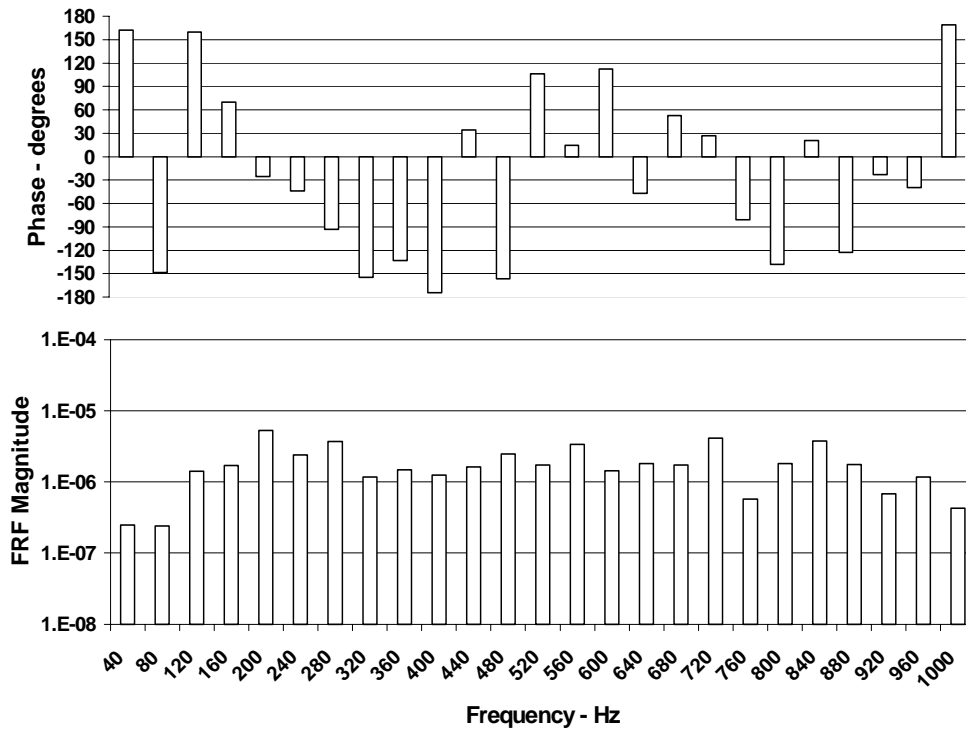
b) Accelerometer EC13 – Firewall Upper Center

Figure 2.35 Simulated Engine Airborne Excitation FRF's.
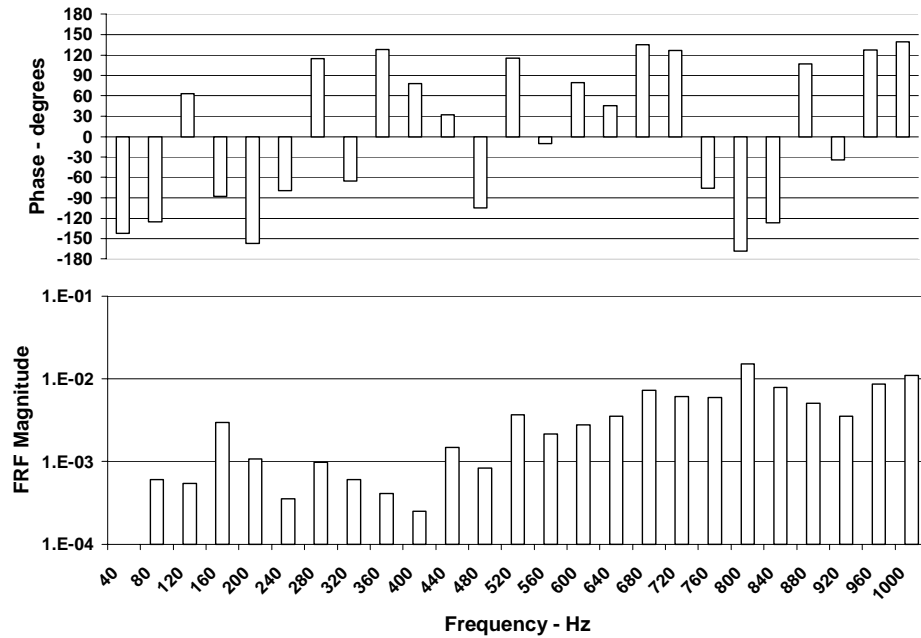
a) Accelerometer AC5 – Instrument Panel Right Side
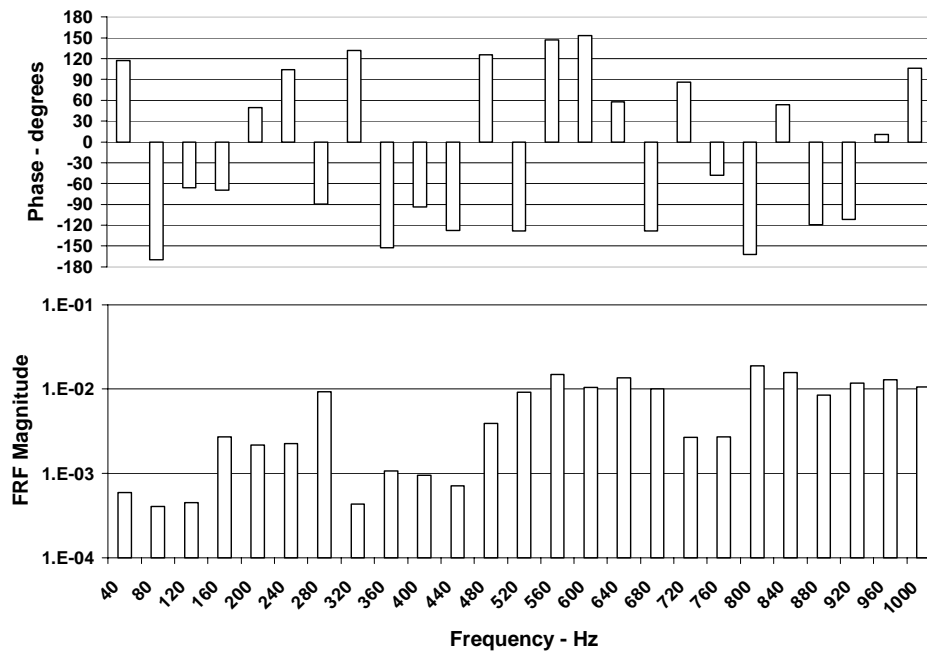
b) Accelerometer EC13 – Firewall Upper Center

Figure 2.36 Simulated Engine/Propeller SBN Excitation FRF's.

AC1 - Pilot

AC2 - Copilot

AC3 - Right Rear

AC4- Left Rear
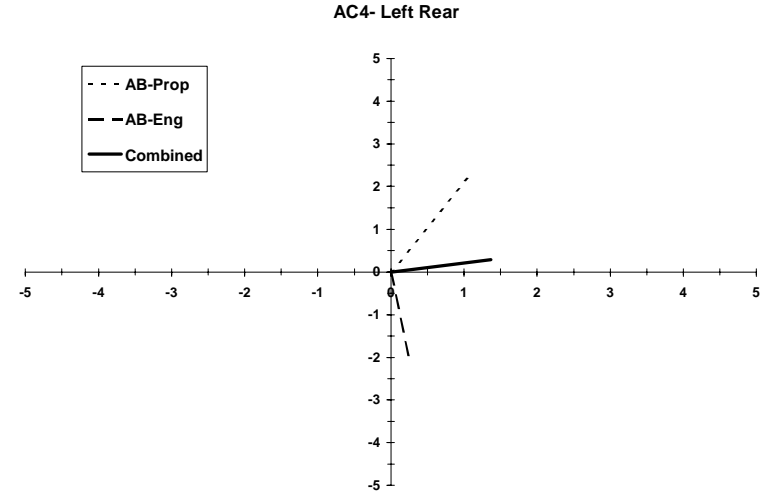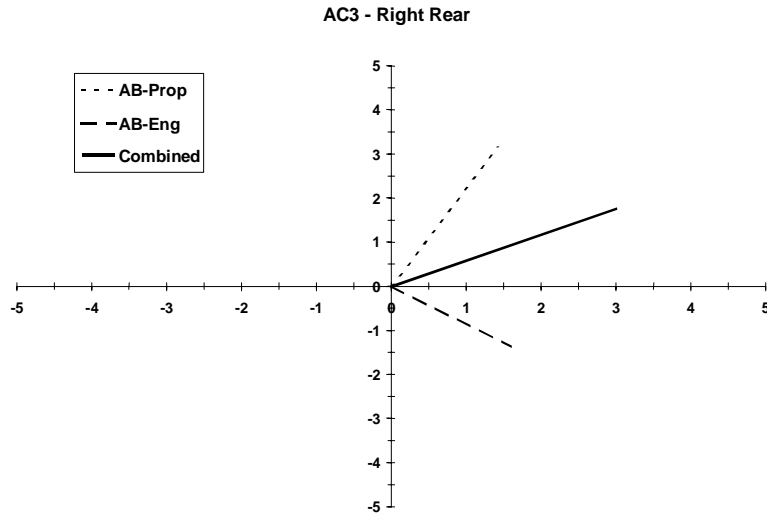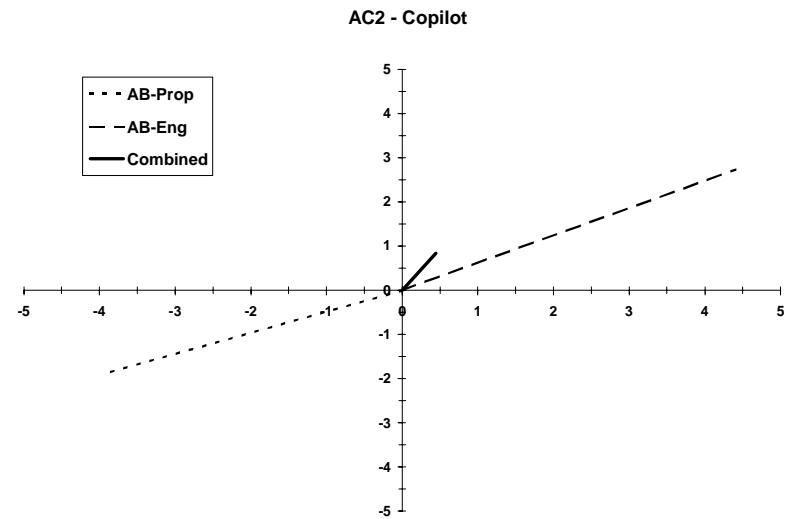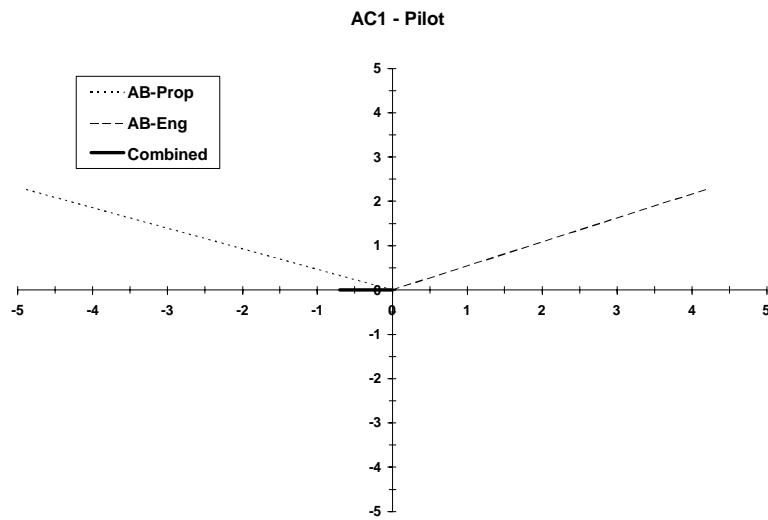
Figure 2.37 Predicted Airborne Contributions: First Propeller Tone @ 80 Hz, Cruise at 75% Power.

3. NOISE SOURCE RANKING OF INTERIOR PANEL GROUPS

In this section, a new method for estimating contributions from panel groups to the interior acoustic field of a vehicle is presented. This approach examines the inverse problem, where pressures in the interior acoustic field are known and, based on an influence matrix, are back-propagated to a known source geometry. The source composition of individual panels, in terms of magnitude and phase, results. A verification example exhibiting execution of the technique is discussed. In addition, this method is applied to in-flight data collected on the Cessna 182E test aircraft. The resulting source panel contribution information is useful in determining which panel groups are dominant and how the radiated fields from individual panel groups combine constructively or destructively to form the resulting acoustic field.

3.1   Acoustic Holography for Vehicle Interiors

As stated, a new method for ranking noise sources for a vehicle interior is defined and verified through an example problem. This technique investigates the inverse problem, estimating the source composition based on pressures measured in a hologram. The method typically combines numerical simulation data with test data to accomplish this task. The numerical simulation data is used to form the influence matrix. The test data consists of pressure measurements collected at the hologram locations. These locations are replicated in the numerical simulation model. The influence matrix technique allows noise sources to be identified for more complex geometries, such as a vehicle interior, where traditional approaches may be limited.

3.1.1 The Inverse Problem

The inverse problem using the influence matrix technique was derived and verified at SwRI under an internal research project [10]. This technique follows the method of conventional Near-field Acoustical Holography (NAH), where pressures are measured in the acoustic near-field, then back-propagated to a defined source geometry to identify contributing sources. The influence matrix technique incorporates an influence matrix constructed using Boundary Element (BE) model simulations. The inverse of this matrix is used to predict the corresponding source distribution based upon the hologram pressures measured in the acoustic field. With the influence matrix technique, these measurements are not restricted to the acoustic near field. In addition, more complex geometries, such as non-planar sources or enclosures, are properly handled with this technique, a distinct advantage over conventional NAH.

The mathematics involved for this method is straightforward. The influence, or $\mathbf{Q}$, matrix is calculated based on the potential source geometry and pressure measurement locations forming the hologram. The expression, $\mathbf{P} = \mathbf{QV}$, relates source velocities, $\mathbf{V}$, to the resulting pressure field, $\mathbf{P}$, generated by these sources at the hologram pressure locations. In the BE model, the sources are composed of "panels" or elements, where velocity boundary conditions are applied. The acoustic pressures are calculated at data recovery nodes, corresponding to the hologram pressure locations, defined in the acoustic medium. In a typical simulation, pressures at each data recovery node are calculated for a given set of source element boundary conditions.

The **Q** matrix is constructed by individually applying a unit velocity boundary condition for each of the source elements and recording the calculated pressures at the data recovery nodes in the hologram space. The inverse, or pseudo-inverse, of the **Q** matrix is then used to predict the velocity distribution of the sources. The pseudo-inverse is defined as follows:

$$\mathbf{A}^+ = \mathbf{B}_2 \mathbf{\Sigma}^+ \mathbf{B}_1^T,$$

where the matrices $\mathbf{B}_1$ and $\mathbf{B}_2$ are formed using the singular value decomposition of **A** defined as,

$$\mathbf{A} = \mathbf{B}_1 \mathbf{\Sigma} \, \mathbf{B}_2^T.$$

The $\mathbf{\Sigma}^+$ matrix is a diagonal matrix composed of the reciprocals of the singular values of **A**. Therefore, using the pseudo-inverse of **Q**, $\mathbf{Q}^+$, the following expression results, relating hologram pressures to source velocities, $\mathbf{V} = \mathbf{Q}^+ \mathbf{P}$. In effect, the pressures measured in the hologram space are projected onto a set of orthogonal basis vectors created by the singular value decomposition of the influence matrix. More clearly, the influence matrix, containing the hologram pressure distributions attributed to each individual source element, is decomposed into a set of orthogonal vectors. The measured hologram pressures are then projected onto this set. The influence matrix is then reconstructed to determine the composition of the potential sources needed to estimate the measured pressure field. The next section presents an example that verifies application of this technique.

3.1.2 Verification Example

In this section, a verification example examining the inverse problem as applied to a general aviation aircraft interior is discussed. The influence matrix technique was used to identify the composition of an arbitrary distribution of sources defined in a BE model. Varying velocity boundary conditions were applied to multiple source elements, producing an acoustic pressure field in the cabin interior. This pressure field was mapped at discrete locations in the hologram space by specifying data recovery nodes. The influence matrix technique was then executed to determine whether these sources could be predicted using only the hologram pressure calculations and inverse of the influence matrix.

The BE model of the aircraft interior is shown in Figure 3.1. In the interest of simplicity, the model includes only the cabin boundary, neglecting seats and other complicating interior features. However, the model is certainly suitable for simulating the acoustic environment of an aircraft cabin, especially at low frequencies, and should prove useful in verifying the influence matrix technique. The model consists of 918 acoustic boundary elements with a characteristic length of 6 inches, resulting in 4 to 5 elements per wavelength at 500 Hz. The pressure hologram consists of 995 data recovery nodes also shown in Figure 3.1. These nodes are located in planes near the side windows and roof, representing potential in-flight measurement locations for microphones. The influence matrix is constructed by completing an individual BE simulation for each potential source, in this case all boundary elements. For each simulation, the boundary condition for the specific element is set to a unit velocity. Thus, the influence matrix has 995 rows by 918 columns.

The velocity boundary conditions selected for the example problem are shown in Figures 3.2 and 3.3. The BE simulation was executed using this velocity distribution for a frequency of 500 Hz, with all of the sources in phase at 0°. The pressure contours calculated at the hologram locations are shown in Figures 3.4 and 3.5. The pressure distribution shown in these figures indicates that the source composition would be difficult to predict based solely on this data. The regions of higher pressures do not necessarily correspond to areas where sources are present. This is expected due to the modal nature of the enclosure response. These hologram pressures were processed using the inverse matrix technique, and a predicted source distribution was calculated. The predicted source composition is shown in Figures 3.6 and 3.7, where the velocity magnitude along the boundary is displayed. Comparison of Figures 3.6 and 3.7 to 3.2 and 3.3 provide verification of the technique. The velocity composition is accurately reconstructed, with the contributing elements easily noted. The sources are also clearly identified in the phase plots shown in Figures 3.8 and 3.9 with the color green corresponding to zero phase. A random phase pattern exists for the noncontributing sources that formed the rigid barrier.

3.2 In-Flight Microphone Array Measurements

This section discusses the in-flight microphone array measurements made aboard the Cessna 182E test aircraft. The aircraft was flown on April 26, 1999, departing and landing at Stinson Airfield in San Antonio, Texas. During the flight, acoustic data was collected at several locations throughout the cabin during cruise conditions to form the hologram data set. The acoustic data was processed and used to implement the influence matrix technique, predicting contributions from panel groups to the overall cabin noise. This activity is reported Section 3.3.

3.2.1 Instrumentation

The array was composed of 8¼-inch ICP microphones mounted in a lightweight, wooden fixture shown in Figure 3.10. The array microphones were spaced 2 inches apart. Spacers and rubber bumpers were affixed to the top and bottom ends of the array, creating an offset of 1¼-inch between the heads of the microphones and the measurement surface. An additional 4¼-inch ICP microphones were positioned in the cabin, mounted at the same locations as the interior microphones used for the previous in-flight data exercise and ground test reported in Section 2. These locations are referred to as AC1 through AC4, corresponding to the pilot, co-pilot, right passenger seat, and left passenger seat positions. A microphone amplifier powered the microphones, and power to the amplifier was provided by the DC power supply running off of internal batteries. The microphone data was recorded using a 16-channel DAT recorder. Before the flight, each of the twelve microphones was calibrated using an acoustic calibrator.

3.2.2 Array Measurements

The hologram data were recorded for the 75 percent power cruise flight condition (C75). These conditions were maintained for the duration of the flight. Array measurements were conducted for 52 locations throughout the cabin. The locations were concentrated around the front windshield, dash, and area below the dash, as well as near the forward and rear side windows, resulting in a total of 416 microphone locations within the cabin. The microphone

---

locations are most easily visualized in the BE model to be discussed in Section 3.3. The microphone array was moved from position to position during flight, with each position denoted by a pair of white markers for aligning the top and bottom of the array. The microphone positions were spaced at a nominal distance of 3" apart, forming grids with a 2" vertical and 3" horizontal spacing. Several representative locations are pictured in Figures 3.11 through 3.16. Data were collected at each location for 1.5 to 2 minutes, so that adequate data would be available for spectral analysis in the frequency range out to 1,000 Hz.

The time history data was post-processed using a signal analyzer capable of producing cross spectra. Using the four fixed cabin microphones as references, cross-spectral functions were computed between these references and the eight array microphones for each of the 52 measurement locations. The data were processed at a sampling frequency of 2.56 kHz with a record size of 1,024 points. This established a bandwidth of 1 kHz with a frequency resolution of 2.5 Hz. A Hanning window was applied and 130 averages were completed for each data set. A typical spectrum measured by one of the hologram microphones is shown in Figure 3.17.

3.3   Acoustic Holography Results

3.3.1 Boundary Element Model

A BE model of the Cessna 182E aircraft cabin was constructed in order to implement the influence matrix technique. This model was generated using the loft surfaces from a CAD model of a typical Cessna 182. The BE model is symmetric about the longitudinal axis and the right half is shown in Figure 3.18. The front seats are included, but are de-featured and modified to simulate the volume of an actual seat and passenger. The BE model is effectively "hard walled," with an infinite impedance present along the boundaries. There are 1,924 elements with a characteristic element length of 4 to 5 inches. Following the guideline of 4 to 6 elements per wavelength, the model is definitely suitable for analysis up to 500 Hz. The hologram data recovery nodes are displayed in Figure 3.19. These nodes correspond to the 416 microphone array measurement locations of the holography flight data.

Initially, the potential sources were limited to elements composing the front windshield, firewall, dash, and the front and rear windows for the GAH evaluation. These 376 elements are shown in Figure 3.20. Limiting the number of potential sources was enacted in an attempt to enhance the prediction capability. If there are more hologram measurement locations than potential sources, the problem is "over-defined" and increased accuracy of source prediction should result. However, since the number of hologram locations is limited, there is a risk of restricting the potential sources too severely, effectively defining an inadequate source group. In this case, there may be actual sources that are not included in the group of potential sources. For a problem such as the aircraft cabin, a balance must be achieved, since a complex source distribution is anticipated.

For the 416-node hologram grid, the influence matrix has dimensions of 416 rows by 376 columns. Influence matrices were formed for several selected frequencies corresponding to prominent blade passage, engine rotation, engine exhaust tones and combinations thereof. The following discussions will concentrate on the results from the 80 Hz and 120 Hz models.

3.3.2 Panel Group Contributions

The in-flight hologram pressure distribution at 80 Hz is shown in Figures 3.21 and 3.22. The front view is looking into the dash and firewall from inside the cabin. The pressure field is quite complex, with pressure extremum spread throughout the hologram region. Based upon this pressure distribution, a predicted velocity composition at 80 Hz is shown in Figures 3.23 through 3.26. For this example, the inverse of the influence matrix was constructed using 100 singular values. The pressure distribution in the hologram, simulated using the prediction velocities, is shown in Figures 3.27 and 3.28. A consistent pressure distribution is observed between the measured and simulated field near the windows; however, simulated pressure magnitudes are lower. The agreement is not as good for the hologram locations near the front windshield, dash, and firewall. Here, certain features in the pressure distribution are replicated while most are absent.

These results led to a second attempt at generating the inverse of the influence matrix. Typically, when increasing the number of singular values used to construct the inverse of the influence matrix, increased accuracy is expected, especially when attempting to reproduce a complex pressure field. However, caution must be exercised in selecting the appropriate number of singular values. The pseudo-inverse of a matrix is calculated using the inverse of the singular values of that matrix. Thus, a sharp decrease in singular value magnitudes can lead to inaccuracies introduced by a poorly composed pseudo inverse. Typically, for the influence matrix technique, a natural break point is sought in selecting the number of singular values necessary to accurately approximate the hologram pressure distribution. The magnitude trend of the singular values for the 80 Hz influence matrix is shown in Figure 3.29. Reviewing this plot, no strong candidate for a break point is clearly evident; therefore, for the second attempt at calculating the pseudo-inverse of the influence matrix, 200 singular values were tried. The source composition for this case is exhibited in Figures 3.30 through 3.33. A dramatic shift in the source distribution is observed for this case when compared to the 100 singular value case. The velocity magnitudes at the firewall have increased substantially, now becoming dominant; however, little change is noted in the hologram locations near the side windows as seen in Figure 3.34. Referring to Figure 3.35, additional features in the hologram pressure distribution near the dash and firewall are now present. In several regions of the hologram, the pressure magnitudes are virtually unchanged. This result could be expected. An increase in the source velocity magnitudes suggests that an increase in the resulting pressure magnitudes will result; however, if the sources are properly phased, they can make up a bound field and result in no additional radiation.

These results are difficult to interpret due to the uncertainty of convergence of the influence matrix inverse. The hologram pressure distributions observed for the 100 and 200 singular value cases are similar, with some refinement present for the increased singular value condition; however, the source compositions are markedly different. The 100 singular value case indicates the dash and windshield are the most pronounced sources at this frequency, while the 200 singular value case points to the firewall as the region with the highest source velocities. This is partially explained by the vector plots of Figures 3.36 and 3.37. These plots decompose the pressures at the four cabin reference microphone locations into contributions from individual panel groups. The cancellation that occurs between the radiated fields created by different panel groups is apparent. The surprising result is that the phase relationships are not consistent

between the 100 and 200 singular value cases. This furthers the possibility that the inverse of the influence matrix has not properly converged. In addition, it is important to note the manner in which the radiated fields from different panel groups combine to produce an overall level at a given location. Application of noise treatment or reduction in vibration levels of a given group may decrease the noise levels, or actually increase them in certain regions.

The SPL values for the 80 Hz case at the 4 reference cabin microphone locations are included in Table 3.1. As shown above, a portion of the hologram pressure field near the windows is reproduced; however, the levels at the microphone locations are not well matched, indicating this portion of the pressure field is not accurately reproduced. Since the hologram locations are concentrated along the boundaries near the sources, other regions of the enclosure may not be as well matched.

Table 3.1 Summary of SPL at Cabin Microphone Locations – 80 Hz.

Location	Location ID	SPL (dB)		
		In-Flight	Predicted	
		Holography Data Flight	100 Singular Values	200 Singular Values
Pilot	AC1	93.5	101	101
Co-pilot	AC2	91.9	98.9	109
Right Passenger	AC3	107	92.5	104
Left Passenger	AC4	109	92.6	98.7

In general, a similar overall trend in the results is seen for the 120 Hz case. The measured hologram pressures are shown in Figures 3.38 and 3.39. The predicted velocity field using 100 singular values to form the influence matrix inverse is shown in Figures 3.40 through 3.43. The simulated pressure field created using these predicted velocities is displayed in Figures 3.44 and 3.45. This case was also run using 200 singular values, and similar results are noted. The predicted velocity field for 200 singular values is shown in Figures 3.46 though 3.49. Again, a sharp increase in velocity magnitudes is noted where the highest levels have now shifted from the windows, windshield, and dash to the firewall. The simulated pressure distribution in the hologram in displayed in Figures 3.50 and 3.51. Again, refinement is observed, especially in the dash and windshield areas. Yet, little change is noted in the region around the windows. The SPL results for the 4 reference microphones for the 120 Hz case are documented in Table 3.2.

3.3.3 Extended Model Results

The results presented thus far indicate that the Cessna 182 source identification exercise included a source field that was perhaps over restricted, as exhibited by the predicted pressure distribution in the hologram. A better match between the actual measured pressures and the predicted pressures calculated from the GAH technique was anticipated; however, if the proper source elements are not included in the analysis, the appropriate features in the hologram cannot be reproduced and the predicted source distribution may not be accurate. To address these issues, additional source elements were added to the inverse matrix technique solution.

Table 3.2 Summary of SPL at Cabin Microphone Locations – 120 Hz.

Location	Location ID	SPL (dB)		
		In-Flight	Predicted	
		Holography Data Flight	100 Singular Values	200 Singular Values
Pilot	AC1	98.3	71.7	92.4
Co-pilot	AC2	98.8	89.5	85.2
Right Passenger	AC3	98.2	91.3	95.9
Left Passenger	AC4	99.3	86.2	92.4

The additional elements were added along each side of the cabin, starting at the back edge of the door, forward to the firewall. The floor and the forward portion of the ceiling were also included. The complete set of potential source elements is shown in Figure 3.52. This figure is compared to Figure 3.20 to show which elements were added. The GAH technique was applied with this source set for the 80 Hz case. The computer run time for a single frequency point exceeded 100 hours. The measured and predicted hologram pressure distributions are shown in Figures 3.53 and 3.54. The three predicted distributions shown are for using 100, 200, and 400 singular values to form the inverse of the influence matrix. The trend shown in these figures is consistent with that seen in the previous results. Increasing the number of singular values used to create the influence matrix inverse results in refinement of the pressure distribution. Numerous features are reproduced in the hologram pressure distribution for the 100 and 200 singular cases, while others are absent. When 400 singular values are included, the match between the measured and predicted hologram field is excellent. In all cases presented here, the levels for the predicted cases are slightly lower than the measured levels.

The predicted source distribution for these cases is seen in Figures 3.55 to 3.58. Again, the trends observed in the previous results are re-established. The 100 singular values case points to the windows, dash, windshield, and trim panels below the dash as areas with high source velocities. The 200 singular values case shows similarities; but as before, the source velocities are much increased and additional regions of high source velocities appear, namely, the firewall. When 400 singular values are used to form the inverse of the influence matrix, the source velocities increase dramatically in magnitude and tend to become more evenly distributed throughout the source elements, no longer confined to specific regions of the boundary.

Insufficient source representation is believed to be the main reason that the GAH technique did not reproduce the hologram pressure distribution using vectors with singular values within 0.001 of the largest singular value. This is supported by the data presented when comparing the 100 singular value results with increased source representation. The source representation for the receiver should span the complete enclosure to ensure all possible degrees of freedom in the representation. The use of the higher order singular values is known to be mathematically destabilizing and results in the unrealistic source velocity predictions.

Measurement of the hologram pressures in the bound field may also produce poor pressure prediction within the enclosure due to the over-emphasis on representation of the bound field. It is important to remember that the GAH technique was devised to use as a source

identification tool. The predicted pressures in the hologram plane are the only check to assure the BE model and GAH technique are performing properly; however, this should not be the end result of the analysis. An accurate representation of the source field is the desired result; however, this is the unknown. One potential improvement would be to acquire the hologram measurements outside of the bound field. Hologram locations should be added particularly in regions of interest, such as passenger locations for vehicles or operator locations for noise generating equipment. This would help "weight" these areas in the processing such that a more accurate pressure field in these regions would result. In addition, the evanescent field features would be de-emphasized.

Another possible complication relates to modeling aspects of the Cessna 182E cabin. The cabin was modeled as a hard walled enclosure. A more accurate representation would include impedance values defined for these walls. Most notably, the aft partition that forms a barrier between the cabin and tail cone is thin and light. Modeling this member as a boundary with finite impedance may modify the modal features of the cabin, especially at the lower frequencies, and improve the accuracy of the results.
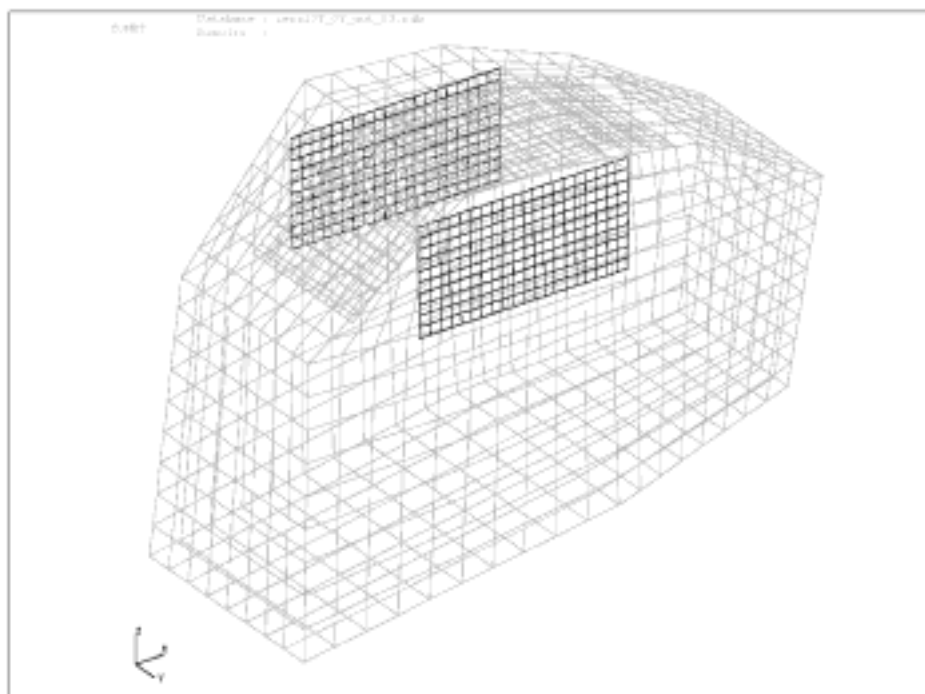
Figure 3.1 BE Model of Aircraft Cabin with Hologram Represented by Data Recovery Nodes.
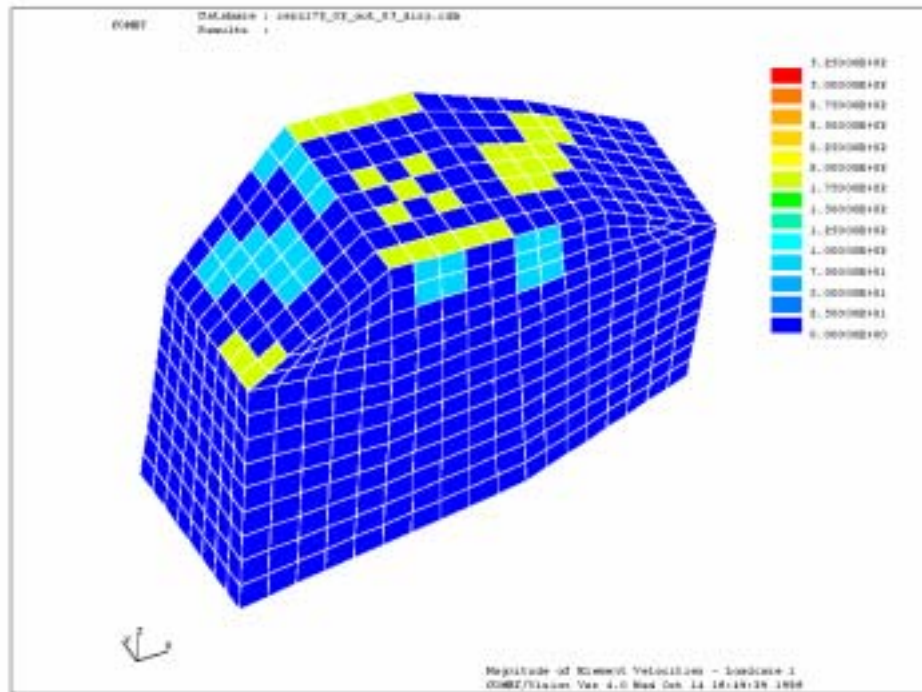
Figure 3.2 Velocity Magnitude Distribution for Verification Problem – Left View.
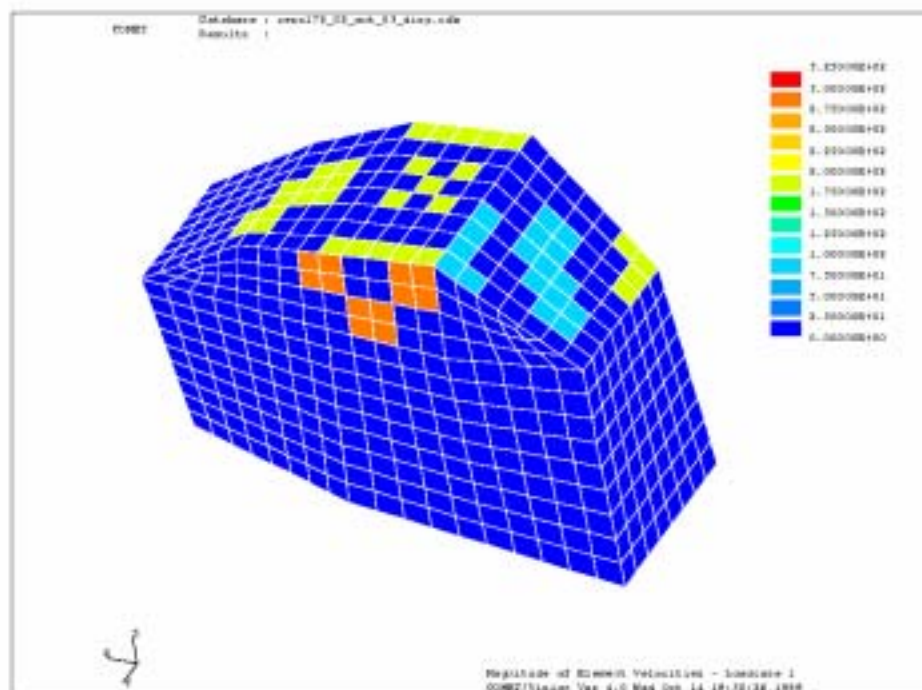
Figure 3.3 Velocity Magnitude Distribution for Verification Problem – Right View.
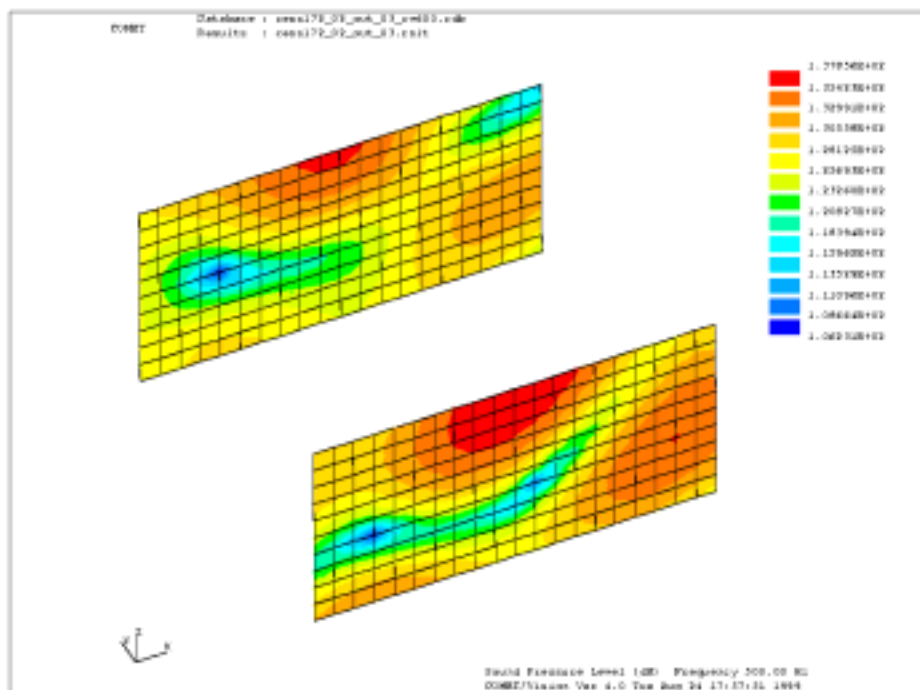
Figure 3.4 Hologram Data Recovery Pressure Contour – Side Panels.
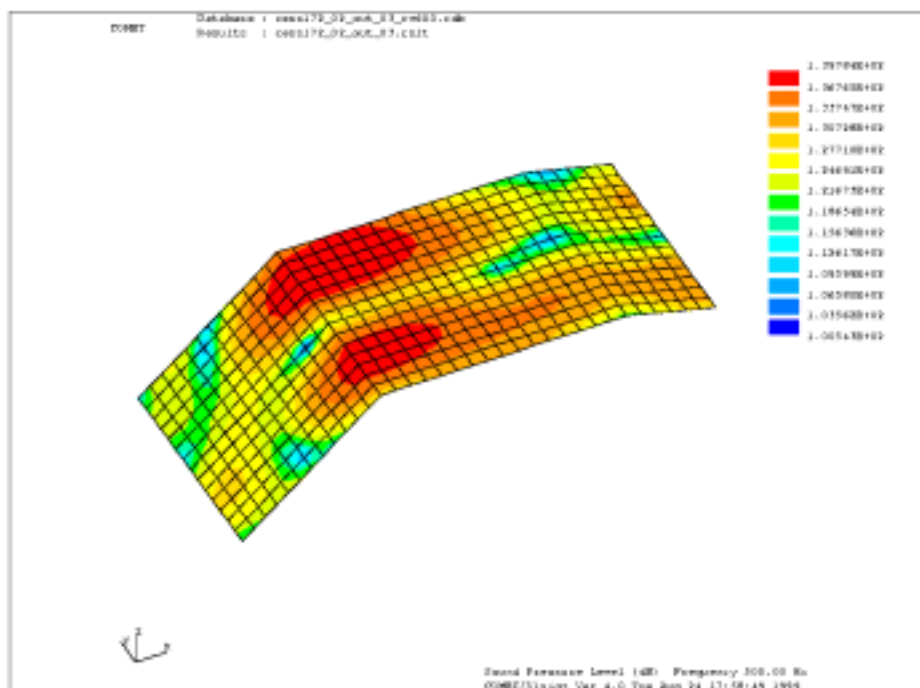
Figure 3.5 Hologram Data Recovery Pressure Contour – Top Panel.
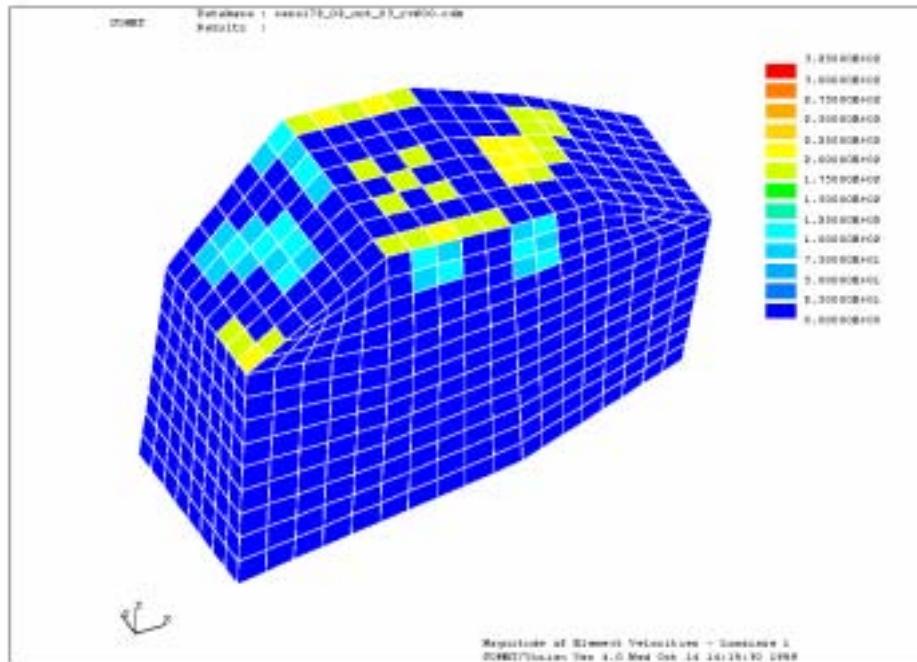
**Figure 3.6 Predicted Velocity Magnitude Distribution for
Verification Problem – Left View.**
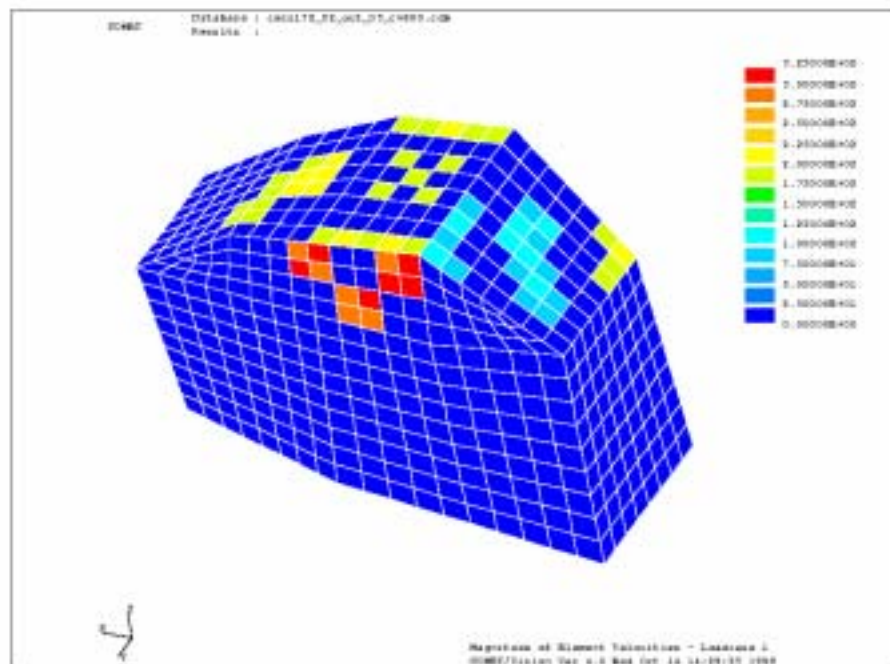
**Figure 3.7 Predicted Velocity Magnitude Distribution for Verification
Problem – Right View.**

Figure 3.8 Predicted Velocity Phase Distribution for Verification Problem – Left View.

Figure 3.9 Predicted Velocity Phase Distribution for Verification Problem – Right View.
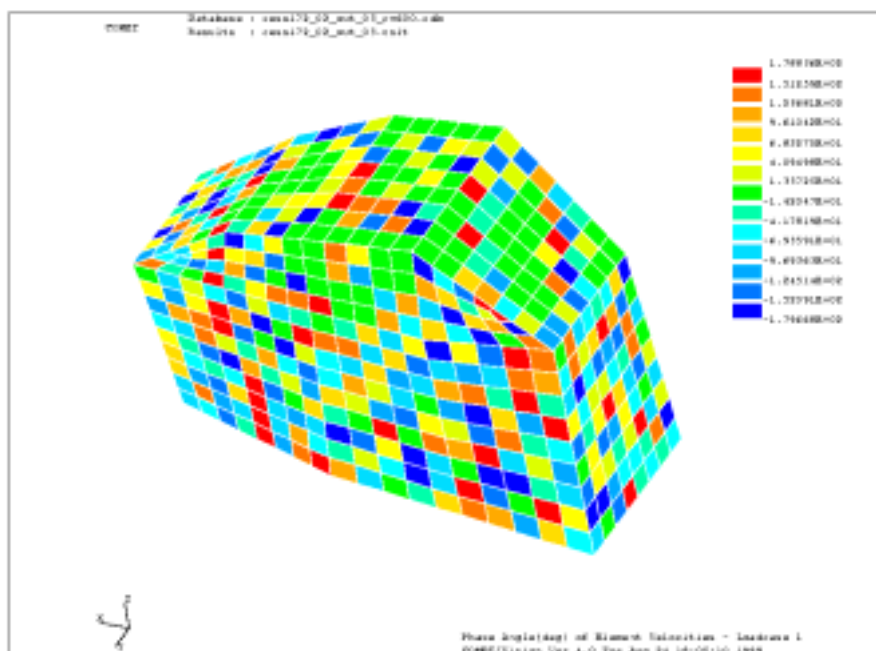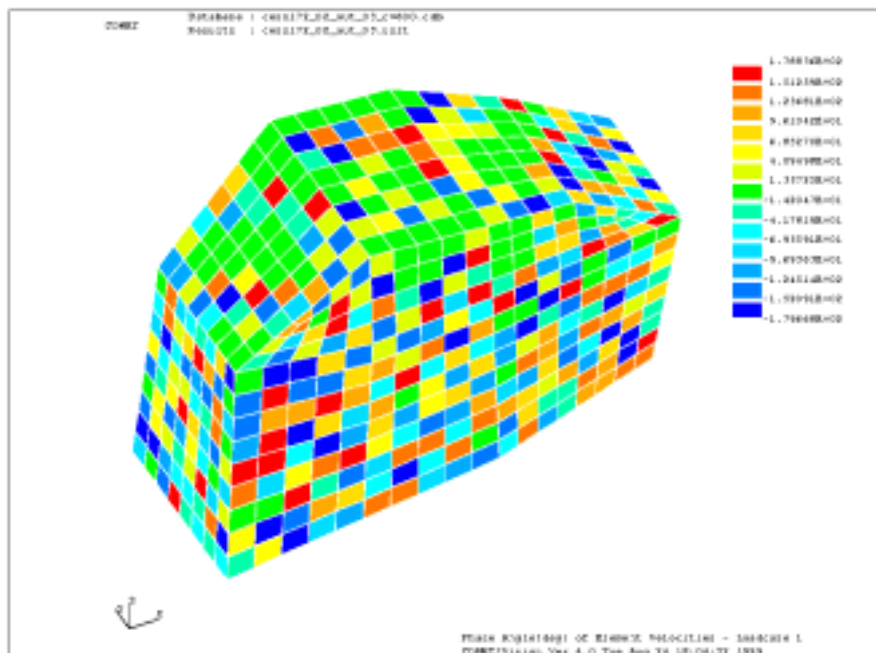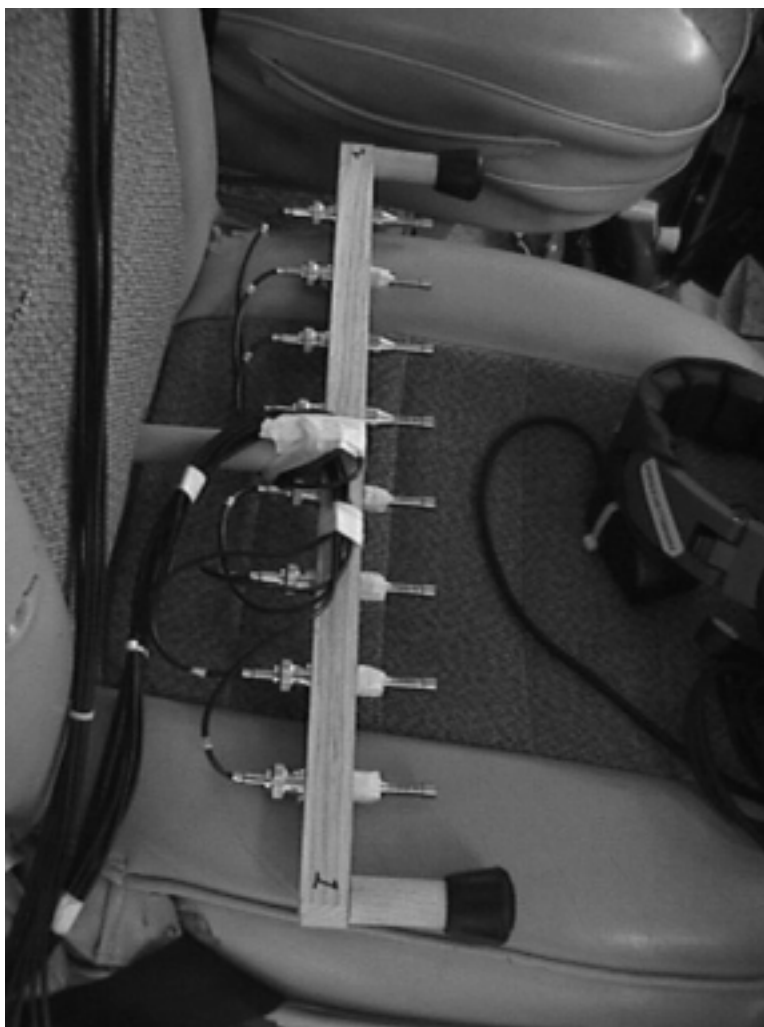
Figure 3.10 Array Microphone Fixture Used for In-Flight Data Collection.

Figure 3.11 Array Measurement Locations for Dash.

Figure 3.12 Selected Array Measurement Locations Along Co-Pilot's Window.
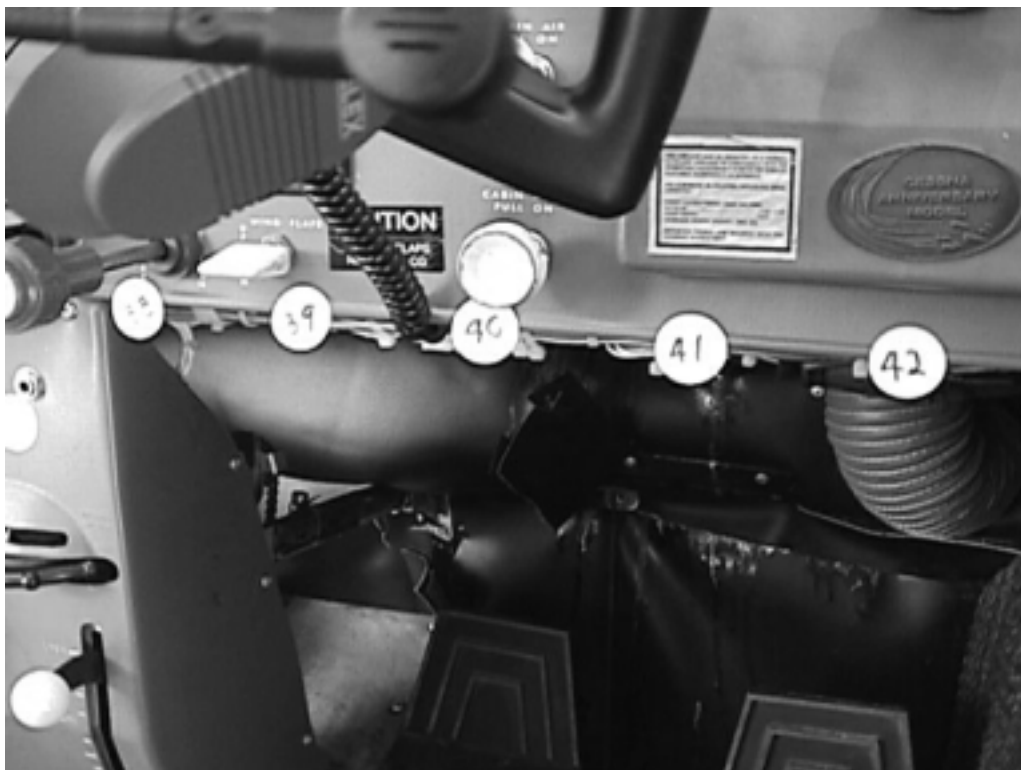
Figure 3.13 Selected Array Measurement Locations Below Dash.

Figure 3.14 Selected Array Measurement Locations Along Left Passenger Window.

Figure 3.15 Selected Array Measurement Locations Along Front Windshield.

Figure 3.16 Selected Array Measurement Locations Along Pilot's Window.
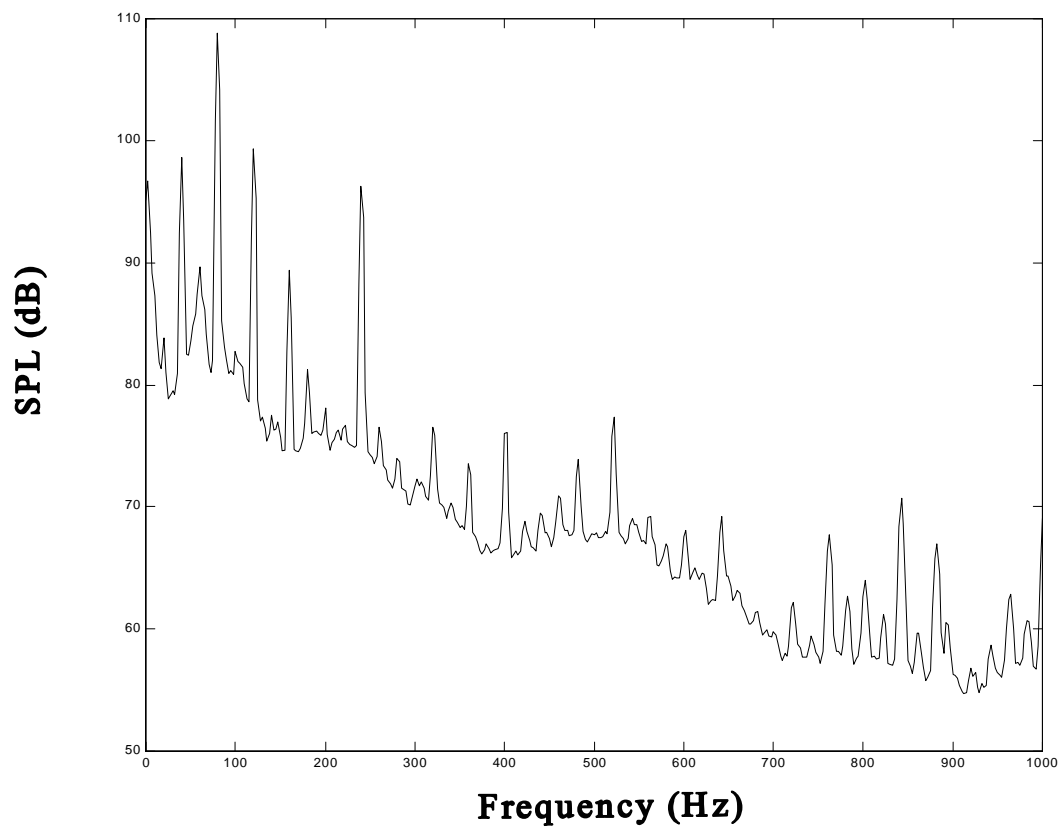
Figure 3.17 Typical Spectra of Array Microphone During Flight.
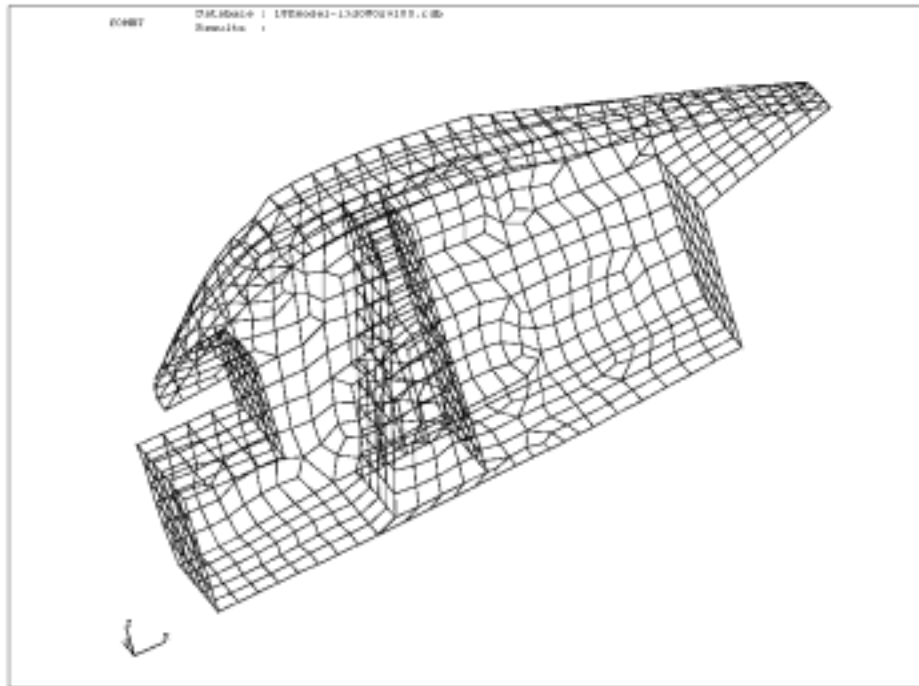
Figure 3.18 Right Side of BE Model.
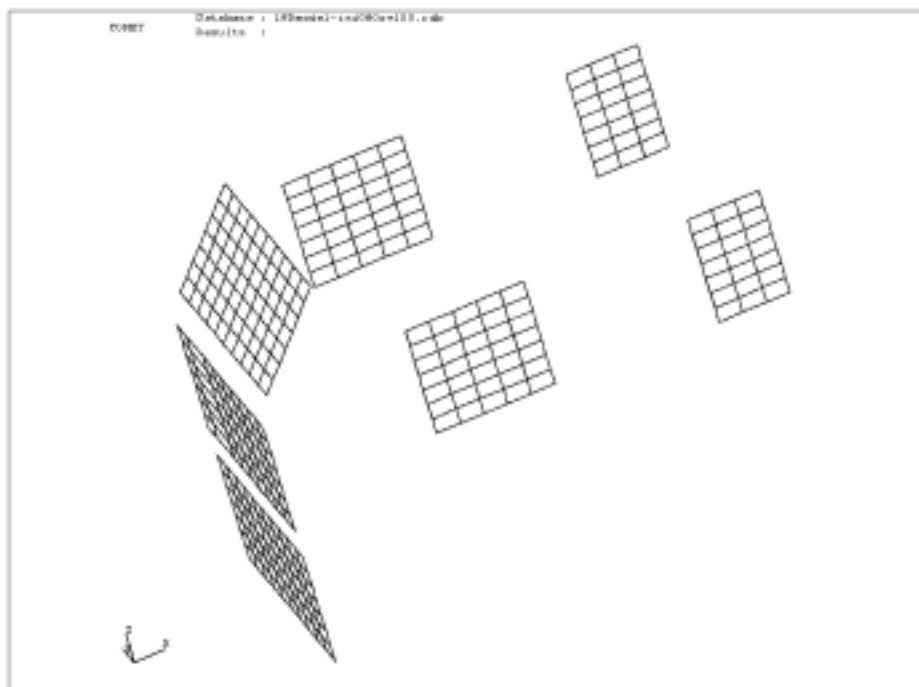
Figure 3.19 Hologram Data Recovery Nodes.
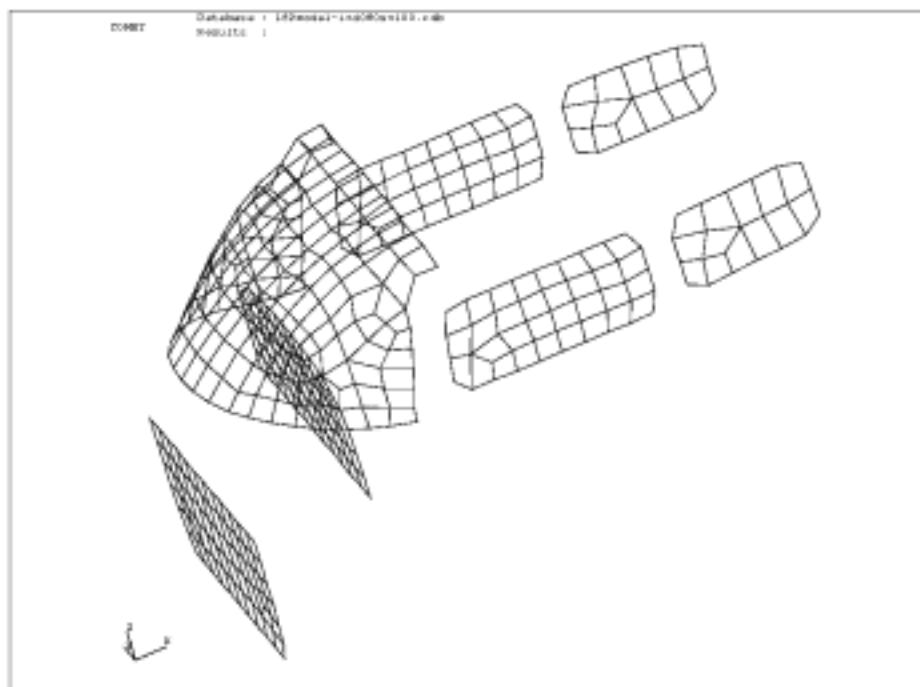
Figure 3.20 Potential Source Elements.
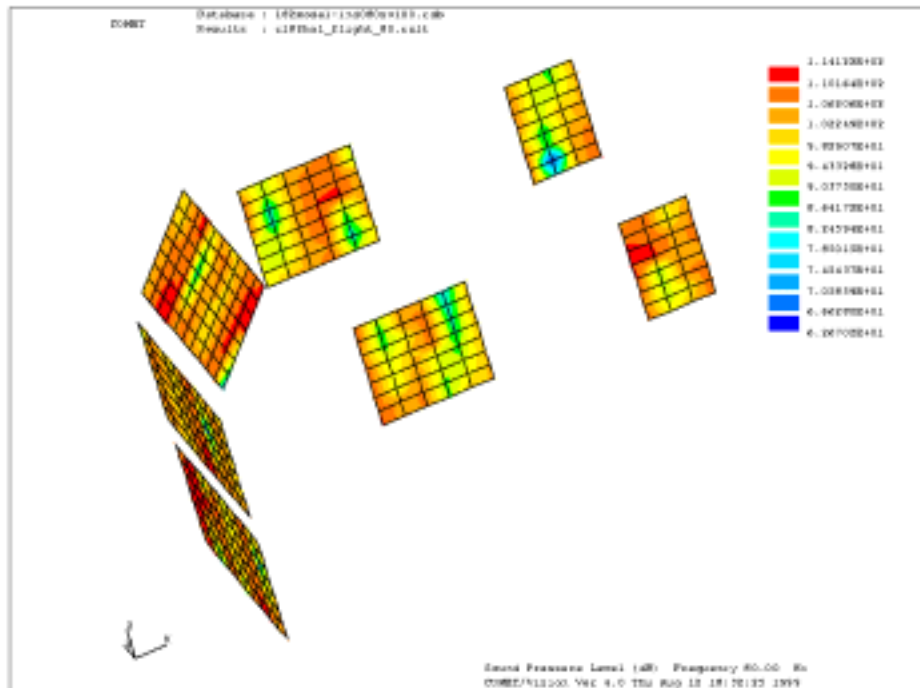
Figure 3.21 In-Flight Acoustic Pressure Measurements at 80 Hz – Isometric View.
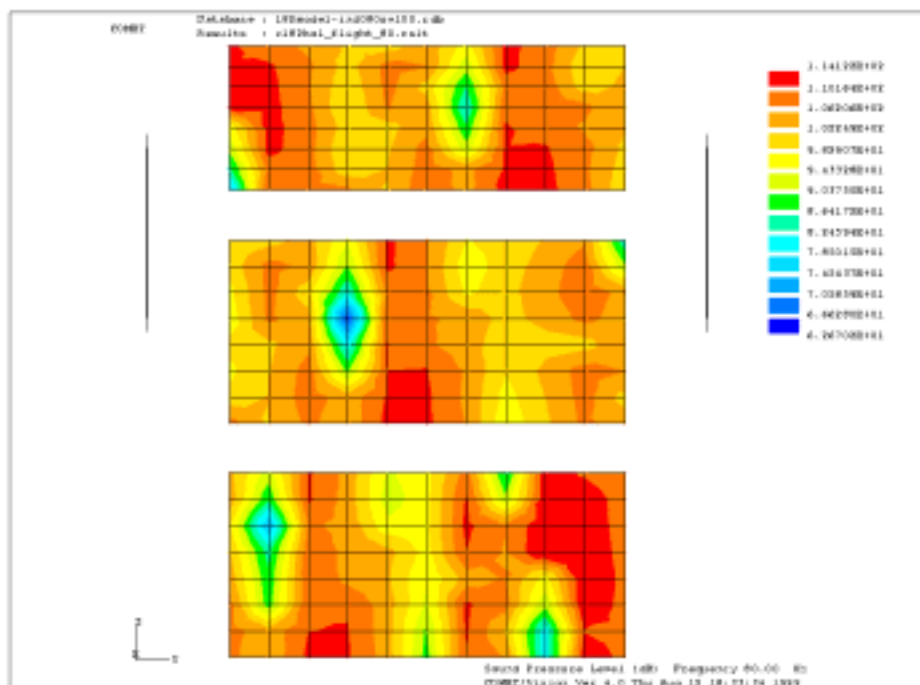
Figure 3.22 In-Flight Acoustic Pressure Measurements at 80 Hz – Front View.
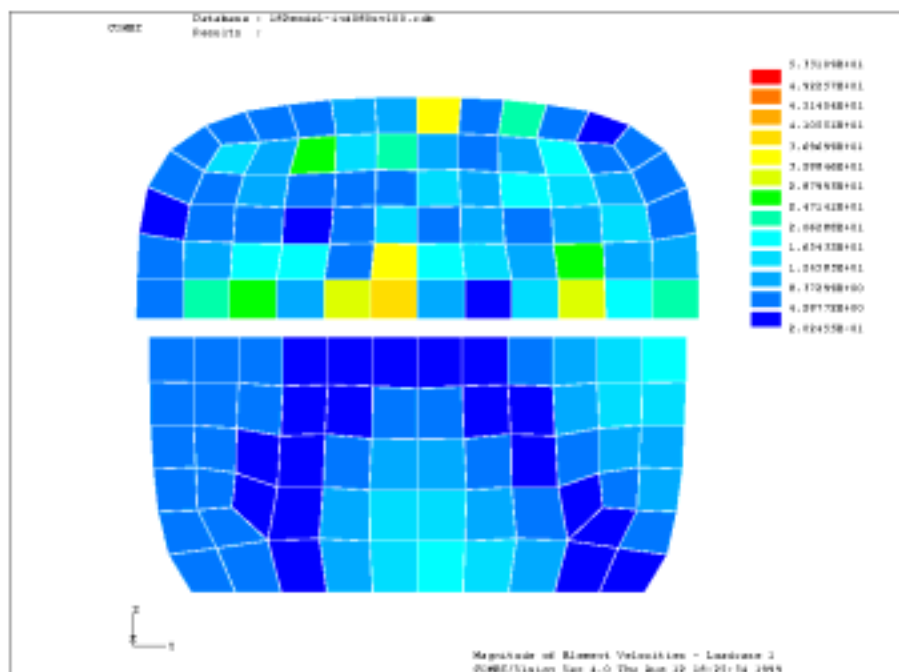
Figure 3.23 Velocity Distribution at 80 Hz Using 100 Singular Values – Dash and Firewall.
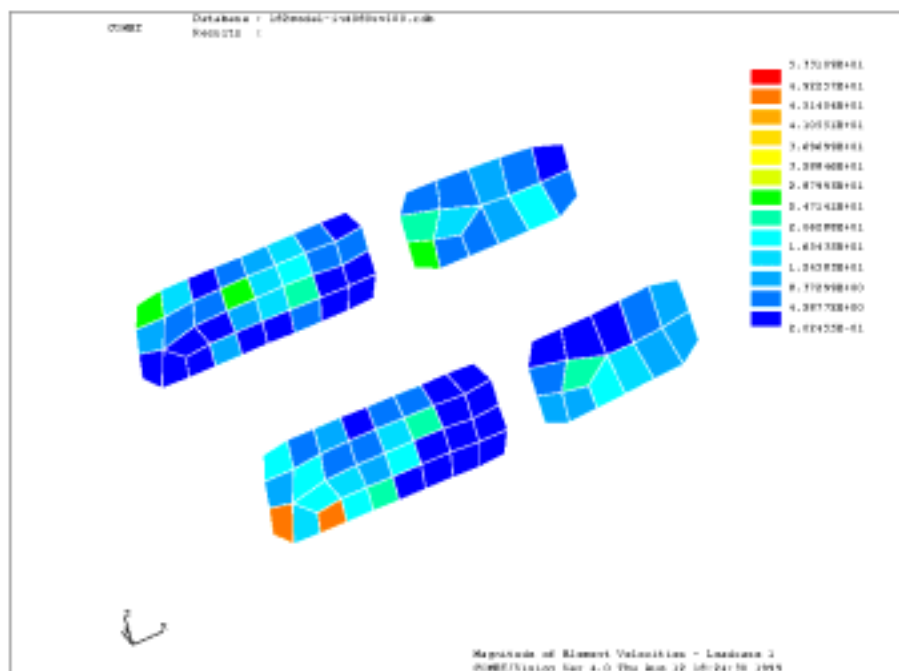
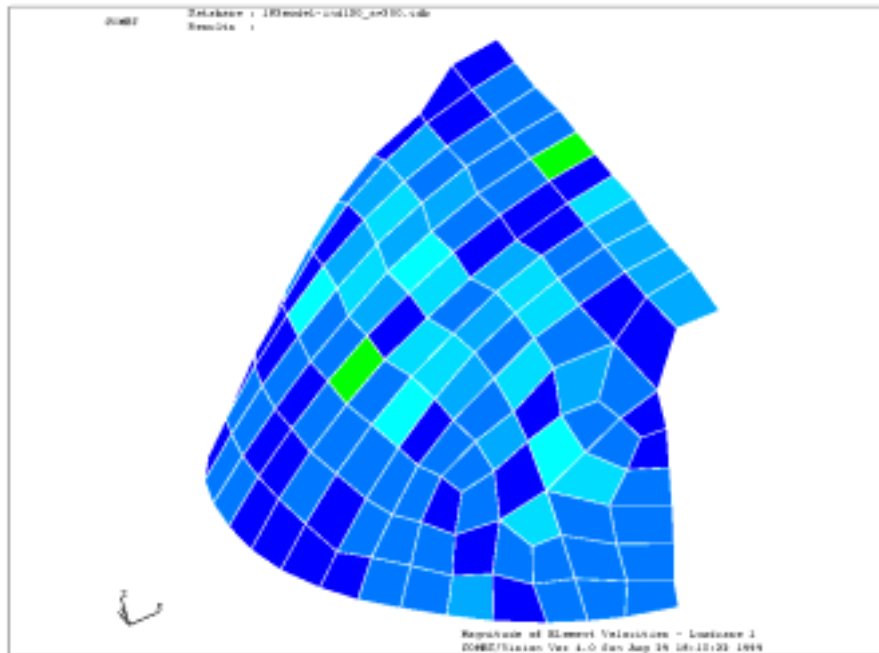**Figure 3.24 Velocity Distribution at 80 Using 100 Singular Values – Windows.**
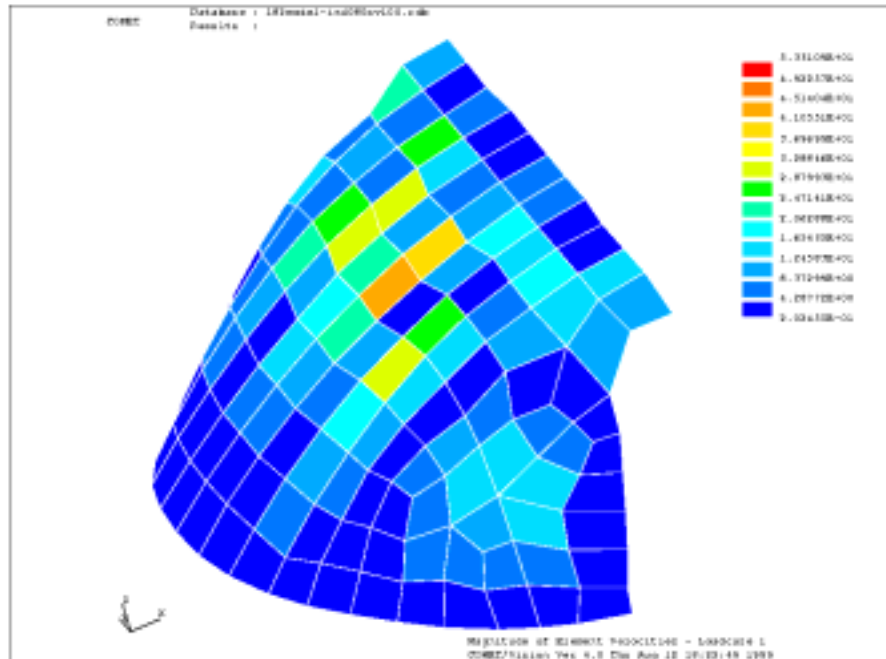
**Figure 3.25 Velocity Distribution at 80 Hz Using 100 Singular Values
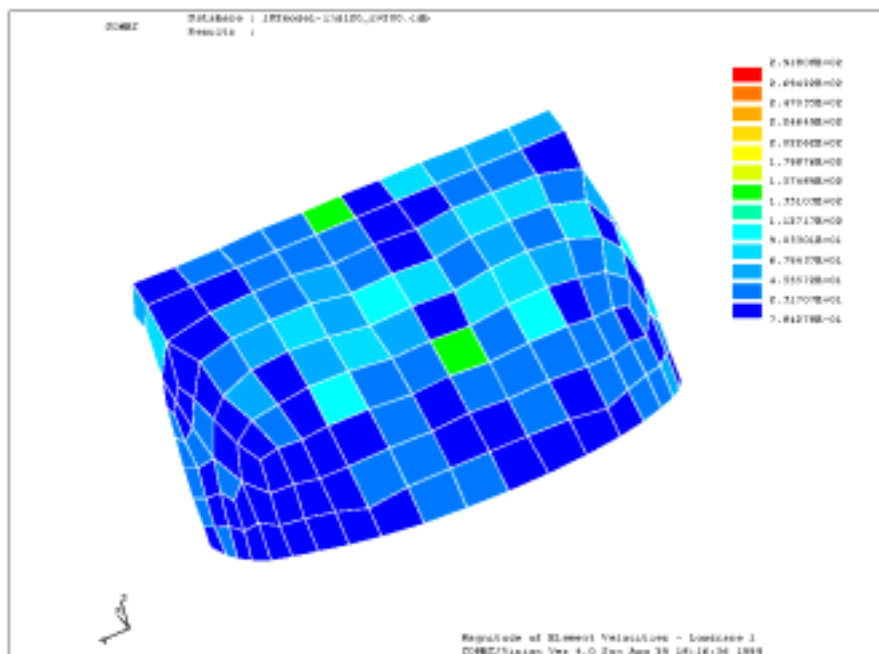– Windshield Side View.**
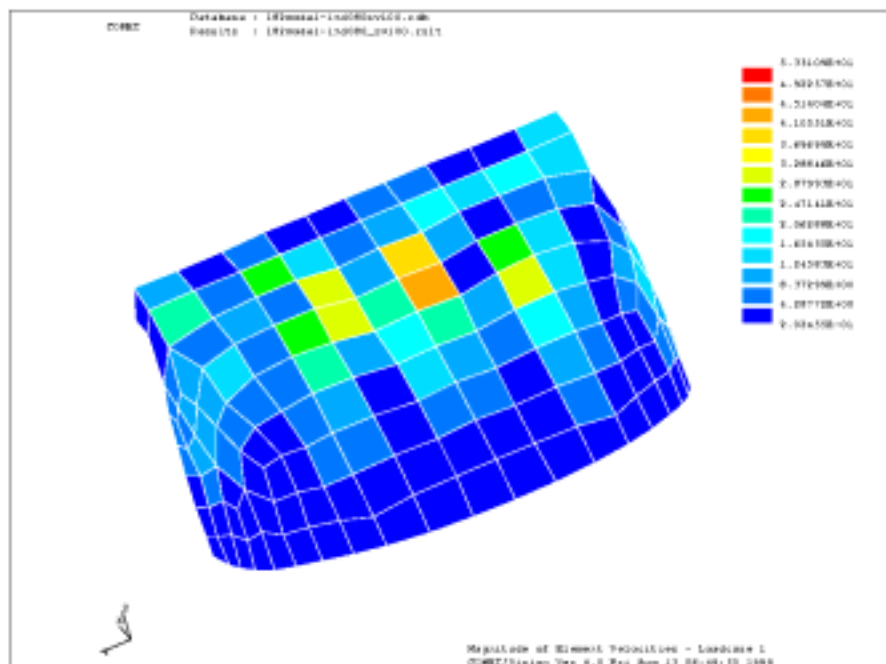
**Figure 3.26 Velocity Distribution at 80 Hz Using 100 Singular Values
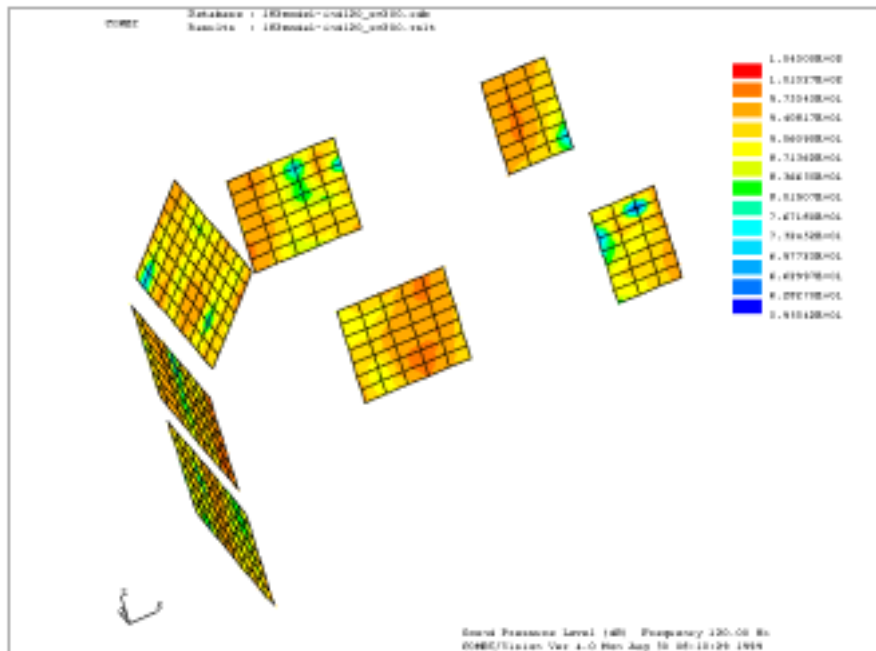– Windshield Front View.**
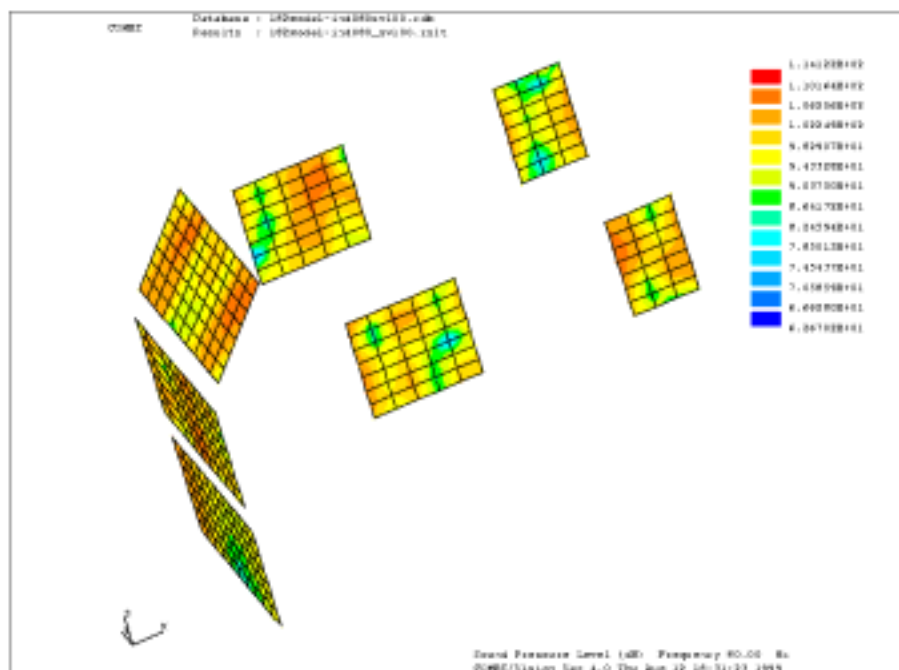
Figure 3.27 Estimated Pressure Field at 80 Hz Using 100 Singular Values – Isometric View.
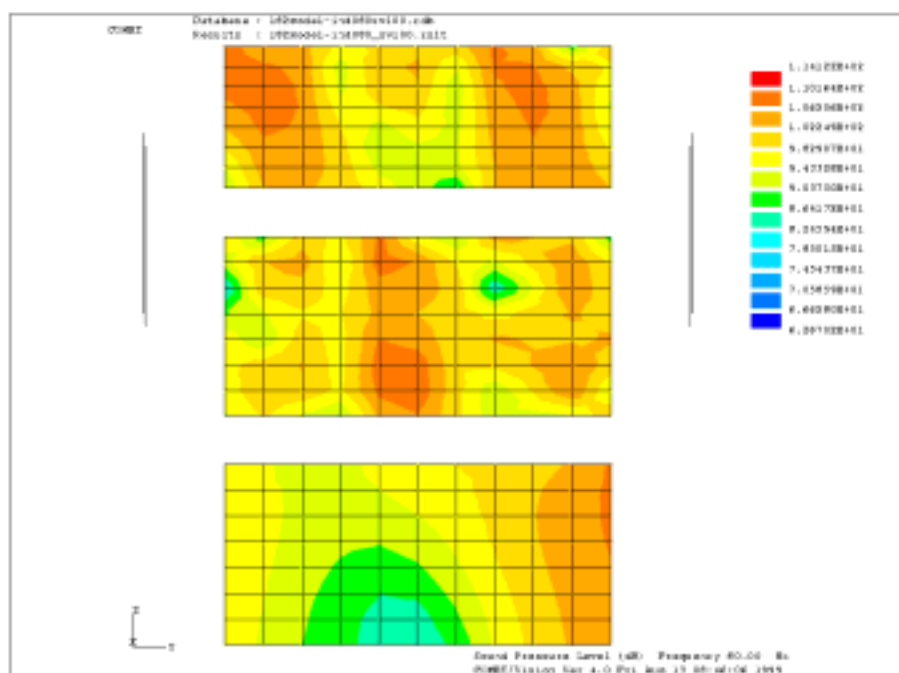
**Figure 3.28 Estimated Pressure Field at 80 Hz Using 100 Singular Values
– Front View.**
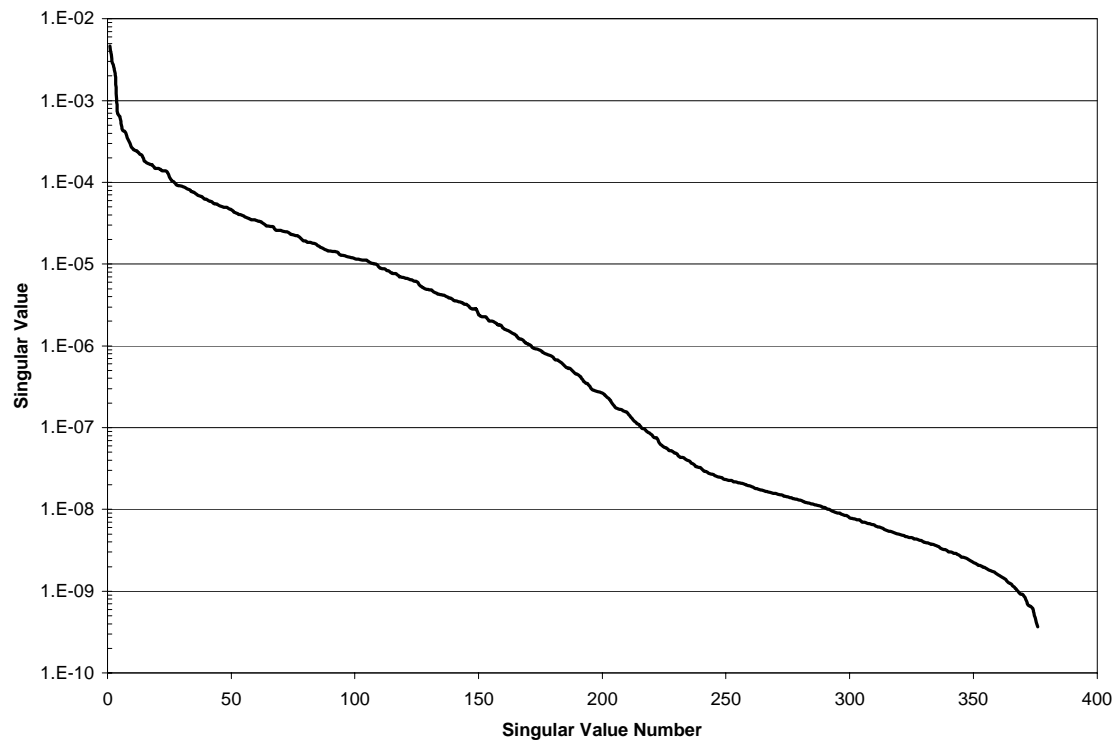
Figure 3.29 Singular Value Trend of 80 Hz Influence Matrix.
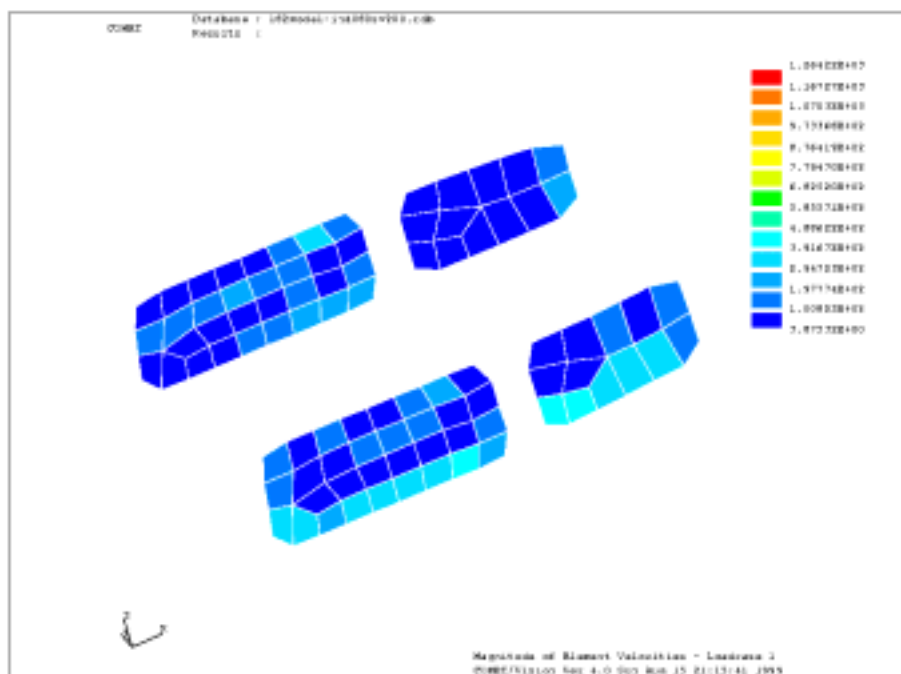
Figure 3.30 Velocity Distribution at 80 Hz Using 200 Singular Values – Windows.
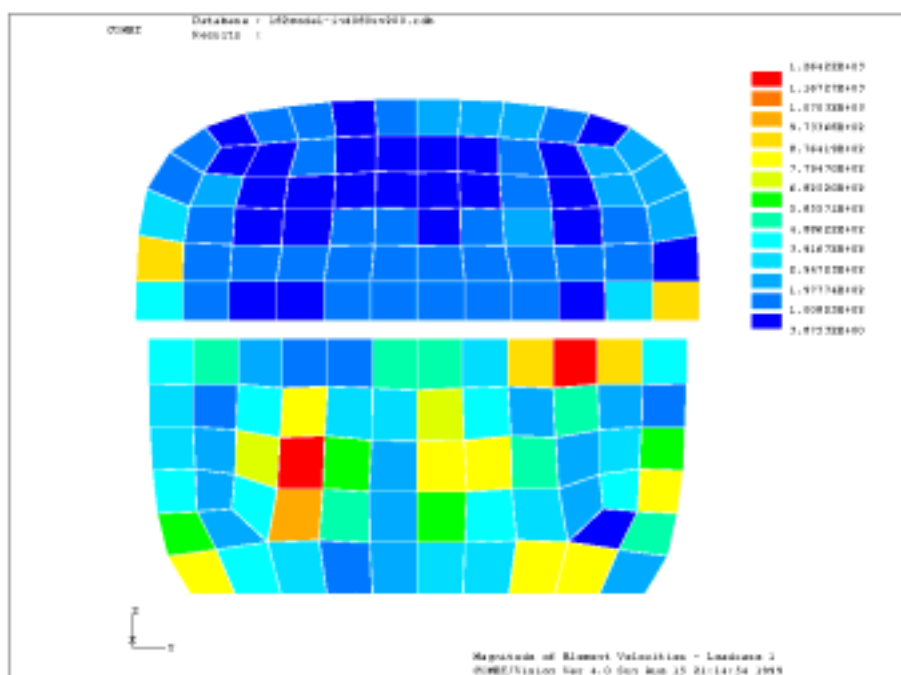
**Figure 3.31 Velocity Distribution at 80 Hz Using 200 Singular Values
– Dash and Firewall.**
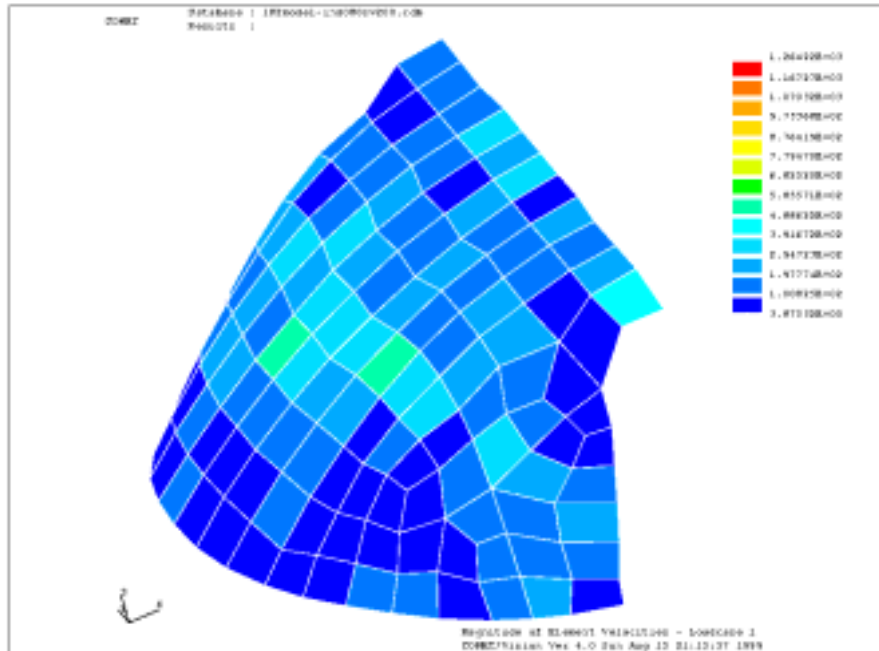
Figure 3.32 Velocity Distribution at 80 Hz Using 200 Singular Values – Windshield Side View.
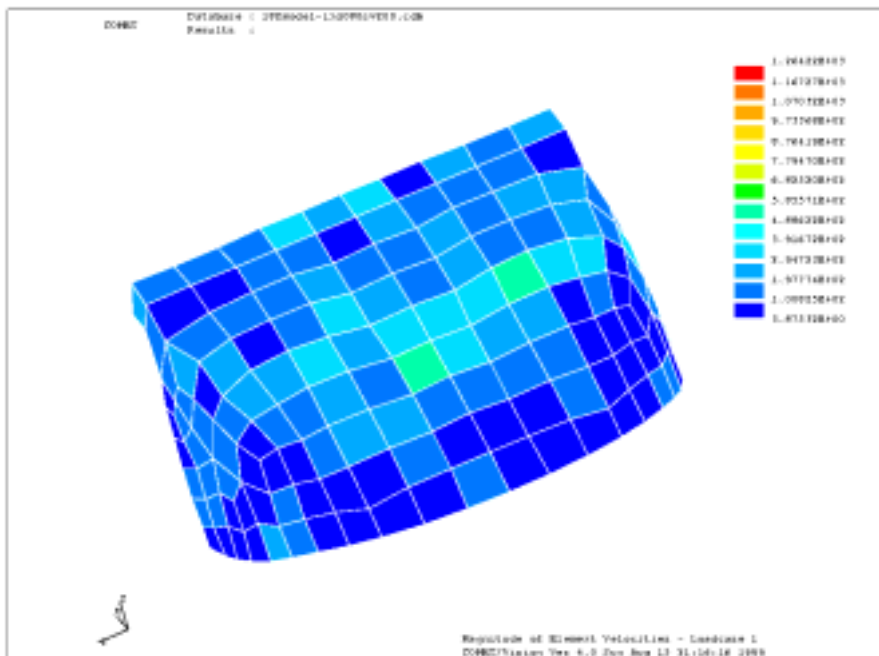
Figure 3.33 Velocity Distribution at 80 Hz Using 200 Singular Values – Windshield Front View.
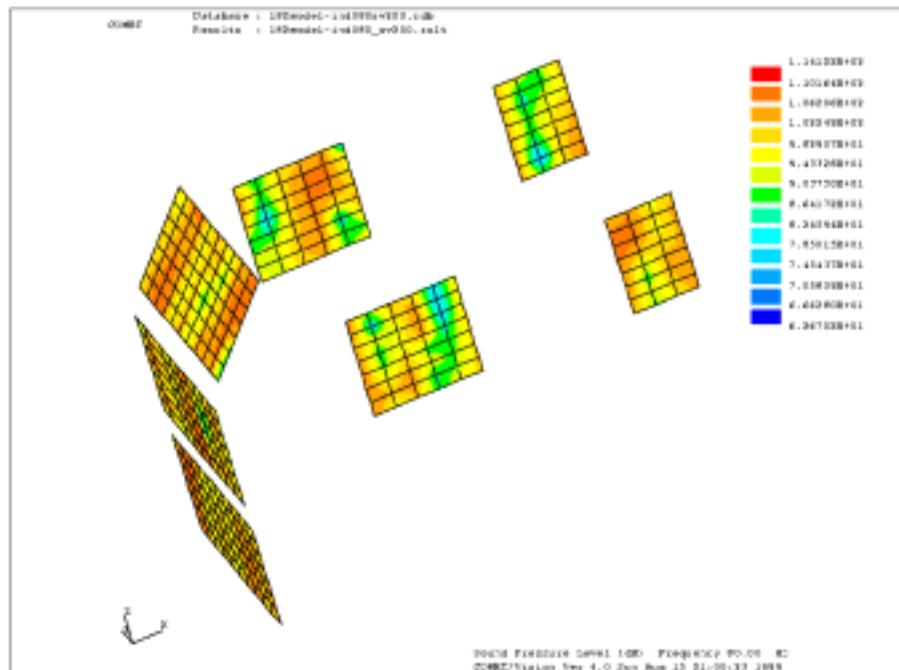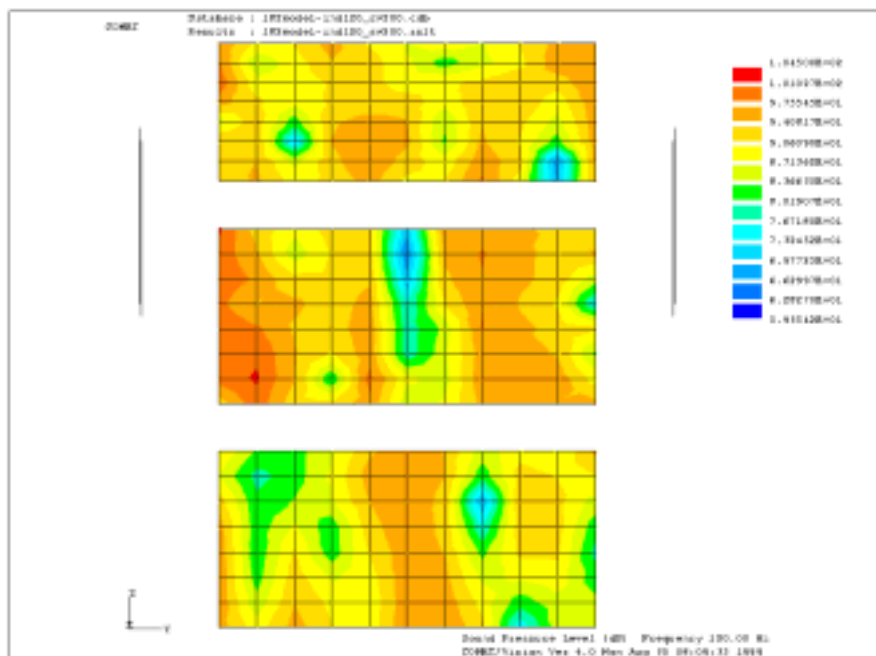
Figure 3.34 Estimated Pressure Field at 80 Hz Using 200 Singular Values – Isometric View.
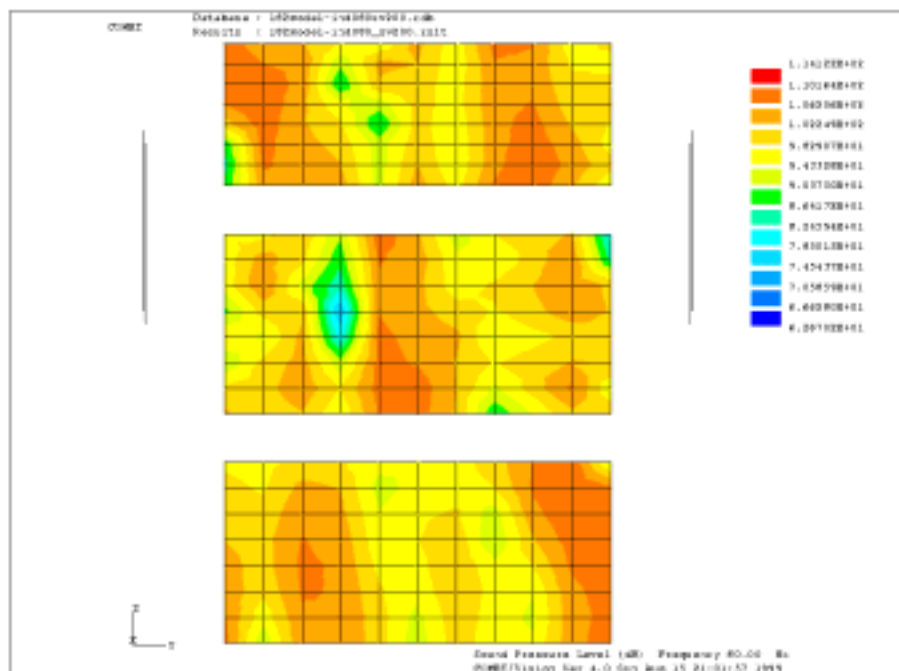
**Figure 3.35 Estimated Pressure Field at 80 Hz Using 200 Singular Values
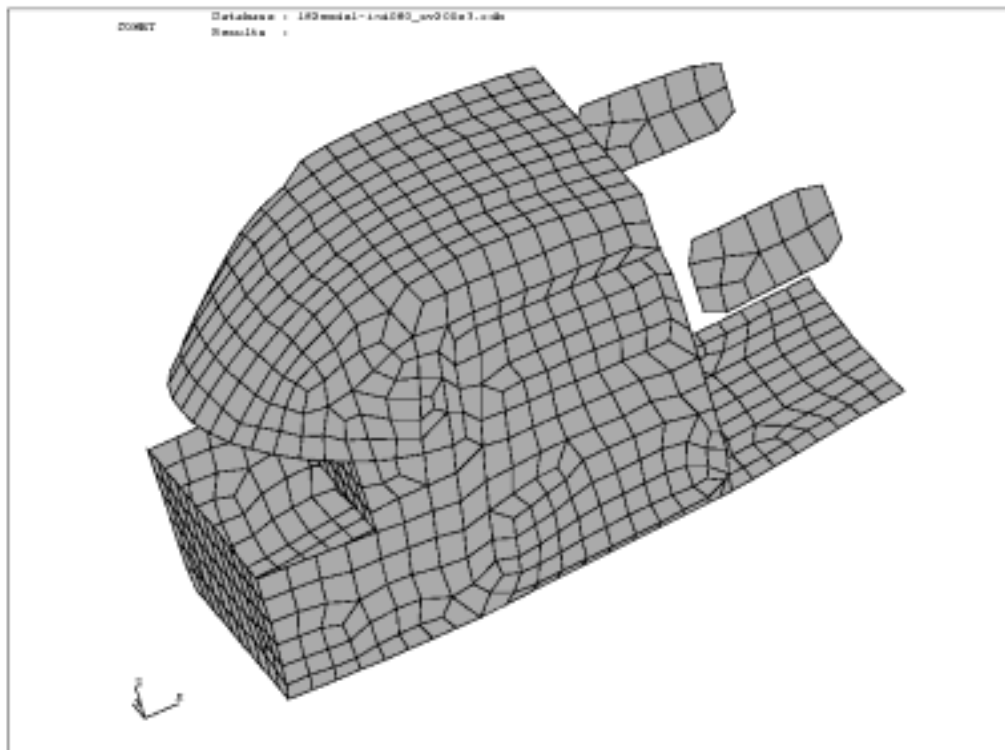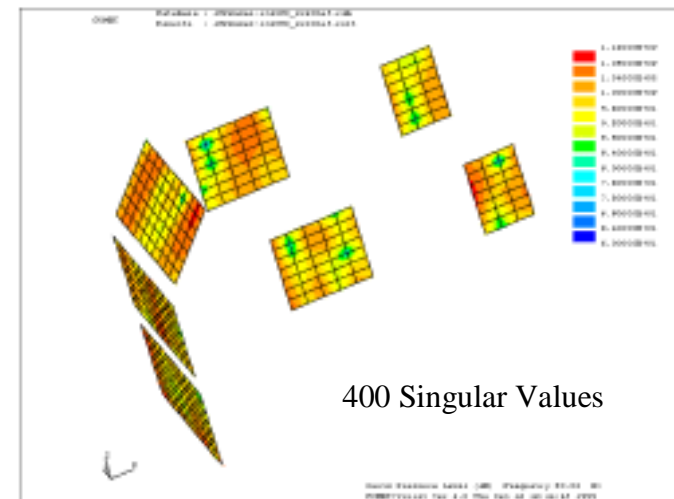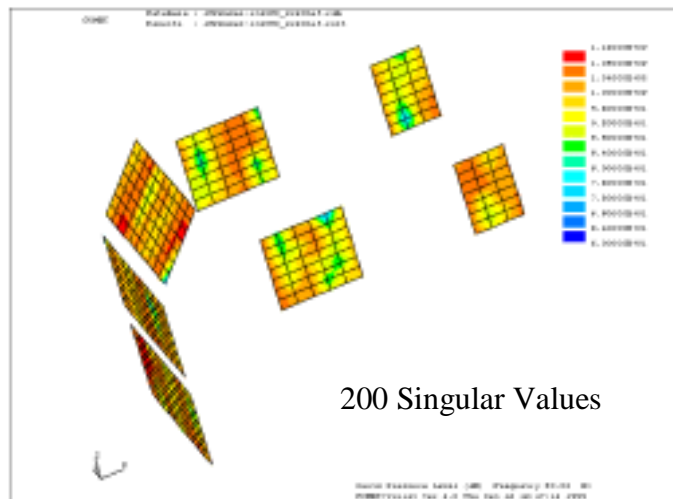– Front View.**
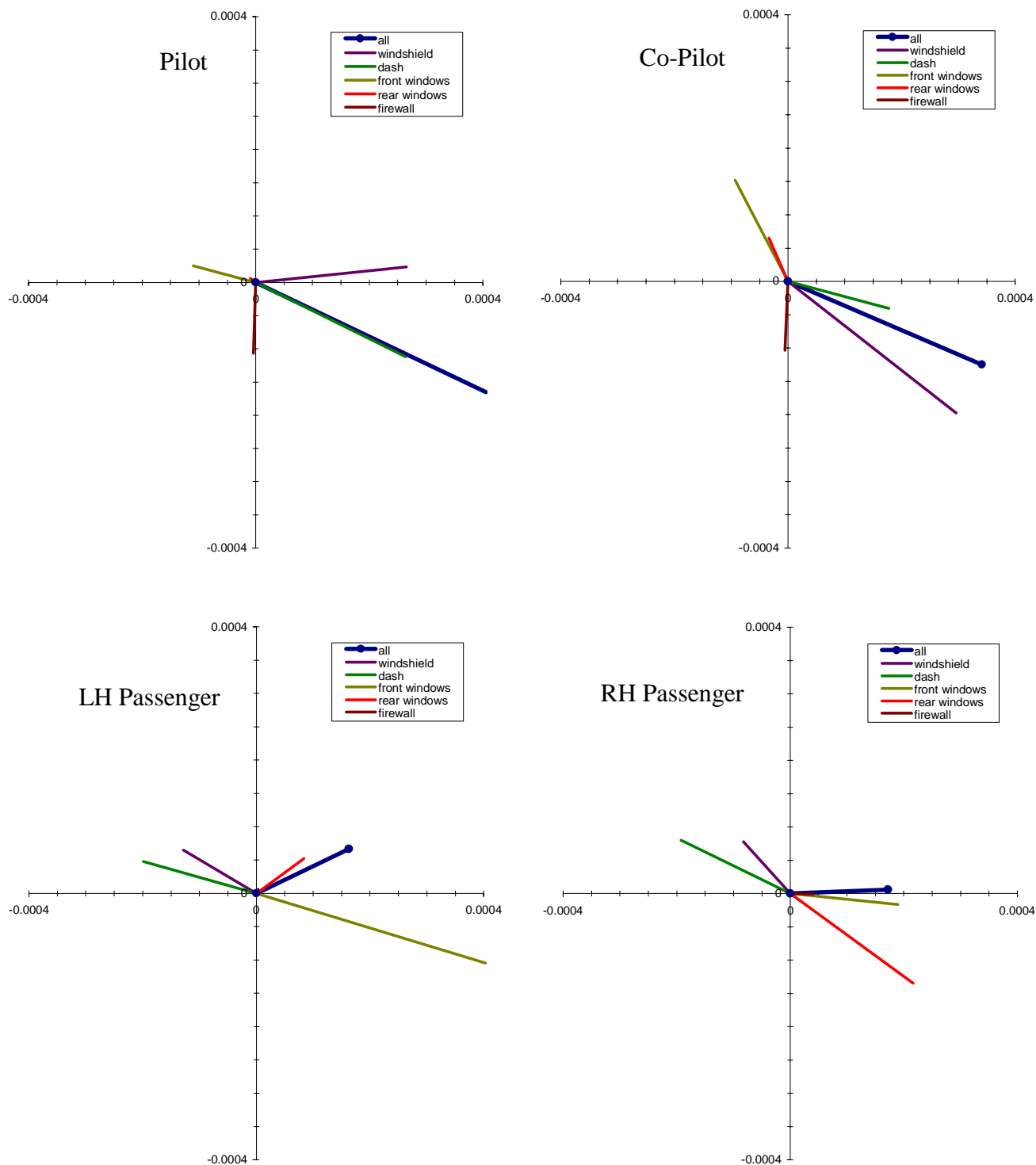
**Figure 3.36 Vector Decomposition of Simulated Pressures
at Reference Microphones – 100 Singular Values.**
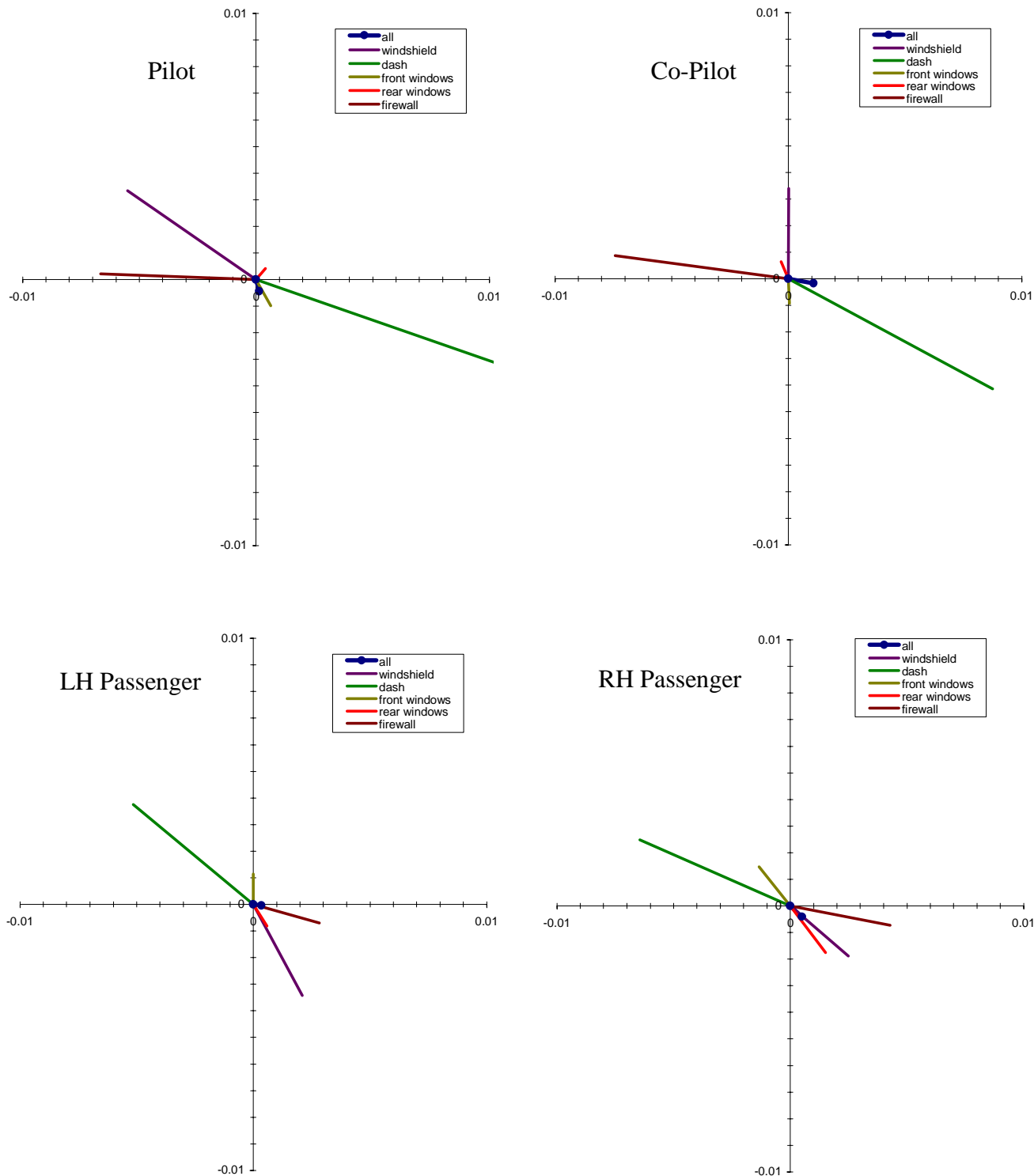
**Figure 3.37 Vector Decomposition of Simulated Pressures
at Reference Microphones – 200 Singular Values**.
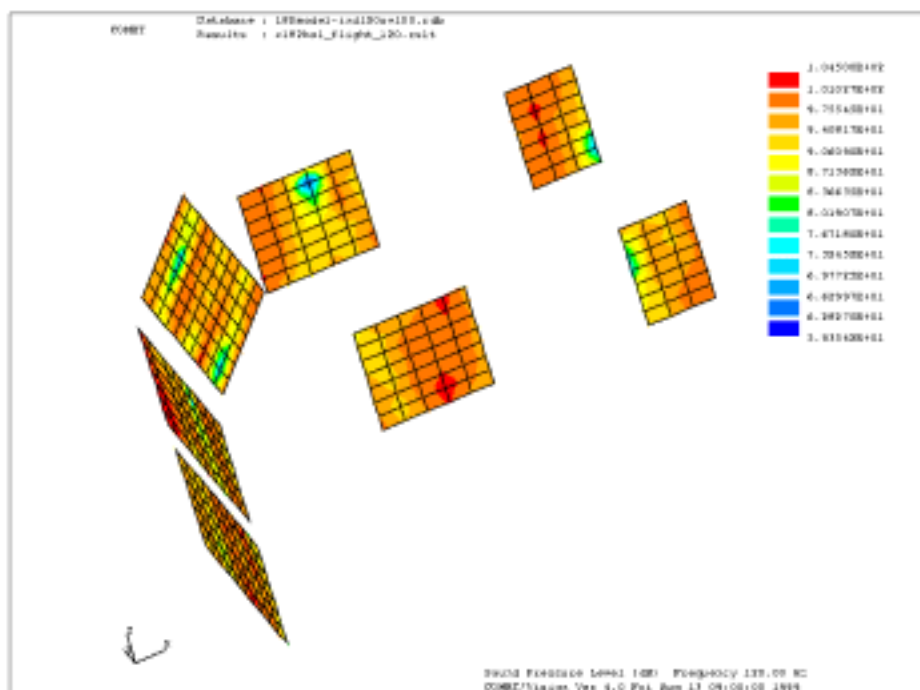
Figure 3.38 In-Flight Acoustic Pressure Measurements at 120 Hz – Isometric View.
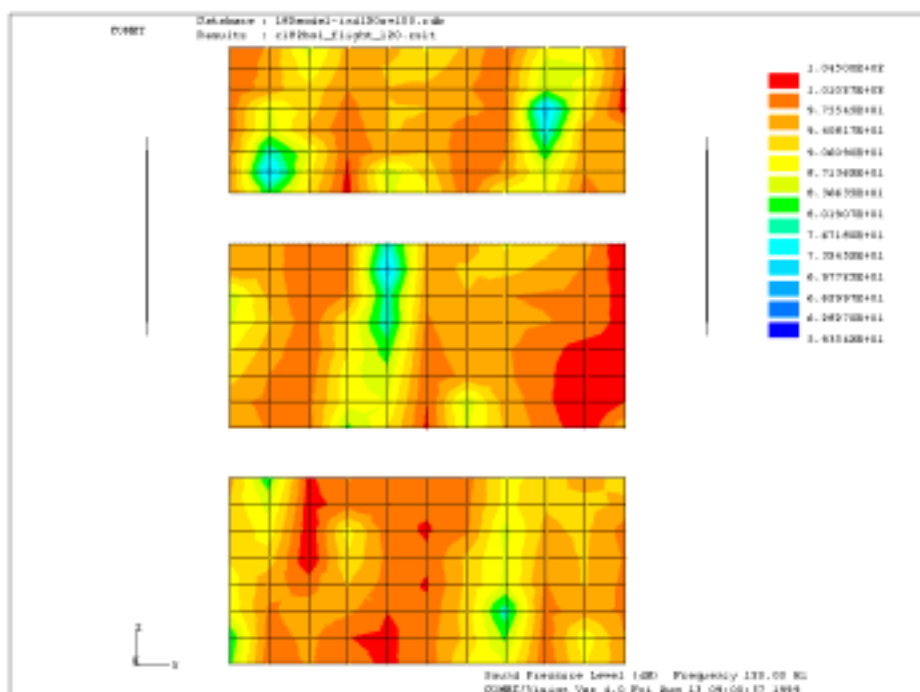
Figure 3.39 In-Flight Acoustic Pressure Measurements at 120 Hz – Front View.
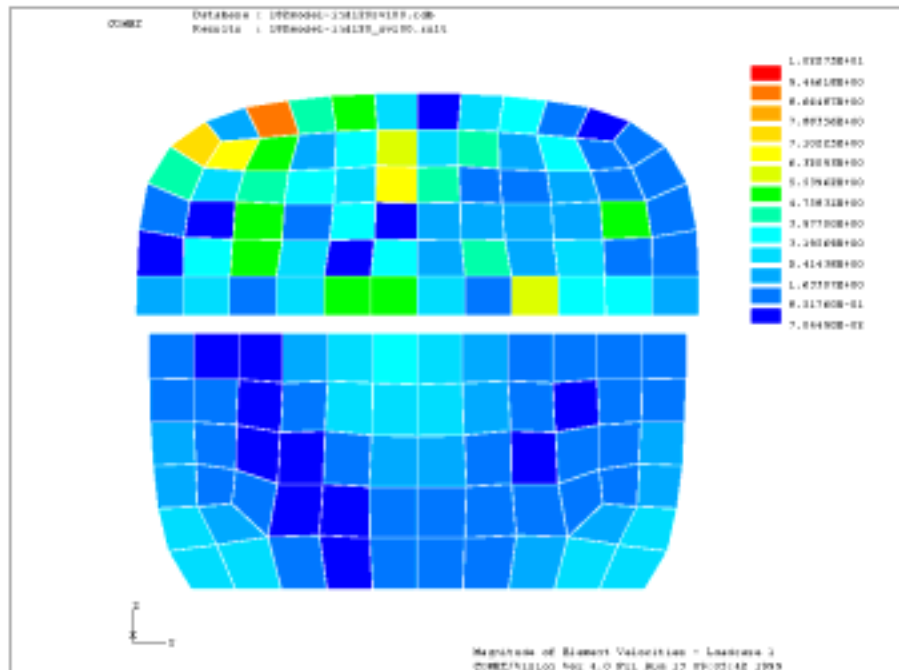
**Figure 3.40 Velocity Distribution at 120 Hz Using 100 Singular Values
– Dash and Firewall.**
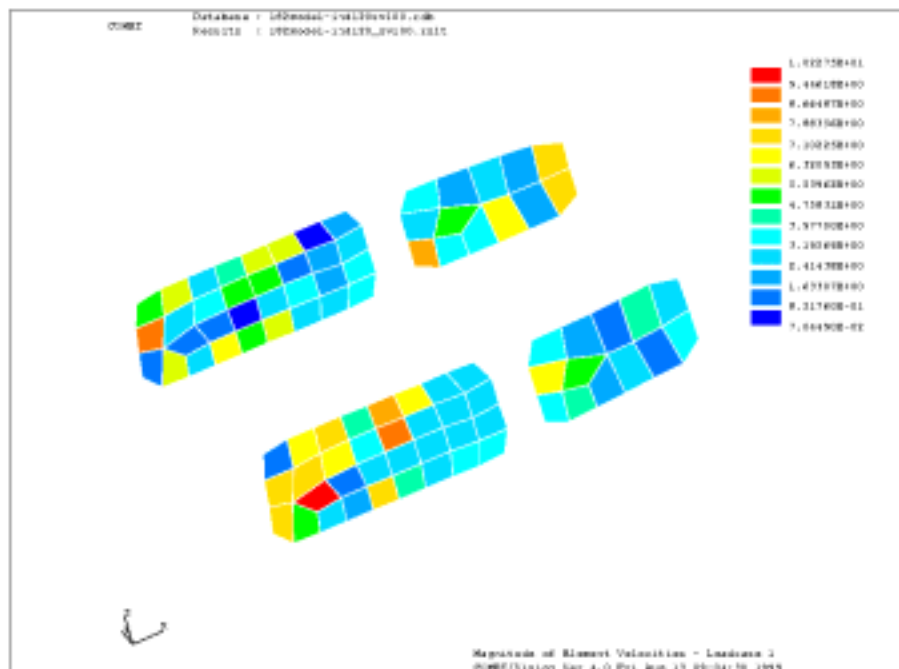
Figure 3.41 Velocity Distribution at 120 Hz Using 100 Singular Values – Windows.

General Aviation Interior Noise: Page 3-32
Part I – Source/Path Identification Technology

Figure 3.42 Velocity Distribution at 120 Hz Using 100 Singular Values – Windshield Side View.

Figure 3.43 Velocity Distribution at 120 Hz Using 100 Singular Values – Windshield Front View.
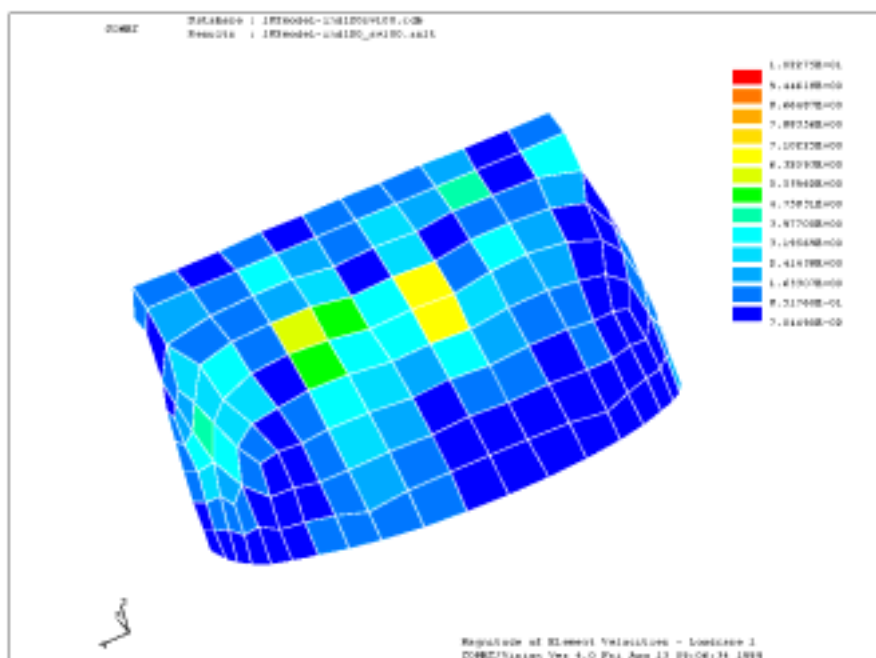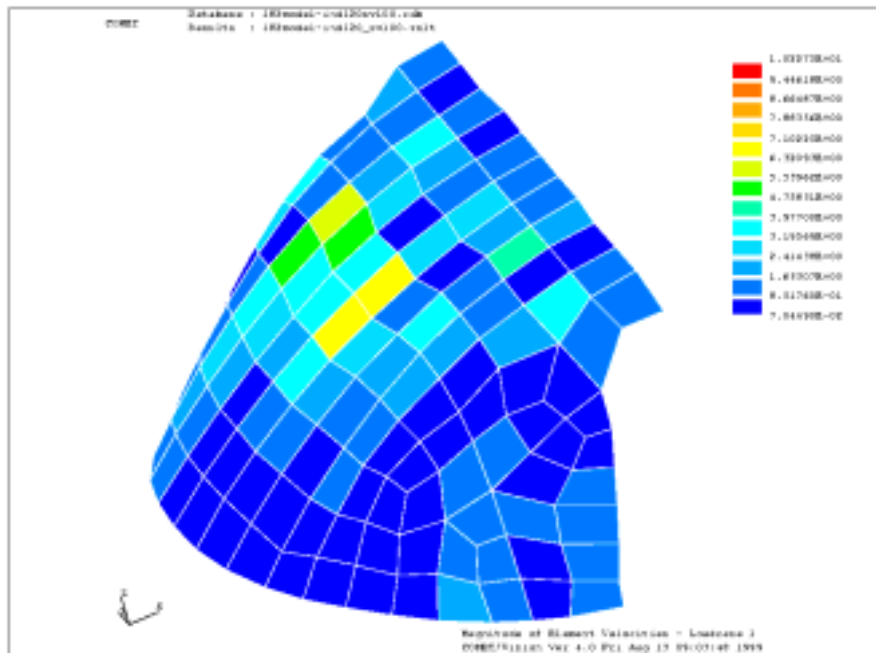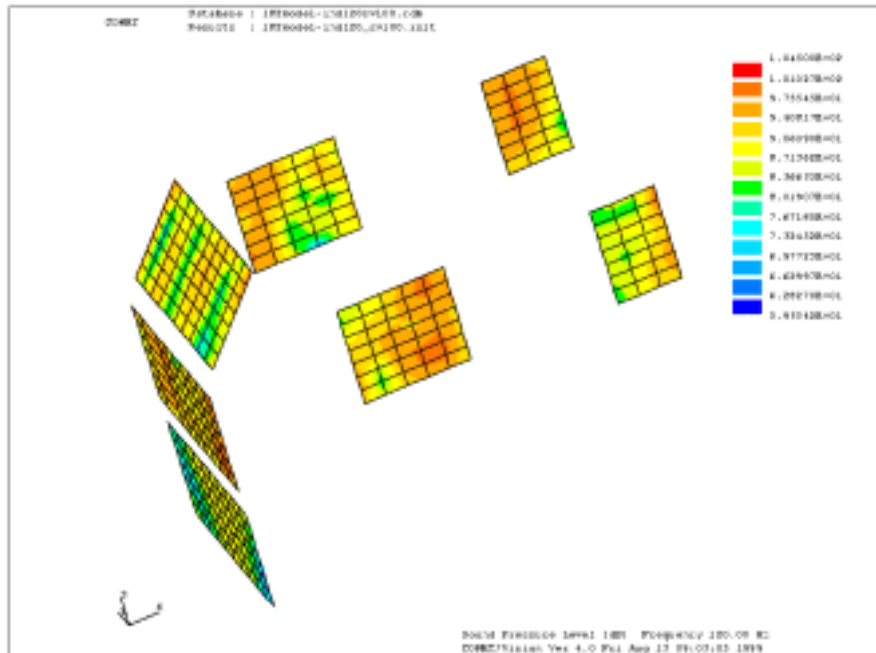
**Figure 3.44 Estimated Pressure Field at 120 Hz Using 100 Singular Values
– Isometric View.**
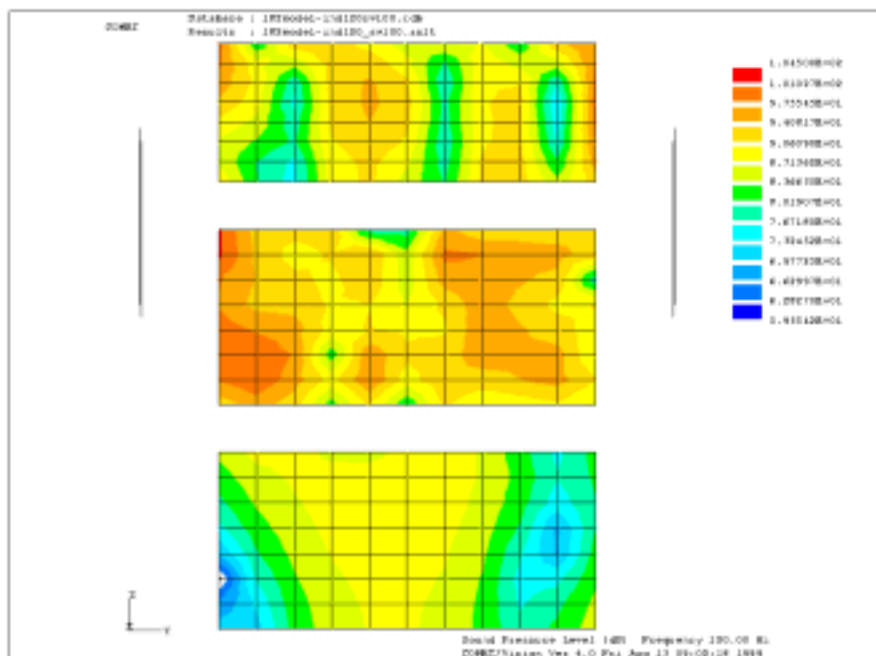
**Figure 3.45 Estimated Pressure Field at 120 Hz Using 100 Singular Values
– Front View.**
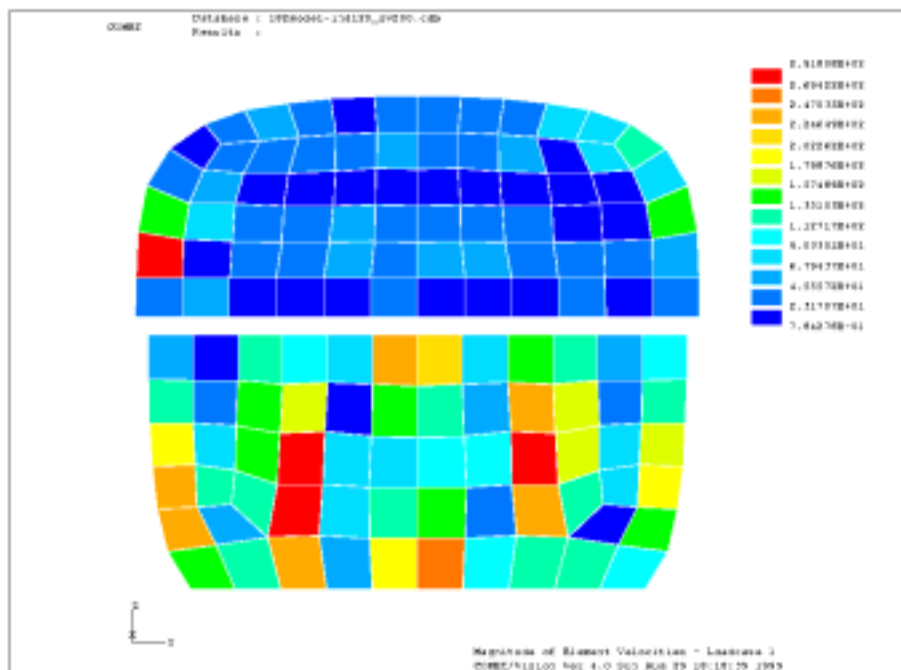
**Figure 3.46 Velocity Distribution at 120 Hz Using 200 Singular Values
– Dash and Firewall.**
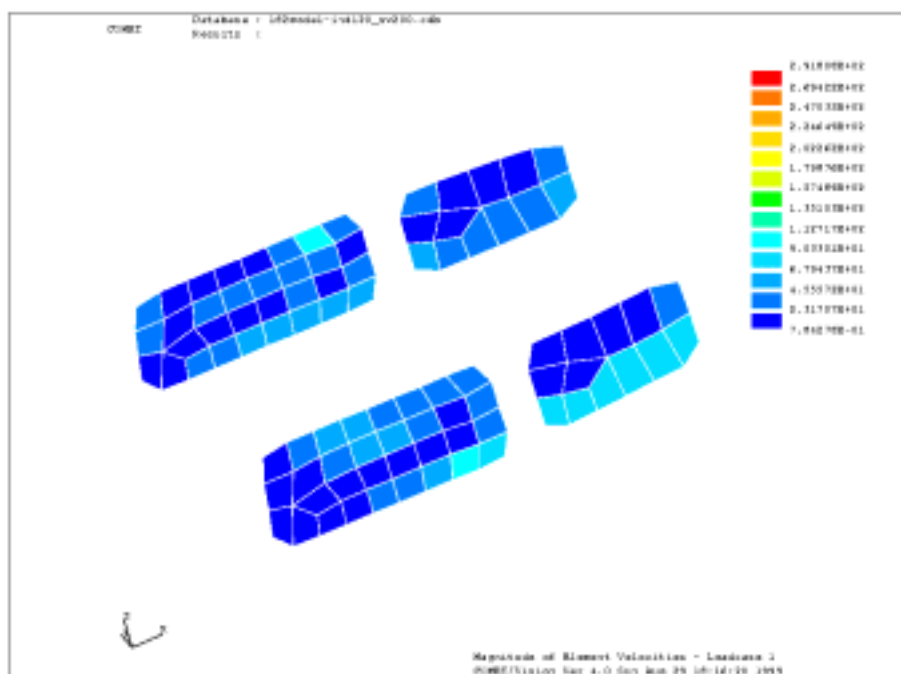
Figure 3.47 Velocity Distribution at 120 Hz Using 200 Singular Values – Windows.

**Figure 3.48 Velocity Distribution at 120 Hz Using 200 Singular Values
– Windshield Side View.**

**Figure 3.49 Velocity Distribution at 120 Hz Using 200 Singular Values
– Windshield Front View.**

**Figure 3.50 Estimated Pressure Field at 120 Hz Using 200 Singular Values
– Isometric View.**

**Figure 3.51 Estimated Pressure Field at 120 Hz Using 200 Singular Values
– Front View.**

Figure 3.52 Extended Source Element Set.
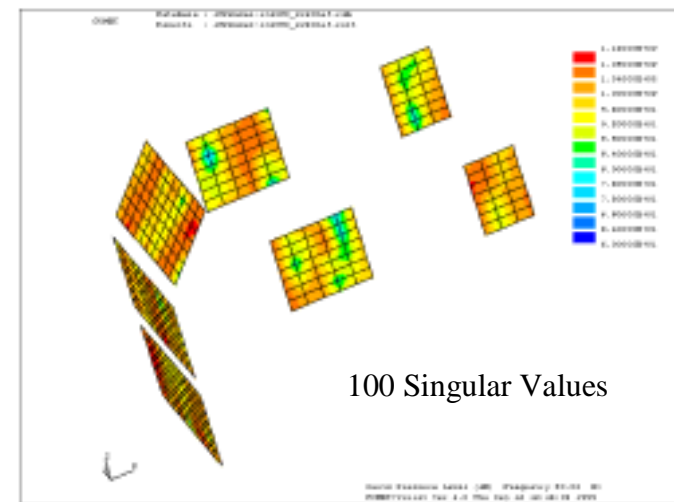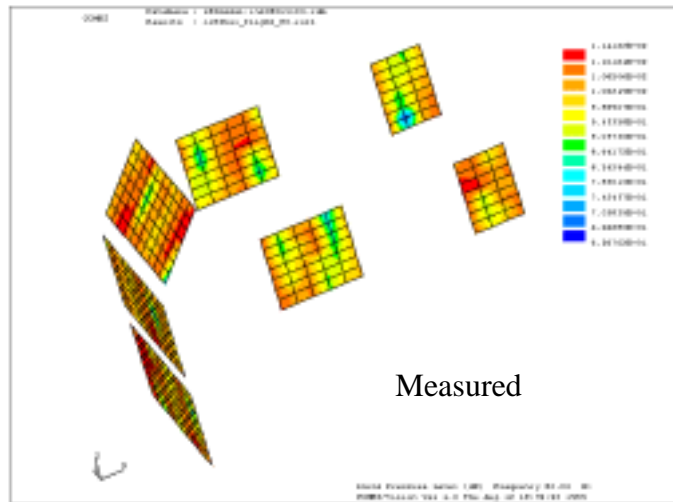
Figure 3.53 Measured and Predicted Hologram Pressure Distributions – Isometric View.
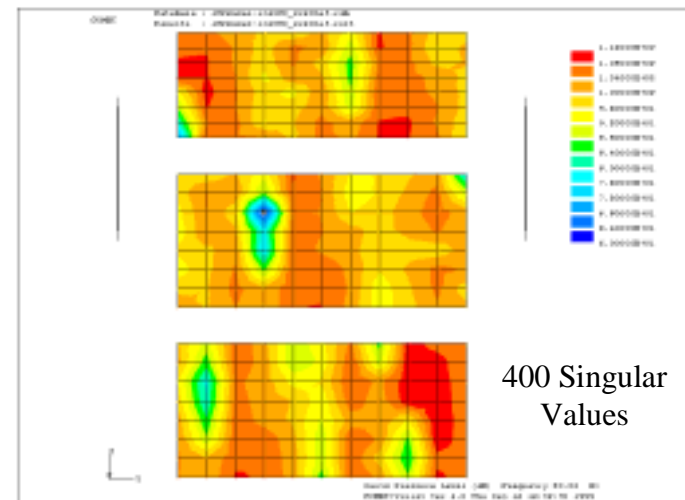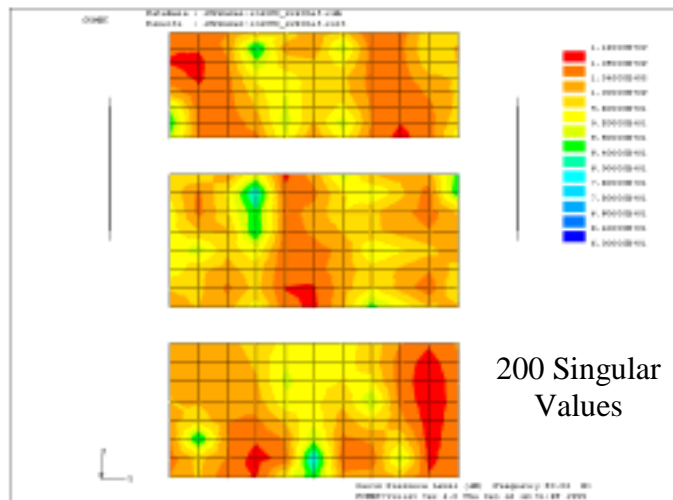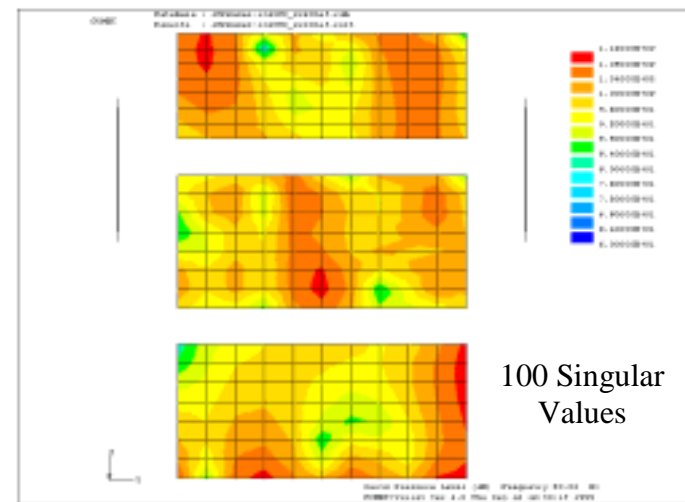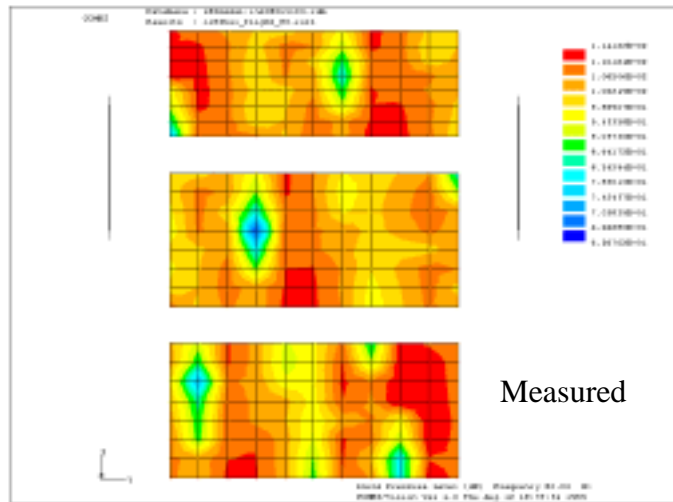
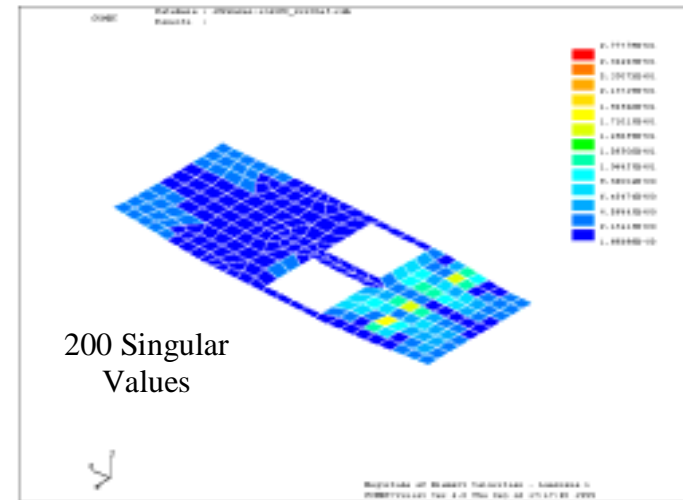**Figure 3.54 Measured and Predicted Hologram Pressure Distributions – Front View.**
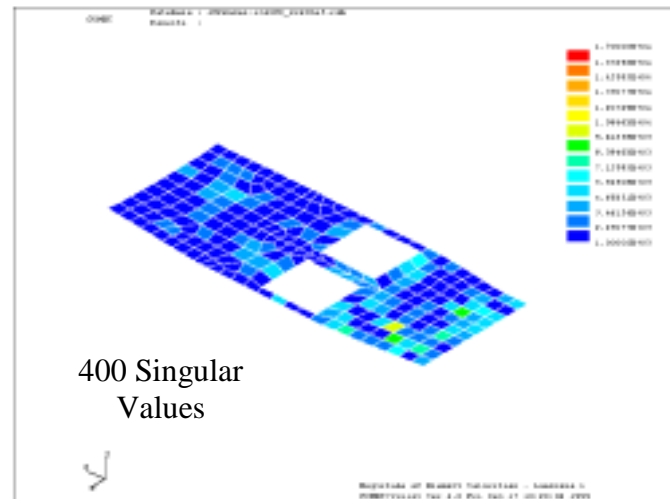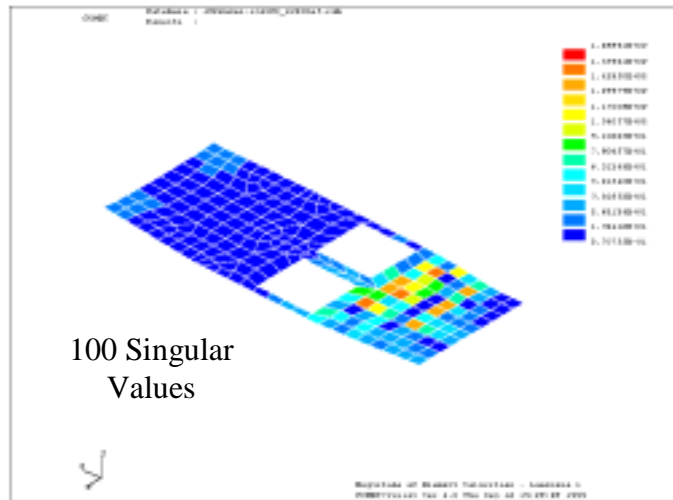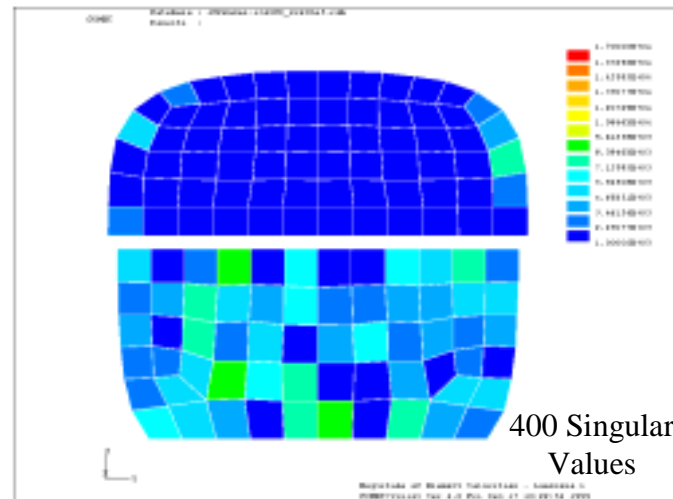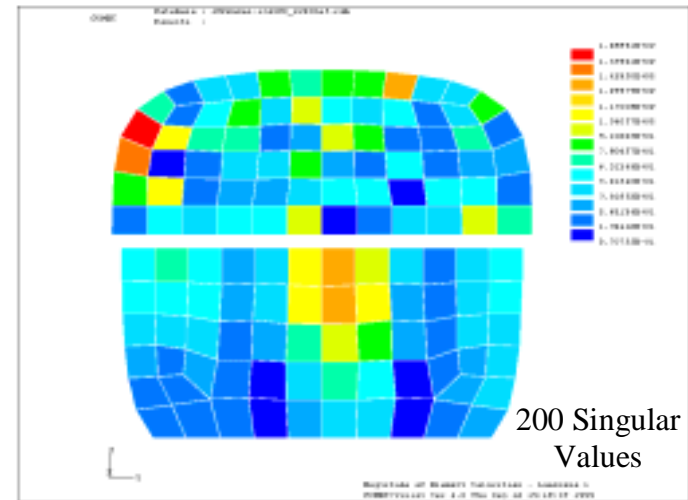
Figure 3.55 Predicted Source Distributions – Floor.
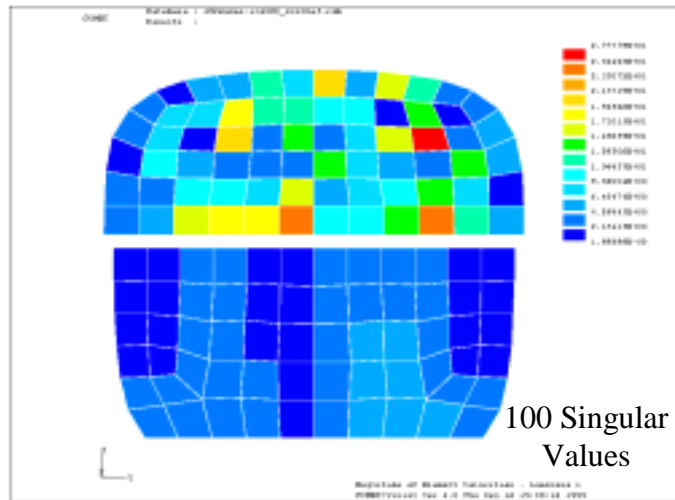
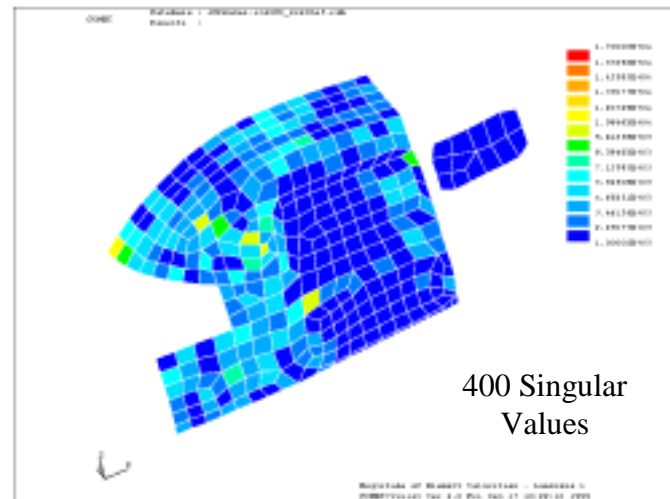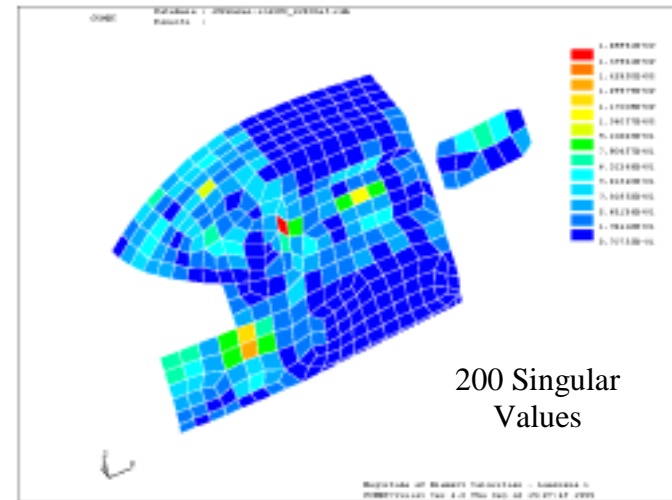**Figure 3.56 Predicted Source Distributions – Dash and Firewall.**
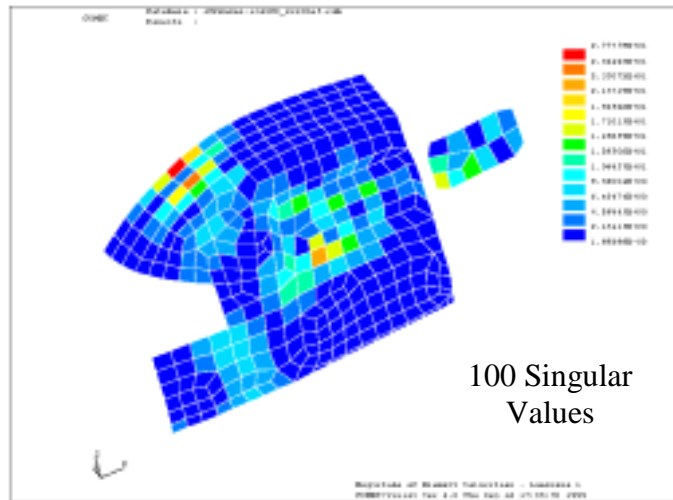
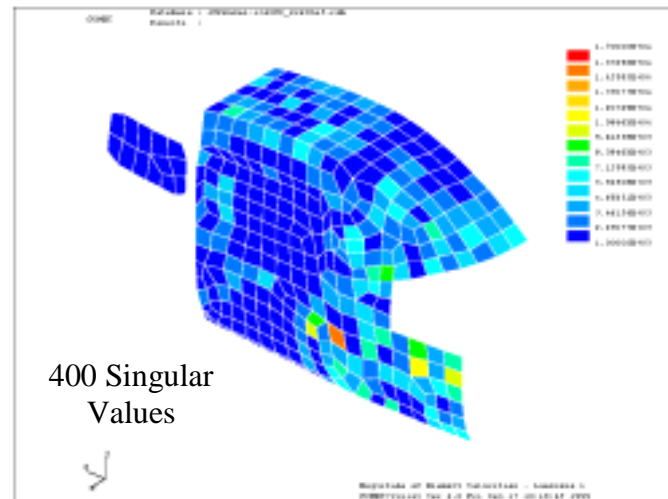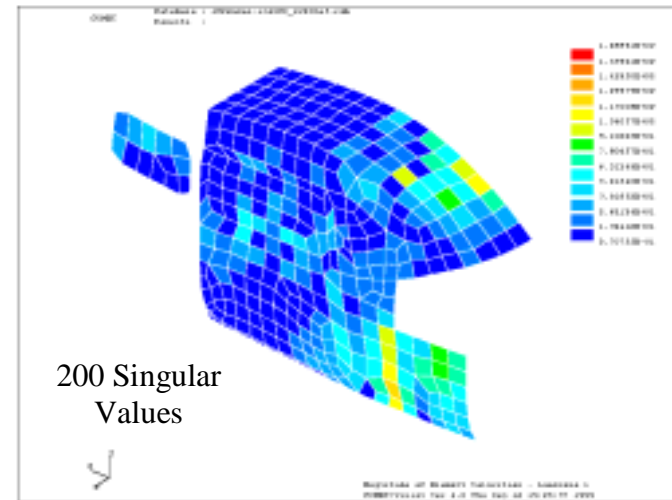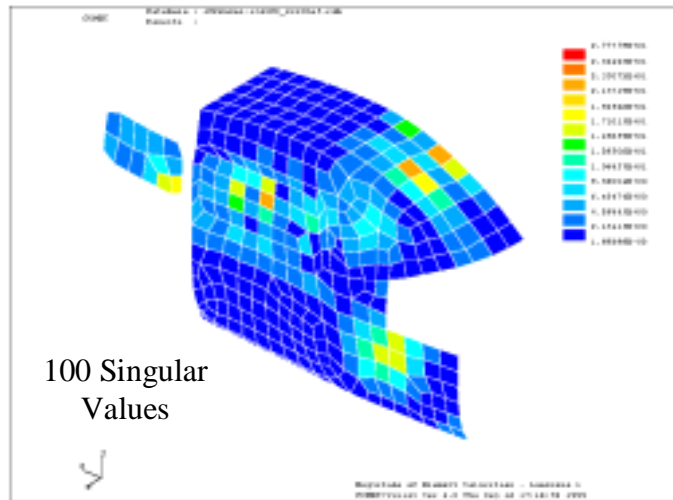**Figure 3.57 Predicted Source Distributions – Left Side.**

Figure 3.58 Predicted Source Distributions – Right Side.

4. CONCLUSIONS

Based on the results presented from Principal Component Analysis (PCA) and Conditioned Response Analysis (CRA) of the Cessna Model 182E in-flight and ground test databases, the following observations and conclusions are made:

The Use of PCA and CRA

1. PCA is a very useful analysis tool to ensure that the measured response parameters of a database are coherent relative to a fixed set of reference signals, such as a set of cabin microphones. In this manner, relative comparisons of response amplitudes within the database may be made with the assurance that they are in themselves coherent responses.

2. Unfortunately, the magnitudes of the response vectors from a PCA analysis do not necessarily translate into equivalent participants in producing the responses at the fixed set of reference signals. For example, the analysis of the Cessna 182E in-flight data showed relatively high levels of vibration of the engine, yet engine structure-borne noise transmission was found to be quite low.

3. CRA can be extremely useful in identifying the potential source contributions from a coherent in-flight data set generated from a PCA.

4. Unfortunately, a brute force application of CRA will most likely lead to poor response predictions from the various source simulations. Employing the following procedures will greatly enhance CRA accuracy:

   - Use caution in selecting the in-flight response parameter set associated with a given source simulation. Employ response parameters that respond well to the simulated source and may be shielded from other potential sources. For example, the engine structure-borne noise simulation parameter set should be restricted to the larger massive engine and engine mount aircraft components that will not be excited easily by airborne noise sources.

   - Initially, remove the effects of structure-borne noise (SBN) transmission from the in-flight data set before evaluating the potential for airborne noise transmission. This should be done independent of the relative contribution of SBN.

   - Separate the microphone and accelerometer parameter data sets into two complementary CRA's and combine the results based on the best match to the in-flight measured cabin noise levels.

Cessna Model 182E Sources and Paths

1. Structure-borne noise transmission from engine/propeller vibration does not appear to be a major source of interior noise.

2. Engine firing exhaust noise is a significant cabin noise source out to the 2nd harmonic of the firing frequency (120 Hz). The path of transmission is believed to be via the firewall.

---

3. The airborne propeller is a significant source out to the 3rd harmonic of the blade passage frequency (80 Hz), with the windshield as a major path.

4. Engine case radiation and/or noise generation within the engine/cowling area is a major source of interior noise. Propagation via the fuselage firewall appears to be the major path.

Identification of the major panel groups contributing to cabin noise in the Cessna Model 182E aircraft was studied using an Acoustic Holography (AH) boundary element modeling technique coupled with an in-flight hologram plane measurement database. The following conclusions are drawn from this limited study:

The AH Modeling Technique

1. The AH boundary element modeling technique shows promise as a prediction tool assisting in noise source identification for aircraft vehicle interiors. Portions of the acoustic field as defined by the hologram pressure distribution were reproduced, indicating agreement between measured data and simulated data.

2. Modeling only the aircraft surface areas where high noise radiation is expected has led to uncertainty regarding identification and ranking of the sources. It is believed that this uncertainty can be eliminated by:

   • Complete representation of the receiving volume by modeling the entire aircraft interior as a potential noise radiator. This will increase the computational complexity of the problem and may require extended hologram measurements.

   • Extending the hologram measurement surface to those areas where low radiation is expected should also improve the convergence of the pseudo inverse solution technique used in the inverse problem solution.

Panel Source Identification

From the limited modeling accomplished to date, the panels in the area of the Cessna Model 182E windshield, windows, and instrumentation panel appear to be dominant sources to the cabin interior. Further analysis is required to confirm this conclusion.

5. RECOMMENDATIONS

In-flight and ground test databases were acquired on a Cessna Model 182E general aviation aircraft and analysis procedures were developed and employed to identify the major noise sources and paths in the aircraft leading to the measured cabin noise levels. The analysis procedures need direct verification through further flight/ground testing and extended AH modeling. The following tasks are recommended:

1. Devise noise control measures to reduce noise transmission across the aircraft firewall and test for effectiveness.

2. Devise noise control techniques to reduce radiation from the aircraft engine case versus the exhaust system and test for effectiveness.

3. Develop interior panel shielding techniques for the windshield, instrument panel, windows, etc., to directly identify their contribution to interior noise.

4. Expand the AH measurement surface to include areas where low noise radiation is expected and expand the AH analysis to modeling of the complete aircraft cabin. Conduct parallel analyses for comparison to the experimental cabin panel shielding test results.

5. Expand the AH modeling to include more detailed cabin features, such as surface absorption.

6. REFERENCES

1. "Detection of In-Flight Propeller-Induced Structure-Borne Noise," by J.F. Unruh, *AIAA Journal of Aircraft*, Vol. 24, No. 7, pp. 441-446, July 1987.

2. "Noise Transmission into Propeller-Driven Airplanes," by J.F. Wilby, *Shock & Vibration Digest*, Vol. 21, No. 6, pp. 3-10, June 1989.

3. "Structure-Borne Noise Transmission in the Propfan Test Assessment Aircraft," by J.F. Unruh, *Noise Control Journal*, Vol. 36, No. 2, March-April 1991.

4. "The Use of Partial Coherence Technique for Identifying Noise Transmission Paths on the MDC UHB Demonstrator Aircraft," by B.N. Tran and M.A. Simpson, AIAA Paper 90-3968, October 1990.

5. "Acoustic Intensity Measurements - A Review," by J. Tichy, AIAA Paper No 84-2310, AIAA/NASA 9th Aeroacoustics Conference, Williamsburg, Virginia, October 1984.

6. "Light Aircraft Sound Transmission Studies: The Use of the Two Microphone Sound Intensity Technique," by K.H. Lyle, M.S. Atwal, and M.J. Croker, *Noise Control Engineering Journal*, Vol. 31, No. 3, pp. 145-153, Nov-Dec 1988.

7. "Nearfield Acoustic Holography: I. Theory of Generalized Holography and the Development of NAH," by J.D. Maynard, E.G. Williams, and Y. Lee, Journal of Acoustic Society of America, Vol. 78, No. 4, 1985.

8. "STSF - A Unique Technique for Scan-Based Near-field Acoustic Holography Without Restrictions on Coherence," Bruel & Kjaer Technical Review No. 1, 1989.

9. *MATLAB The Language of Technical Computing*, The Math Works Inc., Version 5, pp. 4.23-4.25.

10. "Acoustic Holography for Arbitrary Geometry Sources and Receivers", by J.F. Unruh and P.D. Till, Southwest Research Institute, Report 18-9050, September 1999.

REPORT DOCUMENTATION PAGE			Form Approved OMB No. 0704-0188

Public reporting burden for this collection of information is estimated to average 1 hour per response, including the time for reviewing instructions, searching existing data sources, gathering and maintaining the data needed, and completing and reviewing the collection of information. Send comments regarding this burden estimate or any other aspect of this collection of information, including suggestions for reducing this burden, to Washington Headquarters Services, Directorate for Information Operations and Reports, 1215 Jefferson Davis Highway, Suite 1204, Arlington, VA 22202-4302, and to the Office of Management and Budget, Paperwork Reduction Project (0704-0188), Washington, DC 20503.

1. AGENCY USE ONLY (*Leave blank*)	2. REPORT DATE May 2002	3. REPORT TYPE AND DATES COVERED Contractor Report	
4. TITLE AND SUBTITLE General Aviation Interior Noise: Part I - Source/Path Identification		**5. FUNDING NUMBERS** NAG1-2091	
6. AUTHOR(S) James F. Unruh, and Paul D. Till		706-81-14-01	
7. PERFORMING ORGANIZATION NAME(S) AND ADDRESS(ES) Southwest Research Institute San Antonio, Texas		**8. PERFORMING ORGANIZATION REPORT NUMBER**	
9. SPONSORING/MONITORING AGENCY NAME(S) AND ADDRESS(ES) National Aeronautics and Space Administration Langley Research Center Hampton, VA 23681-2199		**10. SPONSORING/MONITORING AGENCY REPORT NUMBER** NASA/CR-2002-211665	

11. SUPPLEMENTARY NOTES
Langley Technical Monitor: Daniel L. Palumbo

12a. DISTRIBUTION/AVAILABILITY STATEMENT Unclassified-Unlimited Subject Category 3 Distribution: Nonstandard Availability: NASA CASI (301) 621-0390	12b. DISTRIBUTION CODE

13. ABSTRACT *(Maximum 200 words)*

There were two primary objectives of the research effort reported herein. The first objective was to identify and evaluate noise source/path identification technology applicable to single engine propeller driven aircraft that can be used to identify interior noise sources originating from structure-borne engine/propeller vibration, airborne propeller transmission, airborne engine exhaust noise, and engine case radiation. The approach taken to identify the contributions of each of these possible sources was first to conduct a Principal Component Analysis (PCA) of an in-flight noise and vibration database acquired on a Cessna Model 182E aircraft. The second objective was to develop and evaluate advanced technology for noise source ranking of interior panel groups such as the aircraft windshield, instrument panel, firewall, and door/window panels within the cabin of a single engine propeller driven aircraft. The technology employed was that of Acoustic Holography (AH). AH was applied to the test aircraft by acquiring a series of in-flight microphone array measurements within the aircraft cabin and correlating the measurements via PCA. The source contributions of the various panel groups leading to the array measurements were then synthesized by solving the inverse problem using the boundary element model.

14. SUBJECT TERMS Noise Source/Path Identification, General Aviation Aircraft, Principal Component Analysis, Acoustic Holography			15. NUMBER OF PAGES 139
			16. PRICE CODE
17. SECURITY CLASSIFICATION OF REPORT Unclassified	18. SECURITY CLASSIFICATION OF THIS PAGE Unclassified	19. SECURITY CLASSIFICATION OF ABSTRACT Unclassified	20. LIMITATION OF ABSTRACT UL

NSN 7540-01-280-5500

Standard Form 298 (Rev. 2-89)
Prescribed by ANSI Std. Z-39-18
298-102